National Technical University of Athens
School of Chemical Engineering
Department of Process Analysis and Plant Design

Diploma Thesis

Microwave-Heated Catalytic Reactor for the Indirect Production of Methanol from Methane: Process Design and Optimization & Techno economic Analysis

Vassiliki Kaperneka

Supervisor: Prof. Georgios Stefanidis

Athens
September of 2023

Abstract

In recent years, stringent environmental regulations have placed increasing pressure on industries to reduce greenhouse gas emissions, as a means of the transition to a sustainable and low-carbon energy landscape. This necessitates the development of innovative processes for carbon capture and utilization (CCU) while concurrently exploring the integration of renewable energy sources (RES) into chemical manufacturing. The goal of this study is to investigate the processes of Dry Methane Reforming (DMR), which utilizes methane and carbon dioxide, the two main greenhouse gases, and methanol synthesis via hydrogenation of CO and CO_2, which are derived from the DMR, in order to finally produce approximately 100 ktonnes/year methanol of purity 99.5%. All the upstream and downstream processes were simulated and optimized in Aspen Plus V11 and afterwards a comprehensive techno-economic analysis was conducted by utilizing the MS Excel. Also, a preliminary estimation of the carbon emissions was employed, using the Ecoinvent 3.9.1 (12/2022) database and the CML v4.8 2016 method. In this thesis three case studies (CS) are employed regarding the feedstock, as well as the heating method of the Dry Methane Reforming process: Firstly, a scenario that employs pure fossil-based methane and carbon dioxide (captured) as feedstock to a conventional heated reactor (i.e., furnaces using fossil fuels) is set as a base (CS1). Then, in the context of chemical industry electrification, a scenario of Microwave-assisted reactor is developed keeping fossil-based methane as feedstock (CS2). Lastly, in an effort to replace fossil fuels with renewable materials, biogas is considered as a feed for the MW-assisted catalytic DMR reactor. Due to the high H_2S composition of biogas, desulfurization system is placed before the DMR reactor (CS3). The methanol production and purification processes are kept the same in all three case studies.

The optimization of the processes regarding the conditions (temperature and pressure), the recycle percentage and the distillation columns' characteristics, lead in the following results, that are the same in all cases: methane conversion in the DMR reactor: 99.5%, CO conversion in the methanol synthesis reactor: 44.8% and total yield 73%. Afterwards, a heat integration is carried out, reducing the energy requirements for hot and cold utilities as following: CS1: 2.3 and 3.1 MW, CS2: 2.3 and 2.3 MW and CS3: 2.4 and 2.4 MW,

respectively. Then, a techno-economic assessment is performed to estimate the operating costs for the year 2023 and the projects' feasibility. The cost drivers of the whole unit resulted to be the H_2 from water electrolysis (3000 eur/tonne), the high pressure steam (6.86 eur/GJ), the grid electricity (100 eur/MWh) and the capital expenditures (CAPEX). Finally, the project appeared to be economically nonviable, with net present values (NPV) ranging from -1.3 to -1.7 billion euro for a total 20-year lifetime.

However, bearing in mind the predicted prices of the H_2, electricity, CO_2 and methanol, four scenario analysis were employed for the year 2050 and only for CS2 (CS1 is not viable in the future due to its high utilization of fossil fuels and CS3 is more costly than CS2):

1. The price for the H_2 was set at 1000 eur/tonne, for the CO_2 34 eur/tonne and for the electricity 20 eur/MWh. The break-even value of methanol resulted to be 1986 eur/tonne, higher than the estimated one (i.e., 630 eur/tonne).

2. An analysis of the economy of scale effect resulted in a zero NPV for a capacity of 3500 ktonne/year (upper limit for industrial scale methanol production according to literature) and a methanol price equal to 1700 eur/tonne

3. A sensitivity analysis for the potential reduction of CAPEX (10-40%) due to the evolution of technology's maturity. The estimated prices of raw materials, electricity and methanol of 2050 were used. The NPV increased, but was not above zero for any CAPEX reduction.

4. Finally, a synergy of all the above was employed. More specifically, the raw materials' and electricity's price of 2050, a capacity of 3500 ktonnes/year MeOH and a 40% reduction of CAPEX due to future maturity of technology were considered in order to find the break-even value of methanol (NPV=0), which resulted to be 1674 eur/tonne (16% reduced compared to the initial 2050 break-even value -1986-, but higher than the estimated one -630-).

Finally, the CO_2 equivalent emissions of all the processes were calculated equal to 1.94, 1.44 and 1.43 $kg_{CO_2-equivalent}/kg_{MeOH}$ for CS 1, 2 and 3 respectively. These values appeared to be comparable to the literature ones, and in fact lower than the some of them (i.e., 5.55 $kg_{CO_2-equivalent}/kg_{MeOH}$ in

the electrochemical reduction of CO_2 method and 12.5-19.8 in the shale gas partial oxidation/SMR method). All in all the project can be considered non profitable in today's economy, but potentially viable in the future "green" economy.

Keywords: CCU; DMR; syngas-to-methanol; methanol; CO hydrogenation; CO_2 hydrogenation; electrification; microwave-assisted; techno-economic analysis; carbon emissions

Περίληψη

Τα τελευταία χρόνια, αυστηροί κανονισμοί περιβαλλοντικής προστασίας έχουν ασκήσει αυξανόμενη πίεση στις βιομηχανίες για τη μείωση των εκπομπών αερίων θερμοκηπίου, ως μέσο για τη μετάβαση σε ένα βιώσιμο και χαμηλού άνθρακα ενεργειακό τοπίο. Αυτό απαιτεί την ανάπτυξη καινοτόμων διαδικασιών για τη δέσμευση και χρησιμοποίηση του άνθρακα, ταυτόχρονα με την εξερεύνηση της ενσωμάτωσης πηγών ανανεώσιμης ενέργειας στη χημική βιομηχανία. Στόχος της παρούσας μελέτης είναι η διερεύνηση των διαδικασιών της ξηρής αναμόρφωσης του μεθανίου, που χρησιμοποιεί μεθάνιο και διοξείδιο του άνθρακα, τα δύο κύρια αέρια θερμοκηπίου, και της σύνθεσης μεθανόλης μέσω υδρογόνωσης του μονοξειδίου και διοξειδίου του άνθρακα, τα οποία προέρχονται από την ΞΑΜ, με σκοπό την παραγωγή περίπου 100 χιλιάδων τόνων/έτος μεθανόλης καθαρότητας 99.5%. Όλες οι διεργασίες προσομοιώθηκαν και βελτιστοποιήθηκαν στο Aspen Plus V11 και στη συνέχεια πραγματοποιήθηκε μια ολοκληρωμένη τεχνο-οικονομική ανάλυση χρησιμοποιώντας το MS Excel. Επίσης, πραγματοποιήθηκε μια προκαταρκτική εκτίμηση των εκπομπών άνθρακα, χρησιμοποιώντας τη βάση δεδομένων Ecoinvent 3.9.1 (12/2022) και τη μέθοδο CML v4.8 2016. Στην εργασία αυτή χρησιμοποιούνται τρεις περιπτωσιολογικές μελέτες (ΠΜ) όσον αφορά την τροφοδοσία, καθώς και τη μέθοδο θέρμανσης της ΞΑΜ: Καταρχάς, θεωρήθηκε ως βάση ένα σενάριο με καθαρή τροφοδοσία ορυκτής προέλευσης μεθανίου και διοξειδίου του άνθρακα, με συμβατική θέρμανση του αντιδραστήρα ΞΑΜ (δηλαδή φούρνοι που καίνε ορυκτά καύσιμα) (πρώτη περίπτωση - ΠΜ1). Στη συνέχεια, στο πλαίσιο του εξηλεκτρισμού της χημικής βιομηχανίας, αναπτύσσεται ένα σενάριο με αντιδραστήρα ΞΑΜ που θερμαίνεται μέσω μικροκυμάτων, διατηρώντας την ίδια τροφοδοσία με την ΠΜ1 (δεύτερη περίπτωση - ΠΜ2). Τέλος, στην προσπάθεια να αντικατασταθούν τα ορυκτά καύσιμα με ανανεώσιμα υλικά, λαμβάνεται υπόψη η χρήση βιοαερίου ως τροφοδοσία στον ΞΑΜ αντιδραστήρα που χρησιμοποιεί μικροκυμάτα για τη θέρμανσή του. Λόγω της υψηλής συγκέντρωσης του βιοαερίου σε υδρόθειο, ένα σύστημα αφαίρεσης θείου, τοποθετείται πριν από τον αντιδραστήρα ΞΑΜ (τρίτη περίπτωση - ΠΜ3). Οι διεργασίες σύνθεσης και καθαρισμού της μεθανόλης παραμένουν ίδιες σε όλες τις περιπτωσιολογικές μελέτες.

Η βελτιστοποίηση των διαδικασιών όσον αφορά τις συνθήκες (θερμοκρασία και πίεση), το ποσοστό ανακύκλωσης και τα χαρακτηριστικά της αποστακτικής στήλης οδηγεί στα ακόλουθα αποτελέσματα, τα οποία είναι ίδια σε όλες τις

περιπτώσεις: μετατροπή μεθανίου στον αντιδραστήρα ΞΑΜ: 99.5%, μετατροπή μονοξειδίου του άνθρακα στον αντιδραστήρα σύνθεσης μεθανόλης: 44.8% και συνολική απόδοση 73%. Στη συνέχεια, πραγματοποιείται η Ενεργειακή Ολοκλήρωση, μείωντας τις ενεργειακές απαιτήσεις για θερμό και ψυχρό μέσο ως εξής: ΠΜ1: 2.3 και 3.1, ΠΜ2: 2.3 και 2.3 και ΠΜ3: 2.4 και 2.4 MW, αντίστοιχα. Στη συνέχεια, πραγματοποιείται μια τεχνο-οικονομική αξιολόγηση για να εκτιμηθούν οι λειτουργικές δαπάνες για το έτος 2023 και εντέλει η βιωσιμότητα του έργου. Τη μεγαλύτερη συνεισφορά στο ολικό κόστος την έιχε το υδρογόνο από ηλεκτρολύση νερού (με 3000 ευρώ/τόνο), ο ατμός υψηλής πίεσης (με 6.86 eur/GJ), η ηλεκτρική ενέργεια (με 100 ευρώ/MWh), καθώς και το υψηλό πάγιο κόστος (ΠΚ). Το έργο εντέλει ήταν οικονομικά μη βιώσιμο σε όλες τις περιπτώσεις, με τιμές της καθαρής παρούσας αξίας (ΚΠΑ) που κυμαίνονταν από -1.3 έως -1.7 δισεκατομμύρια ευρώ για μια συνολική διάρκεια ζωής 20 ετών.

Ωστόσο, λαμβάνοντας υπόψη τις προβλεπόμενες τιμές του υδρογόνου, του ηλεκτρισμού, του διοξείδίου του άνθρακα και της μεθανόλης, πραγματοποιήθηκε μια ανάλυση τεσσάρων σεναρίων για το έτος 2050 και μόνο για την ΠΜ2 (η ΠΜ1 δεν είναι βιώσιμη στο μέλλον λόγω της υψηλής αξιοποίησής ορυκτών καυσίμων και η ΠΜ3 είναι πιο δαπανηρή από το ΠΜ2):

1. Η τιμή για το υδρογόνο ορίστηκε στα 1000 ευρώ/τόνο, για το διοξείδιο του άνθρακα στα 34 ευρώ/τόνο και για την ηλεκτρική ενέργεια στα 20 ευρώ/MWh. Η τιμή νεκρού σημείου της μεθανόλης κατέληξε να είναι 1986 ευρώ/τόνο, υψηλότερη από την εκτιμώμενη (δηλαδή, 630 ευρώ/τόνο).

2. Μια ανάλυση της επίδρασης της οικονομίας κλίμακας που οδήγησε σε μηδενική ΚΠΑ για δυναμικότητα 3500 χιλιοτόννους/έτος (ανώτατο όριο για την παραγωγή μεθανόλης σε βιομηχανική κλίμακα σύμφωνα με τη βιβλιογραφία) και τιμή μεθανόλης ίση με 1700 ευρώ/τόνο.

3. Μια ανάλυση ευαισθησίας για την πιθανή μείωση του ΠΚ (10-40%) λόγω της εξέλιξης της ωριμότητας της τεχνολογίας. Χρησιμοποιήθηκαν οι εκτιμώμενες τιμές πρώτων υλών, ηλεκτρικής ενέργειας και μεθανόλης του 2050. Η ΚΠΑ αυξήθηκε, αλλά δεν ήταν πάνω από το μηδέν για οποιαδήποτε μείωση ΠΚ.

4. Τέλος, υλοποιήθηκε μια συνέργεια όλων των παραπάνω. Πιο συγκεκριμένα, η τιμή πρώτων υλών και ηλεκτρικής ενέργειας του 2050, μια δυναμικότητα 3500 χιλιοτόννων/έτος μεθανόλης και 40% μείωση του ΠΚ

λόγω μελλοντικής ωριμότητας της τεχνολογίας ελήφθησαν υπόψη για να βρεθεί η νεκρή τιμή της μεθανόλης (ΚΠΑ =0), ίση με 1674 ευρώ/τόνο (16% μειωμένη σε σύγκριση με την αρχική τιμή νεκρού σημείου του 2050 -1986-, αλλά υψηλότερη από την εκτιμώμενη -630-).

Τέλος, οι ισοδύναμες εκπομπές διοξειδίου του άνθρακα όλων των διεργασιών υπολογίστηκαν ίσες με 1.94, 1.44 και 1.43 $\mathrm{kg}_{CO_2-eq}/\mathrm{kg}_{MeOH}$ για τις ΠΜ 1, 2 και 3 αντίστοιχα. Αυτές οι τιμές ήταν συγκρίσιμες με τις βιβλιογραφικές και σε ορισμένες περιπτώσεις ακόμα και χαμηλότερες από αυτές (για παράδειγμα, 5.55 $\mathrm{kg}_{CO_2-eq}/\mathrm{kg}_{MeOH}$ στην περίπτωση ηλεκτροχημικής μείωσης του διοξειδίου του άνθρακα και 12.5-19.8 στη μέθοδο μερικής οξείδωσης/αναμόρφωσης μεθανίου με ατμό σχιστολιθικού αερίου). Συνολικά το έργο μπορεί να θεωρηθεί μη κερδοφόρο στη σημερινή οικονομία, αλλά δυνητικά βιώσιμο στη μελλοντική «πράσινη» οικονομία.

Λέξεις-Κλειδιά: δέσμευση και χρησιμοποίηση του άνθρακα· ξηρή αναμόρφωση μεθανίου· αέριο σύνθεσης-σε-μεθανόλη· μεθανόλη· υδρογόνωση διοξειδίου άνθρακα· υδρογόνωση μονοξειδίου άνθρακα· εξηλεκτρισμός· μικροκύματα· τεχνοοικονομική ανάλυση· εκπομπές άνθρακα

Contents

List of Tables

List of Figures

Abbreviations

ACC Annualized Capital Cost

AS Air Separation

ATR Auto Thermal Reforming

CC Composite Curve

CCS Carbon Capture and Storage

CCU Carbon Capture and Utilization

CEPCI Chemical Engineering Plant Industry Cost Index

CF Cash Flow

COG Coke Oven Gases

CS Case Study

CW Continuous Wave

DAC Direct Air Capture

EC Equity Capital

EP Economic Potential

EPB Equity PayBack

GCC Grand Composite Curve

GD Grind Diagram

GHG Greenhouse Gases

GHSV Gas Hourly Space Velocity

GWP Global Warming Potential

HEN Heat-Exchanger Network

HI Heat Integration

HP High Pressure

IPCC International Panel on Climate Change

IRR Internal Rate of Return

LI Loan Installment

LP Low Pressure

MW Microwaves

NG Natural Gas

NPV Net Present Value

NZE Net Zero Emissions

OPEX Operational Expenditure

PV Photovoltaic Panels

PBP PayBack Period

RES Renewable Energy Sources

REV Revenue

RM Raw Material

RV Residual Value

SDS Sustainable Development Scenario

SEI Specific Energy Input

SMR Steam Methane Reforming

STEPS Stated Policies Scenario

TCC Total Capital Cost

TFCC Total Fixed Capital Cost

TRL Technology Readiness Level

WC Working Capital

WT Wind Turbine

Chapter 1

Introduction

1.1 Environmental regulations and carbon utilization

Climate change has become a major concern in recent years due to its impact on the economy, society, and the environment. As a result of human activity-related increases of greenhouse gases (GHGs) in the atmosphere, the Earth's temperature has risen, endangering life as we know it on the planet. Carbon dioxide (CO_2) is the primary GHG responsible for this, as it absorbs infrared light and creates warming effects. Human activities have already contributed to a global warming of 1.0 degree Celsius above the pre-industrial levels, and if present CO_2 emissions continue, the temperature will rise to 1.5 degrees Celsius by 2030. Efforts to limit climate change were launched in 1992 at the United Nations Conference on Environment and Development (UNCED) in Rio de Janeiro. The Paris Agreement in 2016 was a watershed moment in global climate change efforts, with leaders from 195 countries pledging to tackle climate change and keep global warming well below 2 degrees Celsius, compared to the pre-industrial levels by the end of the century. The Paris Agreement Rulebook was agreed as a milestone in implementing the Agreement during the Katowice Climate Summit (COP-24). The International Panel on Climate Change (IPCC) proposes keeping CO_2 emissions at 25-30 gigatonnes (Gt) per year to accomplish the goal of limiting global warming to 1.5 degrees Celsius by the end of the century, which is much lower than the present levels of 58.3 Gt per year. The leading carbon emitting sector is Energy Systems (20.9 Gt per year), with coal generated electricity constituting

half of it. The industrial sector is next, accounting for 13.8 Gt of CO_2-eq in 2023. Figure 1 compares the future carbon emissions in the business as usual scenario, i.e., in case of continuing to produce CO_2 with today's rate (current trends), with the case of achieving the emissions' reduction goals (sustainable development scenario). [1] [2] [3] The European Commission has put forward the European Green Deal (an investment of 600 billion euros), which is a series of measures designed to reduce net greenhouse gas emissions by at least 55% by 2030 compared to 1990 levels. The target is 40% of EU's energy supply to be generated from renewable sources, which implies that the adoption of renewable fuels in industry is crucial. The Green Deal also involves achieving climate neutrality and a circular economy by 2050 (Net Zero Emissions Scenario - NZE), which would necessitate full industrial mobilization. All industrial value chains, particularly those in energy-intensive industries, must strive towards low-emission technology, as well as sustainable goods and services. [4] [5] Wind and solar power, for example, could help reduce CO_2 emissions related to electricity generation. Furthermore, carbon capture technologies could capture CO_2 emissions from industrial operations (i.e., stationary points) before they get released into the atmosphere. [1] [2]

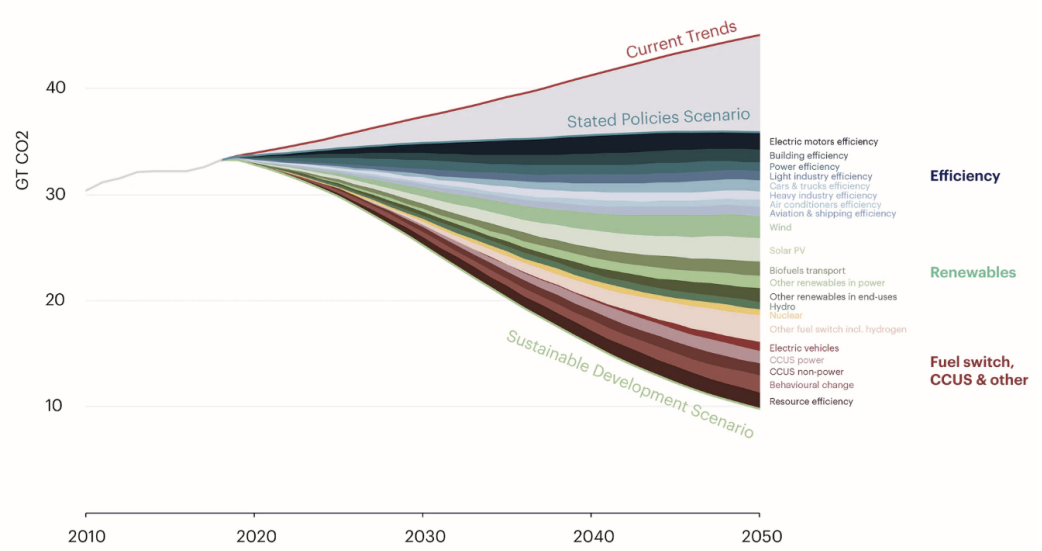

Figure 1: Carbon emissions through time and by measure of NZE in three cases: No climate policies, current policies and pledges & targets. [6]

Carbon capture technologies could be utilized to reduce the quantity of GHGs emitted into the environment, helping to alleviate the effects of climate change, while also creating new revenue streams and financial opportunities and promote sustainable development. CO_2 utilization is the process of absorbing carbon dioxide emissions and utilizing them as a feed-stock to create value-added goods. Carbon capture and storage (CCS), carbon capture and utilization (CCU), and direct air capture (DAC) are all methods that may be employed to make use of CO_2. Carbon Capture and Storage (CCS) generally consists of three steps: capture and compression of emissions from industrial operations or power plants, transport, and storage to a location, where it is injected into deep geological formations or other long-term storage facilities. One example of CCS is the Sleipner project in Norway, where the CO_2 from natural gas production is captured and injected into a saline aquifer beneath the North Sea. Since 1996, the Sleipner project has successfully stored more than 20 million tonnes of CO_2. [1] Carbon Capture and Utilization (CCU) involves capturing CO_2 emissions from stationary points i.e., chemical industry, power plants etc. and using them directly as a carbon source for the production of value-added products. The direct use of CO_2, as it appears in Figure 2, is mainly as a yield booster in various processes, as a solvent and as a heat transfer fluid. Figure 2 also shows the wide range of CO_2-derived products such as synthetic fuels like methanol, various chemicals as urea and polycarbonates, building materials like concrete and aggregates and minerals (eg. carbonates and silica). [1] [2]

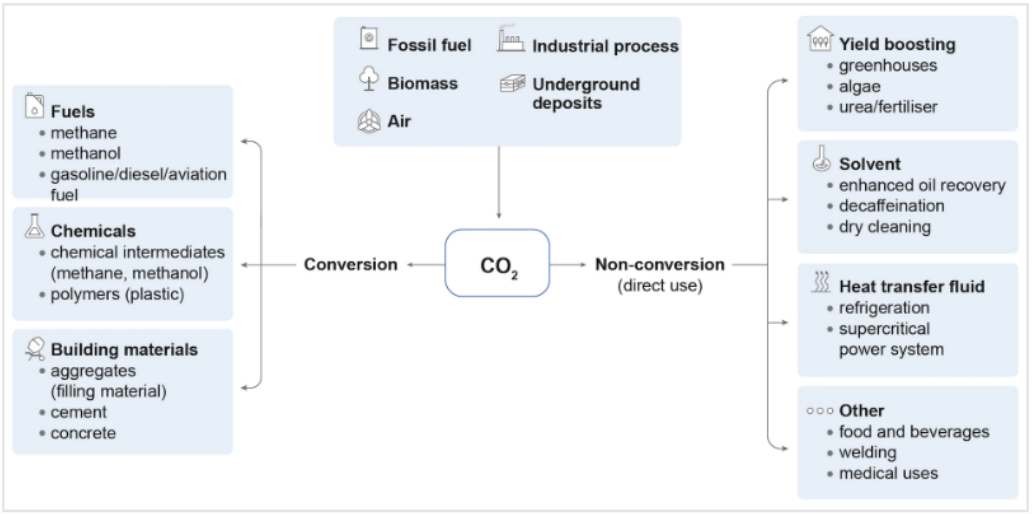

Figure 2: Simple classification of pathways for CO_2 direct use and its conversion to value-added products.

[1]

1.2 Methanol usage and production

Methanol, also known as methyl alcohol, carbinol or wood alcohol, represents one of the most important chemical raw materials. It has the chemical formula CH_3OH, a molecular weight equal to 32.042 g/mol and is often referred as MeOH. In particular, methanol is a colorless, flammable and toxic, neutral and polar liquid that is miscible with water, alcohols, esters as well as most other organic solvents, while being only slightly soluble in fat and oil. Due to its polarity, methanol dissolves many inorganic substances, especially salts. [7] [8] MeOH is readily biodegradable, meaning that it can be broken down and metabolized by microorganisms, reducing the risk of its accumulation in the atmosphere, water, or ground. In general, methanol production does not generate significant environmental problems. Residues and byproducts produced during methanol production are often utilized or processed. [8] It is the simplest aliphatic alcohol and is widely used as a feedstock, solvent, or cosolvent as a C1 building block for the production of various chemicals and materials, such as intermediates and synthetic hydrocarbons, including single-cell proteins and polymers. Most of the methanol produced worldwide is consumed in the production of formaldehyde, MTBE, and acetic acid, as well as other chemicals such as methyl and vinyl acetate, methyl methacrylate, methylamines, and fuel additives, according to the distribution in Figure 3. [7] In addition to the adhesive, paint, silicone, pharmaceuticals, wood, and automotive industries, where methanol is traditionally used, in recent years it has increasingly found application in the energy sector, as an alternative fuel or fuel additive for vehicles, boats and aircrafts. [9] In particular, in 2022 the demand for methanol as a fuel blend component (in gasoline, biodiesel and DME) reached 17 million metric tons. [10]

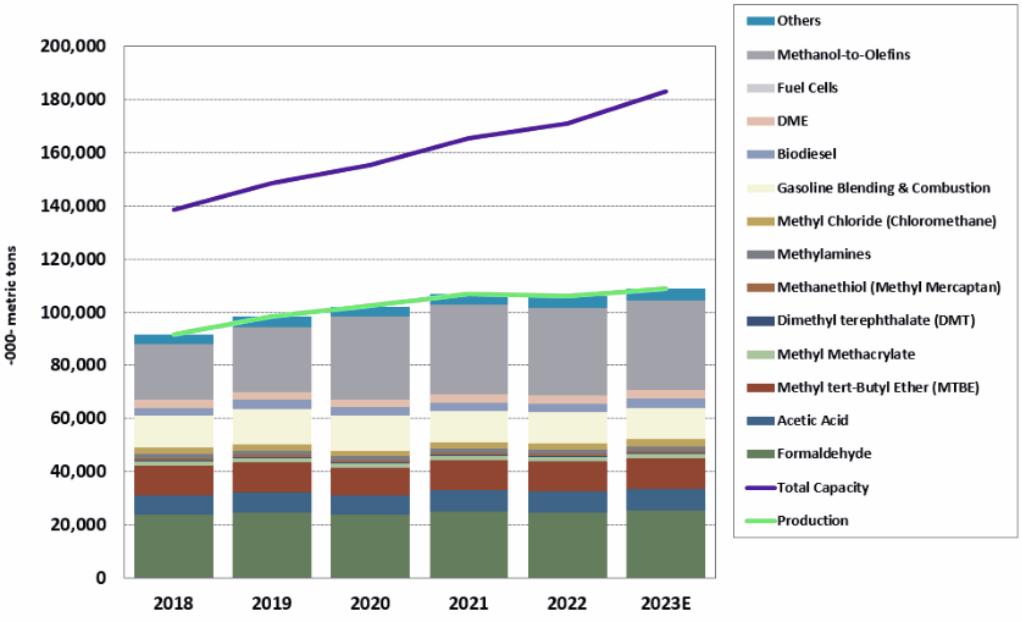

Figure 3: Global methanol demand and supply balance.
[10]

Regarding the methanol Market, over 90 methanol plants worldwide have a total output capacity of approximately 110 million metric tons (Figure 3). The Methanol Institute (MI) maintains records of more than 80 renewable methanol projects throughout the world, which are estimated to produce more than eight million metric tons of e-methanol and bio-methanol annually by 2027 (Figure 4), as it will be discussed below. [10]

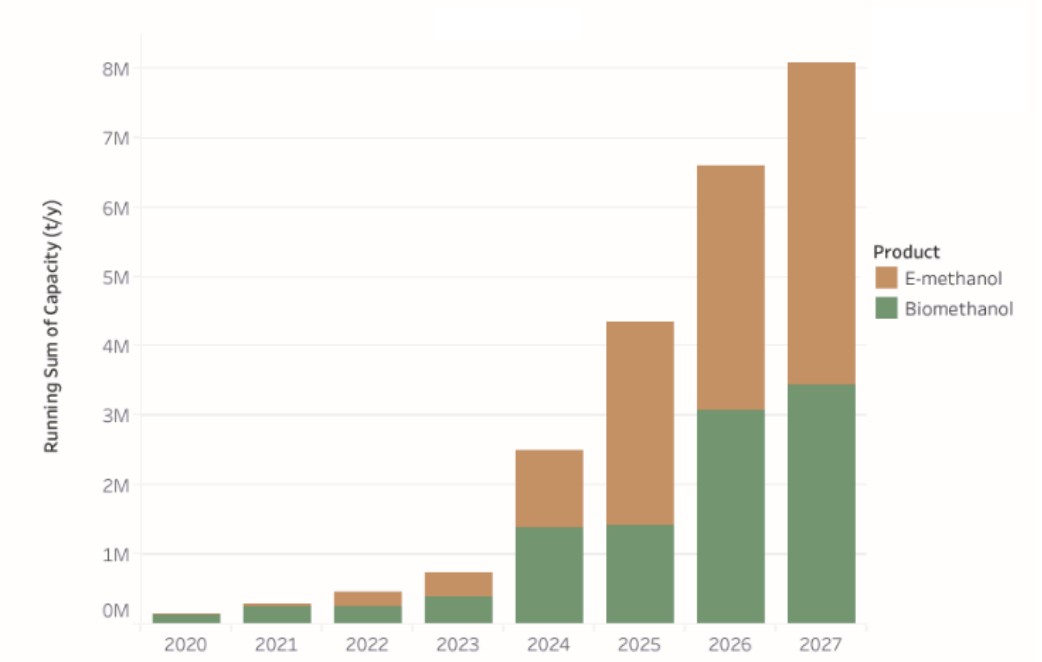

Figure 4: Projected renewable methanol production capacity. [10]

Currently, primarily driven by economic considerations, methanol production relies heavily on fossil fuels. Approximately 65% of methanol production stems from natural gas reforming (referred to as grey methanol), with the remaining 35% predominantly sourced from coal gasification (known as brown methanol). Nevertheless, methanol can also be generated from alternative carbon sources like biomass, by-product streams, or even carbon dioxide derived from various origins, including industrial emissions or DAC. Methanol derived from biomass such as biogas, forestry and agricultural waste, municipal waste and black liquor from the pulp and paper sector is typically called bio-methanol. On the other hand, when produced from carbon dioxide and green hydrogen produced using renewable energy, it is commonly referred to as "e-methanol". [11] A classification of methanol regarding its origins is presented in Figure 5. Given that methanol could be produced utilizing "green" energy and a feedstock of renewable sources as well as captured carbon dioxide, these processes could potentially result in both a closed carbon cycle and a scalability that does not truly have an upper limit. It could drastically reduce the fossil fuel carbon footprint associated with transporta-

tion due to its simplicity of synthesis and wide variety of source feedstocks. [7] Compared with gasoline, methanol creates an improved braking thermal efficiency in combustion systems and even though it emits hydrocarbons at a level comparable to gasoline, due to the way it burns and the fact that it only consists of a single carbon per molecule, it emits much less nitrogen oxide and carbonaceous particulate matter than long-chain hydrocarbons (a characteristic it shares with methane), which leads to being extremely clean burning. Furthermore, methanol has a higher octane rating than gasoline (109 compared to 80 - 98 respectively) resulting in a higher antiknock performance. [9] [12]

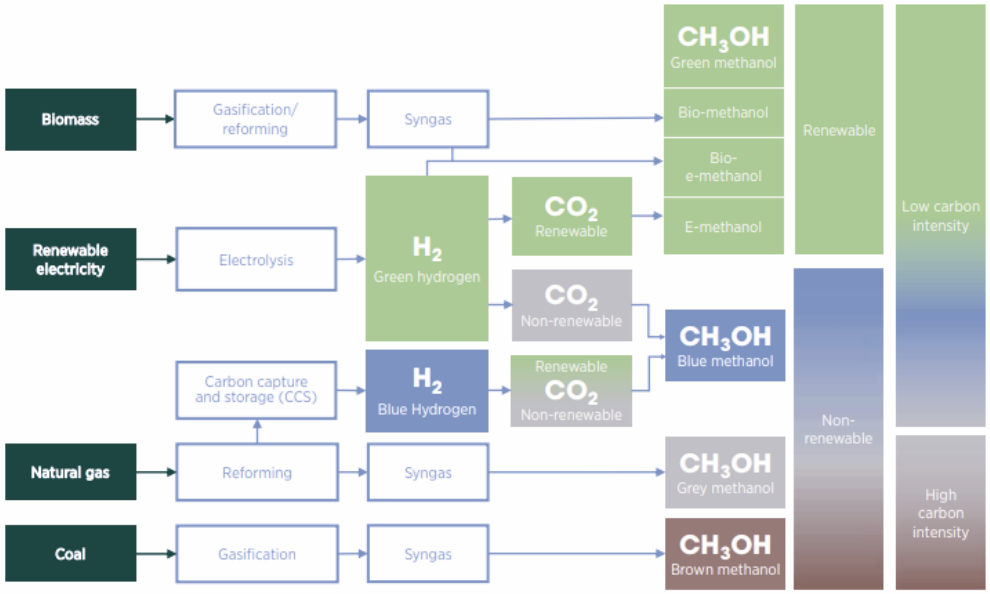

Figure 5: Proposed classification of methanol from various feedstocks. [11]

Historically, methanol production processes have existed since the 1660s. Paul Sabatier, who used metal-based catalysis to hydrogenate a wide range of functional groups, made a major contribution to its development. BASF (Germany) synthesized methanol in 1923 through a metal-based catalytic hydrogenation method at high pressure (25 - 35 MPa and a temperature of 300 - 450 °C). This technique had been the dominant technology for

almost 45 years, until the 1940s when industrially methanol production from electrolytic hydrogen and CO_2 began. Soon after, the invention of the steam methane reforming (SMR) process, which produces syngas (a combination of H_2, CO, and CO_2) using Ni-based catalysts, made it possible to produce methanol at less harsh temperatures and pressures, such as 300 °C and 100 bar. This was the primary idea behind the "ICI process" proposed in 1966. [8] [7] [13] Figure 6 illustrates the methanol production processes through the years. Some other processes that were developed for methanol production, such as the oxidation of hydrocarbons and the Fischer - Tropsch synthesis according to the Synthol process are no longer applicable, especially on an industrial scale. [7] [9] [12]

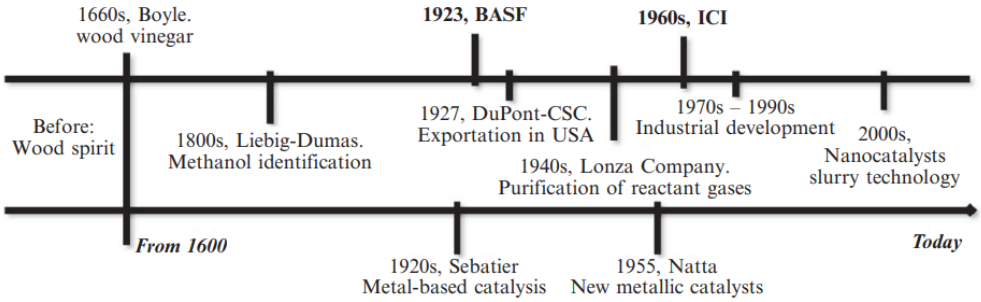

Figure 6: Methanol production milestones throughout history. [7]

The choice of the starting materials for the methanol synthesis is made considering the economy, the energy consumption (usually using the Specific Energy Input), the long-term availability as well as various environmental concerns and regulations. The most common route of the formation of methanol is from synthesis gas and the basic processes that take place are: 1) the production of synthesis gas 2) the conversion of syngas into crude methanol and 3) the purification (distillation) of crude methanol to achieve the desired purity. [7] [9] [8] [12] The two main state-of-the-art routes for methanol production from syngas are: 1) natural gas to methanol via steam methane reforming (SMR) and 2) coal to methanol via coal gasification. In SMR, steam is combined with natural gas (mainly methane) in the presence

of a catalyst, which is often a blend of copper, zinc oxide, and alumina, for them to be catalytically cracked (700 - 1000 °C and 3 - 25 bar) in the absence of oxygen (Equation 1). [7] [8] [14] In general, steam methane reforming presents numerous significant drawbacks. The process demands an abundance of superheated steam at elevated temperatures, leading to considerable operational expenses. Additionally, the process itself is highly endothermic, necessitating temperatures often exceeding 800 - 900 °C, which accelerates catalyst deactivation. To fulfill the energy requirements for the endothermic process, fuel combustion is typically employed, resulting in notable CO_2 emissions. [15] For the coal to methanol route, coal is mixed with oxygen coming from Air Separation (AS) and steam as gasifying agents and under high temperatures (400 - 1500 °C and 5 - 80 bar pressure) syngas is produced (Equation 2). Because this syngas contains low levels of hydrogen, the Water-Gas Shift reaction must take place right after (Equation 3). [7] [8] [16]

$$CH_4 + H_2O \leftrightarrow CO + 3H_2 \ \ (SMR) \tag{1}$$

$$3C + \frac{3}{2}O_2 + H_2O \leftrightarrow 2CO + H_2 + CO_2 \ \ (CG) \tag{2}$$

$$CO + H_2O \leftrightarrow CO_2 + H_2 \ \ (WGS) \tag{3}$$

An important index for the smooth operation of methanol synthesis reactor, via the syngas route, is the stoichiometric number, S, given by the ratio of the difference between hydrogen and carbon dioxide moles, and the summation of the moles of CO_2 and CO (Equation 4). [8]

$$S = \frac{[H_2] - [CO_2]}{[CO] + [CO_2]} \tag{4}$$

The stoichiometry number should have a value of 2.0. Values greater than 2.0 indicate a surplus of hydrogen, while values less than 2.0 signify a deficiency

of hydrogen in relation to the stoichiometry of the methanol reactions. When syngas is created by natural gas reforming, an S value of 2.8 - 3.0 is often obtained. The syngas to methanol route can be described by the following equilibrium reactions (Equations 5, 6, 7 and 8), which take place at a pressure of 50 - 100 bar and a temperature of 200 - 300 °C.

Hydrogenation of carbon monoxide:

$$CO + 2H_2 \leftrightarrow CH_3OH \ \ (\Delta H = 100.46 kJ/mol) \tag{5}$$

Divided into two steps:

Hydrogenation of carbon monoxide:

$$CO + H_2 \leftrightarrow CH_2O \tag{6}$$

Hydrogenation of carbon monoxide:

$$CH_2O + H_2 \leftrightarrow CH_3OH \tag{7}$$

Hydrogenation of carbon dioxide:

$$CO_2 + 3H_2 \leftrightarrow CH_3OH + H_2O \ \ (\Delta H = 61.59 kJ/mol) \tag{8}$$

In addition to the two methanol-forming reactions, the reverse water-gas shift reaction) must be considered (Equation 9).

$$CO_2 + H_2 \leftrightarrow CO + H_2O \ \ (\Delta H = 41.21 kJ/mol) \tag{9}$$

As a typical heterogeneously catalyzed reaction, the synthesis of methanol may be explained by an absorption - desorption process (Langmuir - Hinshelwood or Eley - Rideal). Currently used low-pressure catalysts consist of copper oxide and zinc oxide with one or more stabilizing additives such as alumina, chromium oxide, or mixed oxides of zinc and aluminum. Because of these catalysts' high activity, the reactions can occur at 220 - 230 °C and 50 bar, with a selectivity of 99.5%. [8] Some studies suggest even lower pressures such as 30 bar and 250 °C, using a bimetallic $Cu/ZnO/Al_2O_3$. [17] A high

dispersion of active sites supported by structural promoters is required for low-pressure methanol synthesis. Catalytic stability is important for industries. Methanol synthesis catalysts typically have a lifetime of 2 to 5 years, with the right use. Deactivation of the catalyst may happen due to overheating during operation. This thermal damage may happen after the use of recycled gas compositions that are out of the optimum range, incorrect temperature control, or overloaded catalyst in the startup phase, which results in sintering, i.e., decrease of catalyst active surface area. Furthermore, catalyst poisoning could happen because of the presence of impurities in syngas, such as chlorine- and sulfur-containing contaminants. [7] [9] [12]

Apart from the coal and natural gas to MeOH routes, there are other ways to produce syngas such as the partial oxidation of natural gas, where cracking occurs without the use of a catalyst, and the autothermal reforming (ATR) of natural gas. In addition, syngas may be produced by the dry reforming of coke oven gases (COG), a byproduct of coking plants, over an activated carbon used as catalyst. Furthermore, the gasification of biomass inside a gasifier produces gaseous products, which consist of biogas (CH_4 and CO_2), syngas (H_2, CO_2 and CO), pure hydrogen, and alkaline gases. This gaseous mixture could be considered a form of syngas but not with the quality required for methanol synthesis. [7] [8] [9] [12] Lastly, a promising synthesis route is via Dry Reforming of Methane (DMR). This method has gained interest because of its potential to utilize common low-cost natural gas or biogas, while reducing the carbon footprint. The two main greenhouse gases (CO_2 and CH_4) react at elevated temperatures (800 - 1000 °C), where CO_2 is used as oxidizing agent. The reactions that occur are Equations 10 (consisting of Equations 11 and 12), 13 and 14. [18] [19] [20] [15]

Global DMR Reaction:

$$CO_2 + CH_4 \leftrightarrow 2CO + 2H_2 \ \ (\Delta H = 247kJ/mol) \tag{10}$$

Intermediate Steps:
Methane Cracking:

$$CH_4 \leftrightarrow C + 2H_2 \ \ (\Delta H = 75.6kJ/mol) \tag{11}$$

Carbon Gasification:

$$CO_2 + C \leftrightarrow 2CO \ \ (\Delta H = 172kJ/mol) \tag{12}$$

Side Reactions:
RWGS reaction:

$$CO_2 + H_2 \leftrightarrow CO + H_2O \ \ (\Delta H = 41.2kJ/mol) \tag{13}$$

Boudouard reaction:

$$2CO \leftrightarrow CO_2 + C \ \ (\Delta H = -171kJ/mol) \tag{14}$$

This high temperature required has twofold significance: it is needed for the activation of the two gases and also reduces any catalyst deactivation issues caused by carbon deposition. That said, the greatest barrier to industrial DMR application is the lack of commercial catalysts that confer high efficiencies and are at the same time capable of operating at these temperatures, without being thermally damaged due to metal sintering. The most active elements for the DMR catalysis are reported to be nickel and noble metals (such as Pt, Ru, and Rh) when coupled with a variety of supports, including $Al_2O_3, La_2O_3, Y_2O_3, ZrO_2, TiO_2, MgO, SiO_2$, carbon, and zeolites. Noble metals have great activity and resistance to carbon and coke formation, but their high cost is the principal constraint to their industrial deployment. Nickel-based catalysts, on the other hand, are more "industrial-friendly", but deactivation concerns arise as a result of sintering and carbon deposition on Ni sites under reforming conditions. Apart from the catalysts' research, the high energy demand of the DMR process has led to research of alternative heating methods, such as the use of microwaves. [19] [20] [15]

1.3 Industry electrification - Microwave applications

The global push towards renewable energy sources (RES) to address carbon emissions, as mentioned on Section 1.1, has led to a transition from traditional fossil fuels to electricity in various sectors like transportation, heating, and industry. Wind turbines (WT) and photovoltaic panels (PV) are the RES that are predicted to see the largest growth globally. [21] [22] This transition is often mentioned as "Electrification". In the Net Zero Emissions (NZE) by 2050 Scenario, electrification is one of the key approaches for decreasing CO_2 emissions from energy, only when it is combined with electricity that originated from RES. As the utilization of electricity continues to rise, it brings additional adaptable capacity to the power grid, helping to manage the challenges associated with incorporating fluctuating renewable energy sources. [22] Share of electricity in total final energy consumption has increased at an average annual growth rate of 1.7% from 2016 to 2022, with the biggest rise (4.5%) occurring in 2020. In order to meet the NZE Scenario milestones, the percentage of electricity in total energy demand must rise by 4% every year. This means, that by 2030, 30% of the industrial sectors must be electrified. [22] Today, only 9% of the energy utilized in industry comes from renewables or biofuels, while the rest is fossil fuel based. Industry areas that require lower-temperature heat applications, such as food processing, paper manufacture, and light production, are actively adopting electrification technology. This is facilitated by the integration of industrial heat pumps and electric arc furnaces. [21] In addition, hydrogen generated through electrolysis represents an indirect mode of electrification and holds significance for certain segments of heavy industry. Although costs are anticipated to remain higher compared to direct electrification, its primary application lies in high-temperature procedures where direct electrification is not feasible. [22]

In the context of industrial electrification, chemical industry has been investigating, among others, the development of a large variety of electricity-based chemical reactors, such as electrocatalytic reactors, electrolyzers, plasma-based and microwave-assisted reactors. [23] [24] The first microwave-assisted processes were reported in 1986 and since then this technique has found application in various sectors such as food processing, polymer curing, sterilization, drying, material synthesis and chemical reactions. [15] [25] Rapid

and selective microwave heating has been shown to increase the performance of heterogeneous catalytic processes and has various advantages over conventional heating, including non-contact, fast, and selective heating, rapid heating start and stop, increased safety and ease of automation, elevated heating rates, better heating control, faster reaction rate, better product dispersion, lowered equipment size, and improved energy efficiency. [19] [15] [18] [20] Microwaves, whose wavelength ranges from 1 m to 1 mm corresponding to a frequency range of 0.3 - 300 GHz, create an alternating electromagnetic field as they pass through a material. Polar molecules try to align with the changing electric field produced by microwave radiation resulting in fast rotation in this field. When using microwave reactors, the primary effect that occurs involves thermal influences, which stem from dielectric heating. This effect arises due to the molecular dipoles endeavoring to align with the changing electric field produced by microwave radiation (Figure 7). This alignment generates friction and collisions that lead to heat generation. Consequently, heat is diffused from the molecules themselves via molecular friction and dielectric loss, leading to a more even thermal distribution. Following this, secondary thermal phenomena such as conduction, convection, or radiation might appear. However, for materials like heterogeneous catalysts (e.g., those containing metal nanoparticles on a carbon base), the generated heat can accumulate within these solids, potentially causing overheating or hotspots, which might lead to catalyst sintering and occurrence of unwanted reactions. The capacity of the catalytic material to absorb microwave energy (i.e., to get effectively heated by microwaves) is one of the fundamental determinants influencing the magnitude of these effects. As a result, it is critical to test the dielectric characteristics of catalytic materials under actual process circumstances to determine their sensitivity to microwave heating [15] [25]

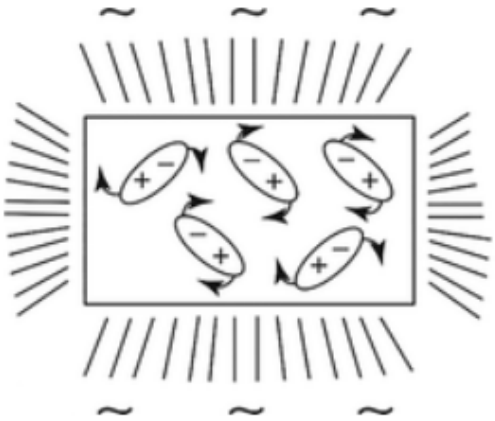

Figure 7: Depiction of thermal microwave effect where heat dissipates from the friction of molecules induced by microwave irradiation.
[15]

As mentioned in Section 1.2, DMR is a highly endothermic process, due to the high thermal stabilities of its reactants. The high energy demand of the DMR and at the same time the shift to electrification of the chemical industry, have led to research of non-conventional heating methods, such as the use of microwaves. Various studies have been conducted, some important of which are presented on Table 1.

Table 1: Catalytic performance of different catalysts recently applied in microwave-assisted dry reforming of methane (DMR).

Catalysts used	CH_4/CO_2 ratio	T (oC)	VHSV (ml/g_{cat} h)	CH_4 conversion (%)	CO_2 conversion (%)	H_2/CO ratio	References
Carbon-based catalysts							
Char	1.0/1.0	800	332	82	98	0.66	[26] [27]
Bio-char	1.0/1.0	800	1200	12	4	-	[28]
Filtracarb FY5	1.0/1.0	800	320	70	79	0.8	[28]
FY5 (Activated carbon)	1.0/1.0	700	400	96.2	97	-	[29]
FY5	1.2/1.0	800	290	60	80	-	[30]
Metal-based catalysts							
40%Ni/CeO_2	1.0/1.0	850	10,200	68	-	1.47	[31]
2%Cr-40%Ni/CeO_2	1.0/1.0	850	10,200	76	-	1.45	[31]
12%Fe/Al_2O_3-SiC	1.0/1.0	750	1200	93	92	0.98	[32]
$Ni_{0.550}Mg_{0.212}Al_{0.238}Pr_{0.0550}$	1.0/1.0	120,000	600	50	61	1.25	[33]
Mixing metal catalysts with microwave-absorbing materials							
FY5+Ni/Al_2O_3	1.0/1.0	800	1500	90	98	-	[34]
CQ+Ni/Al_2O_3	1.0/1.0	800	1500	84	92	-	[34]
Ni/FY5	1.0/1.0	800	1500	85	100	-	[34]
FY5+eFee	1.0/1.0	800	680	72	93	-	[35]
10%Ni/bio-char	1.0/1.0	800	1200	84	89	0.54	[36]
Char+Ni	1.0/1.0	975	2400	87	93	-	[37] [38]
5%Fe-C	1.0/1.0	900	7200	95	99	1.01	[39]
10%Fe-C	1.0/1.0	900	7200	98	100	1.02	[39]
Perovskite catalysts							
7Ru/$SrTiO_3$-MW-1h	45/55	500	9000	99.5	94	0.9	[20]

The synthesis, characterization, and use of ruthenium-doped $SrTiO_3$ perovskite catalysts for microwave-assisted DMR were the topic of a recent research by Gangurde et al. [20]. The catalysts were created using conventional and microwave-assisted (MW) hydrothermal techniques, with the latter achieving a quicker synthesis time and lower temperature. The 7 wt.% ruthenium-doped $SrTiO_3$ catalyst demonstrated the finest dielectric characteristics and was tested for MW-assisted DMR. The authors found that a CH_4:CO_2 vol.% feed ratio of 45:55 maximized methane conversion, attaining 99.5% and 94% CH_4 and CO_2 conversions, respectively, during a 3-hour stability test at 9000 $cm^3/g_{cat}h$ GHSV. [20] The experiments took place within a custom-designed microwave reactor system that was specially built for this purpose. A catalyst-loaded quartz tube, 290 mm in length and 8 mm in inner diameter, was introduced into the microwave reactor setup, depicted in Figure 8. To monitor temperature at specific locations, two N-type thermocouples (able to measure temperatures from -200 to +1250 °C) were strategically positioned at both the upper and lower segments of the catalyst bed. A microwave generator operating in solid-state mode (Miniflow 200 SS, 2.45 GHz) was employed to deliver microwave energy to the catalytic bed. [24] [20] A similar microwave reactor setup is presented in Figure 9. The most significant single-unit continuous wave (CW) microwave generator, known as a magnetron, has a limitation in terms of its maximum

power output: 15 kW at a frequency of 2450 MHz and 100 kW at 915 MHz. Generators operating at 2450 MHz, which have been in production for several decades (e.g., household microwave ovens), offer several advantages such as relatively high power capacity, durability, cost-effectiveness, and the compact size of MW components. Due to the high temperatures that can be reached inside the reactor, the choice of the reactor material becomes critical for successful MW operation, necessitating three key characteristics: (1) a high melting point to withstand high-temperature conditions; (2) resistance to thermal shock; and (3) transparency to microwave, meaning it shouldn't absorb or reflect microwave energy. Thus, materials like ceramics (particularly alumina-based) and aluminum oxynitride (with a melting point above 2000 °C) can be considered for constructing larger MW reactors. Although all experiments regarding the MW-assisted DMR process where conducted in a lab-scale, there have been some pilot-scale units (MW-assisted coal gasification and biomass handling) that opened the way for the development of medium-plants. [23]

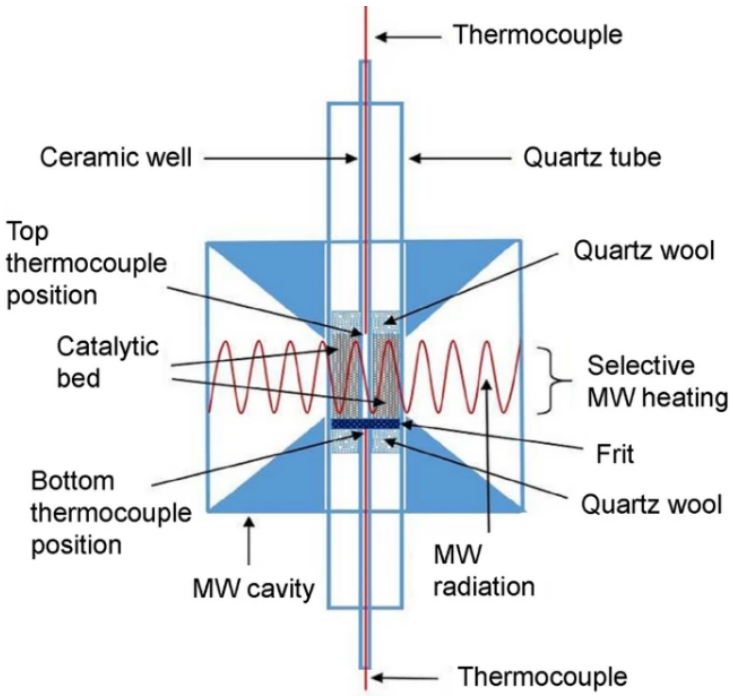

Figure 8: Schematic diagram of catalyst and thermocouple positions in the quartz tube of a lab-scale MW reactor.
[24]

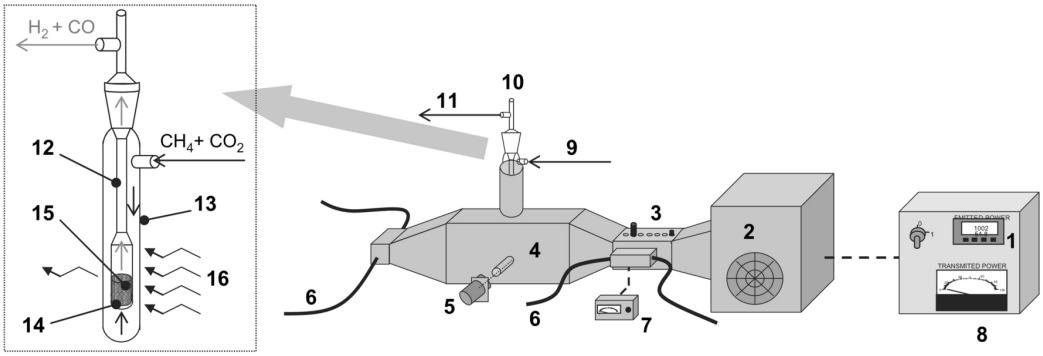

Figure 9: Schematic drawing of the single-mode MW-assisted DMR reactor. Where 1 is input power control unit, 2 is magnetron, 3 is manual two-tub unit, 4 is waveguide, 5 is optical pyrometer, 6 is water sink, 7 and 8 are reflected and transmitted power control, respectively, 9 is inflow gas line, and 10 is quartz reactor-jacket and catalyst/microwave receptor. The schematic drawing of object 10 is inserted at the left side where 11 is outflow gas line, 12 is quartz reactor, 13 is quartz jacket, 14 is porous plate, 15 is catalyst/microwave receptor bed, and 16 is microwave radiation

[28]

1.4 Biogas as an alternative fuel

Given that worldwide energy demand has grown, while conventional energy sources such as crude oil, coal and natural gas are fast decreasing, the turn to renewable sources for energy production, such as biogas, biomass, wind and solar, is crucial. Due to biogas's relatively high composition in methane (40 - 75%) [40] can be used as feedstock for syngas production in the context of power-to-chemicals [41], the global direct use of biogas was estimated to be about 45 Mtoe (million tonnes of oil equivalent). Currently, Europe and North America account for more than 60% of biogas production capacity. Europe, being the biggest biogas-producing region, has over 20,000 biogas plants, the majority of which are located in Germany. Most of them have been developed for on-site generation and co-generation of electricity, with around 500 plants completely dedicated to biogas upgrading. Both the Stated Policies Scenario (STEPS) and the Sustainable Development Scenario (SDS) anticipate a significant increase in the production of biogas for direct use, exceeding twice the current levels and reaching approximately 75 Mtoe by the year 2040. (Figure 10) The majority of this expansion arises from centralized facilities that rely on agricultural and municipal solid waste as feedstock. [6]

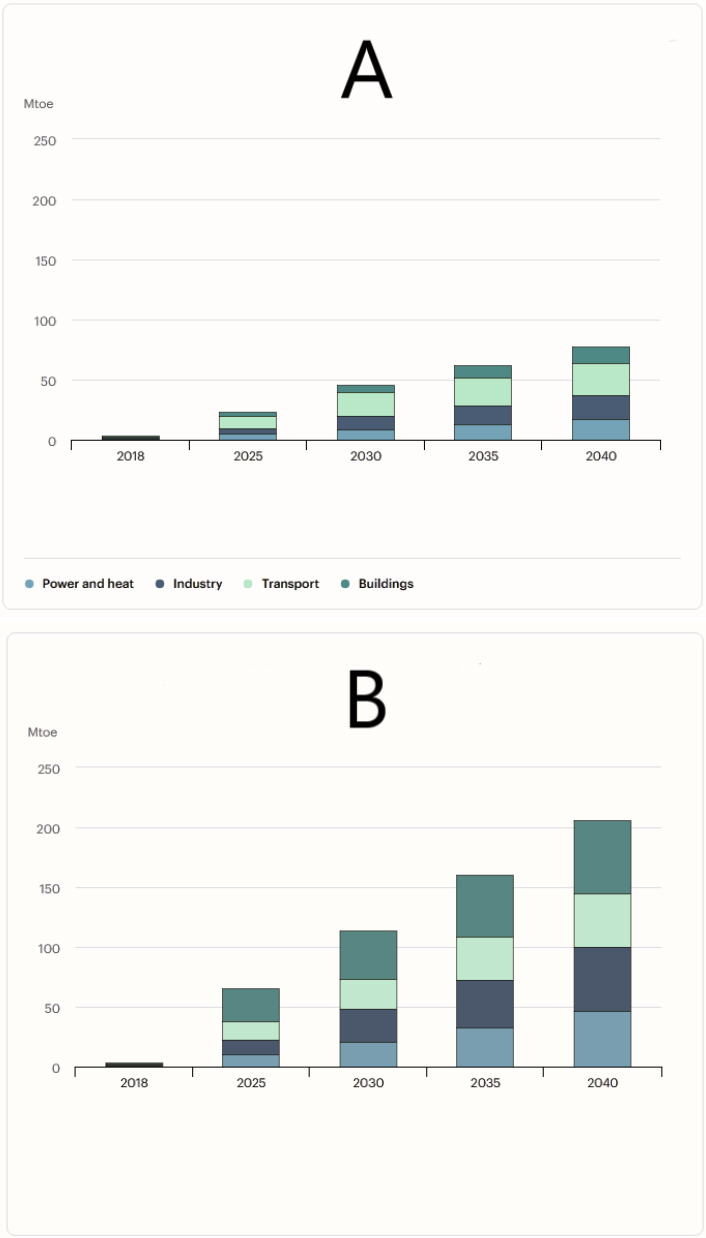

Figure 10: Global biogas demand through 2018 - 2040 by sector in the Stated Policies Scenario (A) and the Sustainable Development Scenario (B).

[6]

Biogas is a versatile and sustainable renewable energy source created by microorganisms decomposing organic materials (food wastes, cellulosic biomass, and animal waste) in the absence of oxygen, a process known as anaerobic digestion. This natural process happens in plenty of anaerobic environments, including landfills, wastewater treatment facilities, and biogas plants. Apart from methane, biogas also includes carbon dioxide and trace quantities of other gases, such as hydrogen sulfide, ammonia and water. Table 2 shows the composition ranges of plant-produced biogas, landfill gas and natural gas. [42] [40] [43]

Table 2: Composition of biogas, landfill gas and natural gas.

[40] [43]

Component	Biogas	Landfill Gas	Natural Gas
Methane (%)	40-75	35-65	87-97
Carbon dioxide (%)	25-55	15-40	0.1-1.0
Hydrogen sulfide (ppm)	50-5000	0-100	NA
Ammonia (%)	0-1	0.0005	NA
Water (%)	0-10	1-5	NA
Nitrogen (%)	0-5	15	0.2-5.5
Oxygen (%)	0-2	1	0.01-0.1
Hydrogen (%)	0-1	NA	traces-0.02

Landfill gas has various disadvantages regarding its use for industrial purposes such as large composition variations due to differences in sources of municipal solid waste, low efficiency of gas collection at landfills, fluctuating gas production leading to unstable gas supply for industrial processes and questionable long-term sustainability. [44] [45] Compared to natural gas, biogas includes a high composition of carbon dioxide. This fact makes biogas a great candidate for feedstock in Dry Methane Reforming. The only downside is that it contains certain impurities that must be eliminated, the most significant of which is the hydrogen sulfide (H_2S). (H_2S) removal is necessary to ensure the safe utilization of biogas and to prevent damage to downstream equipment and infrastructure due to the corrosion hydrogen sulfide causes to the metallic parts of engines, pipes, pumps, compressors, gas storage tanks

etc. Almost all metallic catalysts like Ni, Fe, Co catalysts and some platinum or palladium-based hydrogenation and reforming catalysts are poisoned by hydrogen sulfide. Furthermore, because it is a colorless, combustible gas with a rotten egg odor, it may be detected at low concentrations ranging from 0.0005 - 0.3 parts per million (ppm). However, in high concentrations, a person's sense of smell may be lost, posing a major risk to people's health due to mistaken assumptions that it is no longer present. Regarding human health, there is loss of smell, acute respiratory problems, eye discomfort, and loss of consciousness at concentrations of 100 - 1000 ppm, with instant mortality over 1000 ppm. Lastly, H_2S is potentially hazardous to the environment since it may be transformed to sulfuric acid, resulting in acid rain. When H_2S is emitted as a gas, it lingers in the atmosphere for an average of 18 hours before being oxidized to sulfur dioxide (SO_2) and sulfuric acid (H_2SO_4). [46] [40] [47] [43]

Therefore, there is an emerging need of biogas desulphurization in order to be utilized industrially. The permitted level of H_2S in a gas stream is determined by the end use and the applicable regional regulations. For example, pipeline gas in the United States and Denmark must have an H_2S level of 4 ppm, but reformer and fuel cell applications often demand it to be less than 1 ppm. Desulfurization procedures are essentially divided into two primary categories: physicochemical techniques and biological techniques. Furthermore, they can be classified as microbiological procedures, chemical absorption, membrane separation, cryogenic distillation, advanced oxidation processes, adsorption processes using clay materials, zeolites, metal-impregnated silica, raw and modified activated carbons, etc. (Figure 11) Biological desulfurization employs microorganisms to convert sulfur compounds into elemental sulfur, offering an environmentally friendly approach with relatively low operational costs. However, this method requires extended retention times for optimal sulfur removal and can be influenced by fluctuations in process conditions. Chemical absorption achieves high efficiency in sulfur removal and can accommodate diverse sulfur compounds and varying gas flow rates. Nonetheless, it involves chemical consumption, leading to operational expenses, and generates chemical waste that demands proper treatment. Membrane separation provides continuous sulfur removal and can handle diverse gas flow rates. Nevertheless, it requires an initial investment for membranes and associated equipment, and its efficiency might be affected by gas composition and pressure variations. Cryogenic distillation and advanced oxidation pro-

cesses have really high overall cost and therefore are not industrially-friendly. Lastly, adsorption is effective for removing even low sulfur concentrations and allows for the regeneration and reuse of adsorbents. Some of these solids have high selectivity, meaning that H_2S can be adsorbed without the simultaneous adsorption of other gases like CO_2. This is an extremely important advantage in the case of using biogas as a feedstock for DMR, given that a molar ratio of around 1:1 needs to be obtained. The only disadvantage is that solid adsorption necessitates frequent replacement or regeneration of adsorbent materials. [42] [40] [43] [47] [48] Some of the most important and efficient solids for the adsorption of hydrogen sulfide are presented in Table 3.

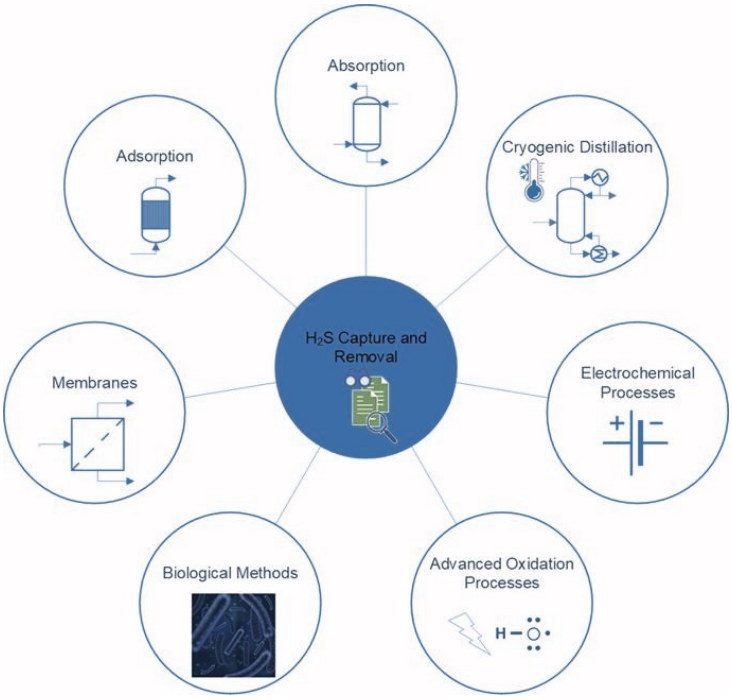

Figure 11: The main techniques for biogas desulphurization. [48]

Table 3: Adsorption capacity and removal efficiency of H_2S for various solids.

Material	Feed	Amount of H_2S in Feed	H_2S Breakthrough Concentration	Removal Efficiency	Breakthrough Capacity (mg/g)	Reference
Zeolites						
Natural zeolite	Biogas	-	-	0.94	-	[49]
5M acid treated diatomite	Biogas	-	-	-	6.87	[50]
Industrial molecular sieves (IMS)	36% CO_2, Ar and H_2S at 1 atm and 298.15 K	3000 ppm	-	equilibrium	57.7	[51]
13X Ex-Cu	Pure CO_2	1000 ppmv	0-20 ppmv	0.98	14	[52]
NaX (13X)	N2 and H_2S at 1 bar and 298.15 K	50 ppmv	2.5–5.0 ppmv	0.93	8.94E-5 – 1.84E-4	[53]
NaA	N2 and H_2S at 1 bar and 298.15 K	15 ppmv	1 ppmv	0.933333333	13.95	[54]
Fe-X	N2 and H_2S at 1 bar and 298.15 K	110–126 ppmv	5.5-6.3 ppmv	0.95	10.01	[55]
Metal Oxides						
ZnFe2O4	N2, O_2, H_2O and H_2S at ambient conditions	1000 ppm	100 ppm	0.9	1.6	[56]
Iron Oxide	Landfill gas	50 ppm	-	-	6.4	[57]
ZnO	N2, CO, H_2, CO_2, H_2O and H_2S at 673.15–873.15 K	100 ppmv	20 ppmv	0.8	673	[58]
DMO-5	N2, CO, H_2, CO_2, and H_2S at 823.15 K	2000 ppmv	100 ppmv	0.95	250	[56]
AMDS	N2 and H_2S at 1 bar and 298.15 K	110–126 ppmv	5.5–6.3 ppmv	0.95	8361	[57]
Carbon-based Sorbents						
GAC	CH_4, CO_2, O_2, and H_2S at 293.15–298.15 K	932–2350 ppm	100 ppm	0.952380952	615–1293	[59]
ZnAc2–CAC	N2 and H_2S at ambient temperature	5000 ppmv	5–10 ppmv	0.999	2.37	[60]
AC	N2, O_2, H_2O and H_2S at 303.15 K	850 mg/m^3	0.1 ppmv (0.15 mg/m^3)	0.999823529	3.4	[61]
Zn/AC	N2, O_2, H_2O and H_2S at 303.15 K	850 mg/m^3	0.1 ppmv (0.15 mg/m^3)	0.999823529	38.5	[61]
Mg0.2Zn0.8/AC	N2, O_2, H_2O and H_2S at 303.15 K	850 mg/m^3	0.1 ppmv (0.15 mg/m^3)	0.999823529	113.4	[61]
Mg/AC	N2, O_2, H_2O and H_2S at 303.15 K	850 mg/m^3	0.1 ppmv (0.15 mg/m^3)	0.999823529	32.7	[61]
BAX (wood-based AC)	N2, O_2, H_2O and H_2S at ambient conditions	1000 ppm	100 ppm	0.9	5.6	[61]
10 wt% ZnFe2O4/BAX	N2, O_2, H_2O and H_2S at ambient conditions	1000 ppm	100 ppm	0.9	122.5	[61]
CaCO3/CH, CaO/CH	N2, O_2, and H_2S at 303.15 K	1000 ppmv	50 ppmv	0.95	<100-9100	[62]
PC, NC, NPC	N2, O_2, H_2O and H_2S at 303.15 K	1000 ppmv	50 ppmv	0.95	12.5-426.2	[63]
NMCS-0–5	N2, O_2, H_2O and H_2S at ambient conditions	1000 ppm	250 ppm	0.75	48	[64]
N-PCNF-1/2–800-40%	N2, O_2, H_2O and H_2S at 1 atm and 298.15 K	1000 ppm	50 ppm	0.95	3340	[65]
AGA	N2, O_2, and H_2S at 303.15 K	1000 ppmv	50 ppm	0.95	3190	[66]
Metal Organic Frameworks and Porous Organic Polymers						
CuBTC	N2 and H_2S at 1 bar and 298.15 K	99.6 ppm	5 ppmv	0.949799197	17.1–56.3	[67]
Cu(BDC)0.5(BDC-NH_2)0.5	N2 and H_2S at 298.15 K	500 ppm	50 ppm	0.9	128.4	[68]
ED-ZIF-8 1st	CH_4, CO_2, H_2S, and He at 2 bar and 298.15 K	3 vol%	1500 ppmv	0.95	3299	[69]
MOF-199 (CuBTC)	N2 and H_2S at 1 bar and 298 K	10 ppmv	1 ppmv	0.9	40	[70]
MOF-5	N2 and H_2S at 1 bar and 298 K	10 ppmv	1 ppmv	0.9	1.2	[70]
UiO-66-NH_2	N2 and H_2S at 1 bar and 298 K	10 ppmv	1 ppmv	0.9	0.04	[70]
CBAP-1-EDA	N2 and H_2S at 1 bar and 298 K	10 ppmv	1 ppmv	0.9	0.033	[70]
CBAP-1-DETA	N2 and H_2S at 1 bar and 298 K	10 ppmv	1 ppmv	0.9	0.026	[70]
Composite Materials						
SBA-15-PEI-25	N2, O_2, and H_2S at 298.15 K	1000 ppm	50 ppm	0.95	26.58	[71]
HKUST-1/GO-PEI	N2 and H_2S at 1 bar and 298.15 K	99.6 ppm	5 ppmv	0.949799197	30.67–55.55	[67]
CuO/SiO_2	N2 and H_2S at 1 bar and 423.15 K	100 ppm	5 ppm	0.95	32–363	[72]
CuO/SiO_2	N2 and H_2S at 303.15 K	850 mg/m^3	0.15 mg/m^3	0.999823529	145.6	[73]
ZnO/SiO_2	N2 and H_2S at 303.15 K	850 mg/m^3	0.15 mg/m^3	0.999823529	28.6–108.9	[73]
Co_3O_4/SiO_2	N2 and H_2S at 303.15 K	850 mg/m^3	0.15 mg/m^3	0.999823529	114.3	[73]
20 wt% ZnO/MCM-41	N2, H_2O, and H_2S at 298.15 K	500 mg/m^3	1.5 mg/m^3	0.997	54.9	[74]
20 wt% ZnO/SBA-15	N2, H_2O, and H_2S at 298.15 K	500 mg/m^3	1.5 mg/m^3	0.997	41	[74]
30 wt% ZnO/MCM-48	N2, H_2O, and H_2S at 298.15 K	500 mg/m^3	1.5 mg/m^3	0.997	53.2	[74]
Waste-based Adsorbents						
Halloyfill (halloysite based adsorbent)	-	-	-	0.99	21.3	[75]
Fly Ash	H_2S in air at 1 bar and 298.15 K	750 ppm	-	-	12.6-15.9	[76]
Biochar	H_2S in air at 1 bar and 298.15 K	50 ppm	-	-	382	[77]
Iron-modified bentonite	Outlet gases of refinery	-	-	-	32.3	[78]

1.5 Concept description and Main scope

In this work a DMR-MEOH plant producing around 100 ktonnes/year of methanol (99.5% purity) was developed in Aspen Plus V11. In this unit, the first subunit was a Dry Methane Reformer that produced syngas. This syngas, after reaching the desired conditions and composition with the addition of hydrogen (derived from electrolysis), was inserted in the CO/CO_2 hydrogenation reactor. The methanol that was produced from the latter was purified by removing any impurities in a distillation column. Three case studies were investigated regarding the feedstock as well as the heating utility of the DMR reactor. Firstly, a scenario of a pure feed of methane and carbon dioxide (captured) with conventional reactor heating (fossil fuels) was set as a base. Then, in the context of the Electrification of the Chemical Industry, a scenario of Microwave-assisted reactor was developed. Lastly, in an effort to replace fossil fuels with renewable materials, biogas was considered as a feed for the MW-assisted catalytic DMR reactor. Due to the high H_2S composition of biogas, a desulfurization system was placed before the DMR reactor. The methanol production and purification processes were kept the same in all three case studies.
The main goals of this work were:

- Detailed modeling of all the processes in Aspen Plus V11 software, based on literature data.
- Optimization of the developed synthesis setup and applied process conditions.
- Design of a Heat Exchanger Network by application of pinch analysis.
- Implementation of an economic study and investigation of the viability of the plant under current market conditions. Conduction of a series of sensitivity analyses to understand the barriers of viability.
- Configuration of a preliminary greenhouse gases' emissions estimation.
- Overall comparison, regarding the energy demand, the total cost, and the environmental impact, between the three scenarios, as well as some state-of-the-art processes for methanol production, retrieved from the literature.

Chapter 2

Method

2.1 Model description

This work focuses on the development and determination of a methanol production unit with a capacity of around 100 ktonnes/year of methanol (99.5% purity). Three case studies were developed regarding the syngas production: DMR with conventional heating and a pure feed of CO_2 and CH_4 (base case), DMR with microwave heating and a pure feed of CO_2 and CH_4 and lastly DMR with microwave heating and biogas feed. In all three cases the methanol production and purification steps are exactly the same, while the difference arises in the syngas production step. These abovementioned processes were designed using the software Aspen Plus V11. In order to minimize the total cost (materials, utilities, etc) these processes were optimized regarding the conditions (pressure & temperature), the recycle and purge of streams, and the total energy demand (heat integration). Furthermore, an economic analysis was performed for each case study, as well as a sensitivity analysis regarding the prices of electricity and hydrogen in order to investigate the feasibility and viability of the unit. The three case studies were compared. A comparison was also conducted between these scenarios and some state-of-the-art processes for methanol production, such as natural gas-to-methanol, coal-to-methanol and biomass-to-methanol.

2.1.1 Case study 1: Conventional DMR with pure feed

For the first case study a dry methane reforming unit was developed in Aspen Plus. The thermodynamic model that was chosen was the cubic equation of state Peng-Robinson, given that it generates accurate results for light gases even in high temperatures and pressures and that there are no polar mixtures in the processes. The feed consisted of pure CO_2:CH_4 55:45 molar ratio [20] at 20 °C and a pressure of 1 bar. This feed was preheated to 500 °C and then inserted to the DMR reactor. The reactor was simulated using the RGibbs unit in Aspen Plus. The desired conversion was 99.5% of methane. The pressure was kept at 1 bar (most usual pressure for DMR [79]) and in order to find the temperature that produce this conversion a sensitivity analysis was conducted. As it appears on Figure 25 (Appendix) the temperature must be 900 °C. Bimetallic and monometallic (Ni) catalysts are preferred compared to noble metals due to their low-cost. An appropriate catalyst for these conditions is Ni on Al_2O_3. [79]

2.1.2 Case study 2: MW-assisted DMR with pure feed

For the second scenario, Gangurde's et al. research was used as a literature base [20]. The feed consisted of pure CO_2:CH_4 55:45 molar ratio [20] with a temperature of 20 °C and a pressure of 1 bar, just like in the first case study. Reactor's conditions were 1 bar and 500 °C resulting to 99.5% conversion of CH_4. Before entering the reactor, the feed was preheated at 500 °C. The catalyst used for this process (ruthenium-doped $SrTiO_3$ perovskite) was synthesized by Gangurde et al. Due to the utilization of microwaves for this synthesis a better distribution of the active sites was achieved. That fact, in combination with the thermal microwave effect where heat dissipates from the friction of molecules induced by microwave irradiation (as mentioned on Section 1.3) result in lower energy demand in comparison with conventional heating of the DMR reactor. The efficiency of the microwaves was considered 90%.

2.1.3 Case study 3: MW-assisted DMR with biogas feed

For the last case study, the DMR process was kept the same as on the second scenario. However, the feed changed using biogas instead of pure methane - carbon dioxide mixture. The composition of the biogas was assumed to be 60% CH_4 and 40% CO_2 with 2000 ppm H_2S, while the temperature and pressure were 20 °C and 1 bar respectively. Due to the need of desulfurization, as discussed on Section 1.4, a pretreatment of the biogas was needed before its entrance to the DMR reactor. The technique that was chosen was the one of solid adsorption (for the reasons mentioned on 1.4), using as adsorbent dried sewage sludge, because of its selectivity to H_2S (CO_2 should not be removed given that it is needed for the DMR reaction) and its low cost. [80] The desulfurization system was assumed to be consisted of 5 adsorption columns and 1 regeneration column, in order to be able to consider continuous flow. Knowing that the regeneration efficiency decreases 2.6% on average in each regeneration cycle, and assuming 14 regeneration cycles before reloading the bed with fresh adsorbent, the lifetime of the adsorbent is estimated to be 118 days. Finally, the amount of adsorbent needed (for this study's capacity) is 122 tonnes per year. The pressure drop across the adsorption beds is very low (only about 14 Pa), resulting to a non significant power consumption. The adsorption beds operate at 20-25 °C and 1 bar. [80] Consequently, the energy demand of the desulfurization columns was assumed to be zero. Regarding the regeneration column, it operates at high temperature and atmospheric pressure, leading to 2.4 ktonnes of high pressure steam demand per year. This desulfurization system has an efficiency of 90%, meaning that the biogas produced contains 200 ppm H_2S, [80] which is acceptable for this specific study. The fixed beds were simulated on Aspen Plus using a Component Separator. Due to the really low concentration of hydrogen sulfide, it was considered as non present in the next processes. The regeneration unit was not simulated for simplicity reasons, given that it did not interfere with the rest processes.

2.1.4 Methanol synthesis and purification

Regarding the methanol production these conditions were chosen: a stoichiometric number of 2.5, a pressure of 35 bar and a temperature of 230 °C. [9] [17] The effect of pressure and the effect of temperature on the CO conversion were examined using Aspen Plus, i.e. an RGibbs reactor, and are presented on Figure 26 and Figure 27 (Appendix) respectively. Although a lower pressure and temperature of the chosen appear to result in higher CO conversion, based on thermodynamics, no research has shown the same results yet, given that the reactions discussed in Section 1.2 cannot occur in such low temperature and pressure. In order to reach a stoichiometric number of 2.5, hydrogen needs to be added (the design specs tool of Aspen Plus was used). The mixture was compressed using a multi-compression system created by combining five compressors in series, with each compressor capable of increasing the pressure by around three times. In addition, an efficiency of 85% was considered for each compressor. Due to the need of keeping the temperature relatively low, inside the compressors a heat exchanger was added before each compressor that kept the temperature at 170 °C. The unit that was used to simulate the CO and CO_2 hydrogenation reactor in Aspen Plus was the RYield one. The reactions used were 5, 8 and 9 and the conditions the ones discussed above. The CO and CO_2 hydrogenation reactions have low conversions, as discussed before, resulting in a high concentration of reactants in the outlet. In order to reduce the waste/emissions as well as the supply of raw materials, a recycle of these reactants is necessary. Firstly, methanol and water need to be separated from the mixture so that methanol can be obtained. A Flash separator was used in Aspen Plus and the aim was to reclaim all of the produced methanol, at the bottom of the Flash. The pressure was kept at 35 bar so that no further compression would be needed (extra cost). The effect of the temperature on the methanol and water reclaim as well as the impurities at the bottom were produced via sensitivity analysis in Aspen Plus and the results are shown on Figure 28. The chosen temperature was 3 °C. Ideally, the top stream would be recycled completely, but because of the existence of methane, which does not react in the methanol synthesis reactor, a total recycle of the stream would result to methane accumulation problems. Consequently, a purge stream was inserted via a separator. The lowest purge stream fraction (of the total flash's top stream) achieved was 0.07. Anything lower than that could not be calculated in Aspen Plus due to the methane accumulation. The bottom of the Flash was directed to a

distillation column in order to obtain as a final product methanol of purity 99.5%. Before entering the column, the stream was preheated at 50 °C and a turbine was used in order to lower the pressure to 1 bar. A step-wise sensitivity analysis was conducted aiming to maximize the methanol purity and reclaim in relation to the number of stages, the reflux ratio as well as the distillate molar vapor fraction. Firstly, a distillate molar vapor fraction of 0.1 an a reflux ratio of 1.6 were chosen and a sensitivity analysis regarding the number of stages was carried out. As presented in Figure 29 (Appendix) after the eleven stages a plateau appears and there is no change in methanol reclaim (95.3%) nor its purity (99.5%). Following this, a sensitivity analysis for the effect of reflux ratio was studied, by keeping the number of stages at 11 and the distillate molar vapor fraction at 0.1. As it appears in Figure 30 (Appendix) the methanol purity and reclaim is not affected significantly, while the reboiler and condenser duty increases with reflux ratio's increase. A purity of exactly 99.5%, which is desired, is obtained with a reflux ratio of 1.6. Lastly, the distillate molar vapor fraction's effect was investigated for 11 stages and 1.6 reflux ratio. As showed in Figure 31 (Appendix) any value lower than 0.1 is not in agreement with the desired purity. All in all the characteristics of the distillation column are presented in Table 4. For all the case studies it is assumed that the compressors and the turbine have an efficiency of 85%.

Table 4: The distillation column's characteristics for the production of high purity (99.5%) methanol.

Item	Assumption/Value
number of stages	11
feed stage	5
type of condenser	partial vapor liquid
type of reboiler	Kettle
reflux ratio (molar)	1.6
molar vapor fraction	0.1
reflux rate	583 kmol/h
heat duty	11.8 MW

Two indicators used for the technical evaluation of the projectwhere F_{MeOH} is the the annual methanol production (ktonnes/year) and F_{feed} is the total

mass flow per year of the materials in the process feed (carbon dioxide, methane, hydrogen for the first two case studies and biogas and hydrogen for the third). In addition, the Specific Energy Input (SEI), that shows the energy demand per kg of methanol produced, was calculated using Equation 19, where Q is the total energy demand of the unit (MW) and F'$_{MeOH}$ is the flow of the final product (kg/s). SEI is a very important indicator because of its ability to make of a fair comparison between different methods. Lastly, considering that green electricity was used, the energy share of RES can be determined (the energy demand refers to the heat duty needed).

$$Yield\% = \frac{F_{MeOH}}{F_{feed}} * 100\% \tag{15}$$

$$SEI = \frac{Q}{F'_{MeOH}} \ [MJ/kg_{MeOH}] \tag{16}$$

The process flow diagrams (PFD) (one for each case study) are illustrated in Figure 12, Figure 13 and Figure 14.

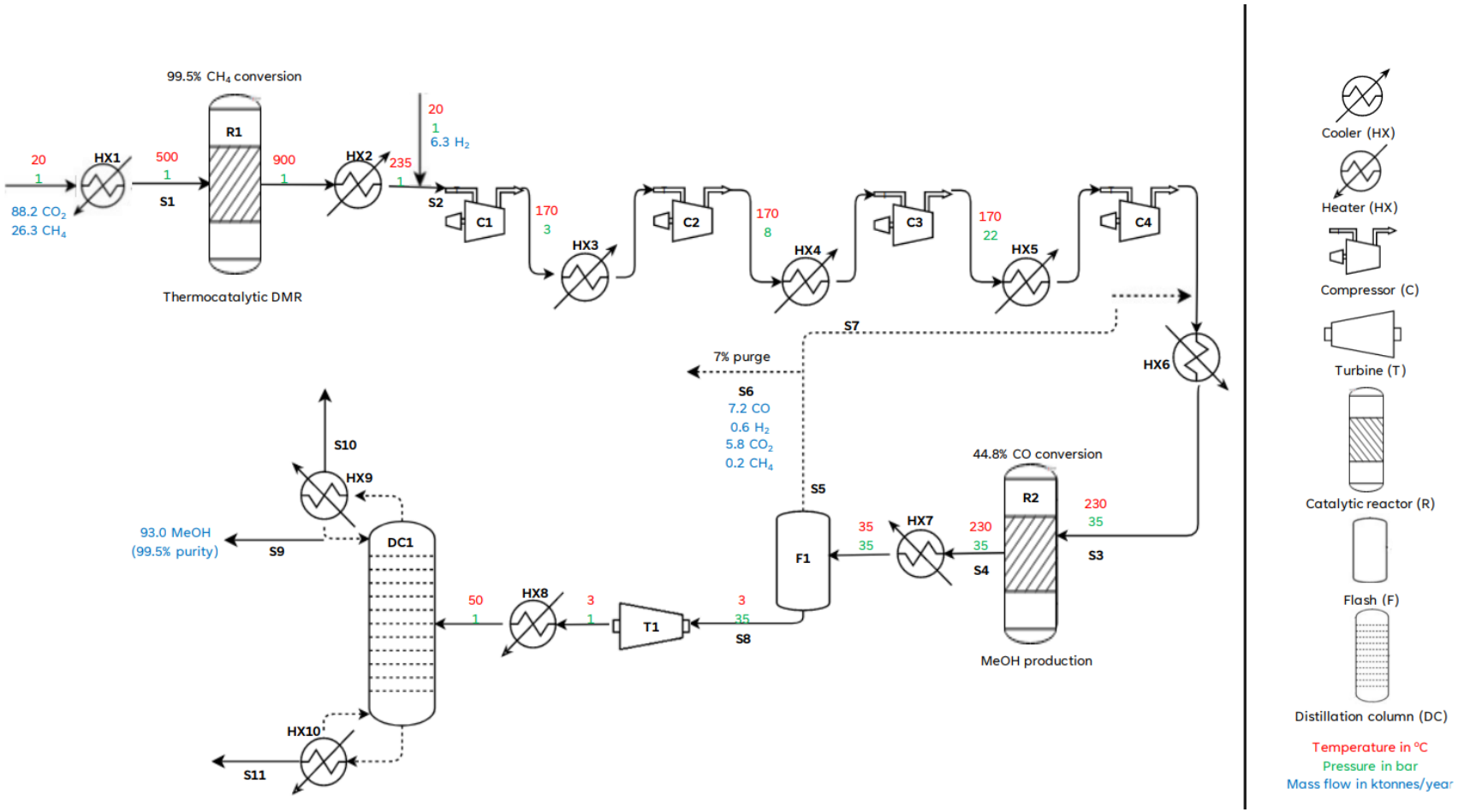

Figure 12: Process Flow Diagram for Case Study 1: Conventional DMR heating with pure feed.

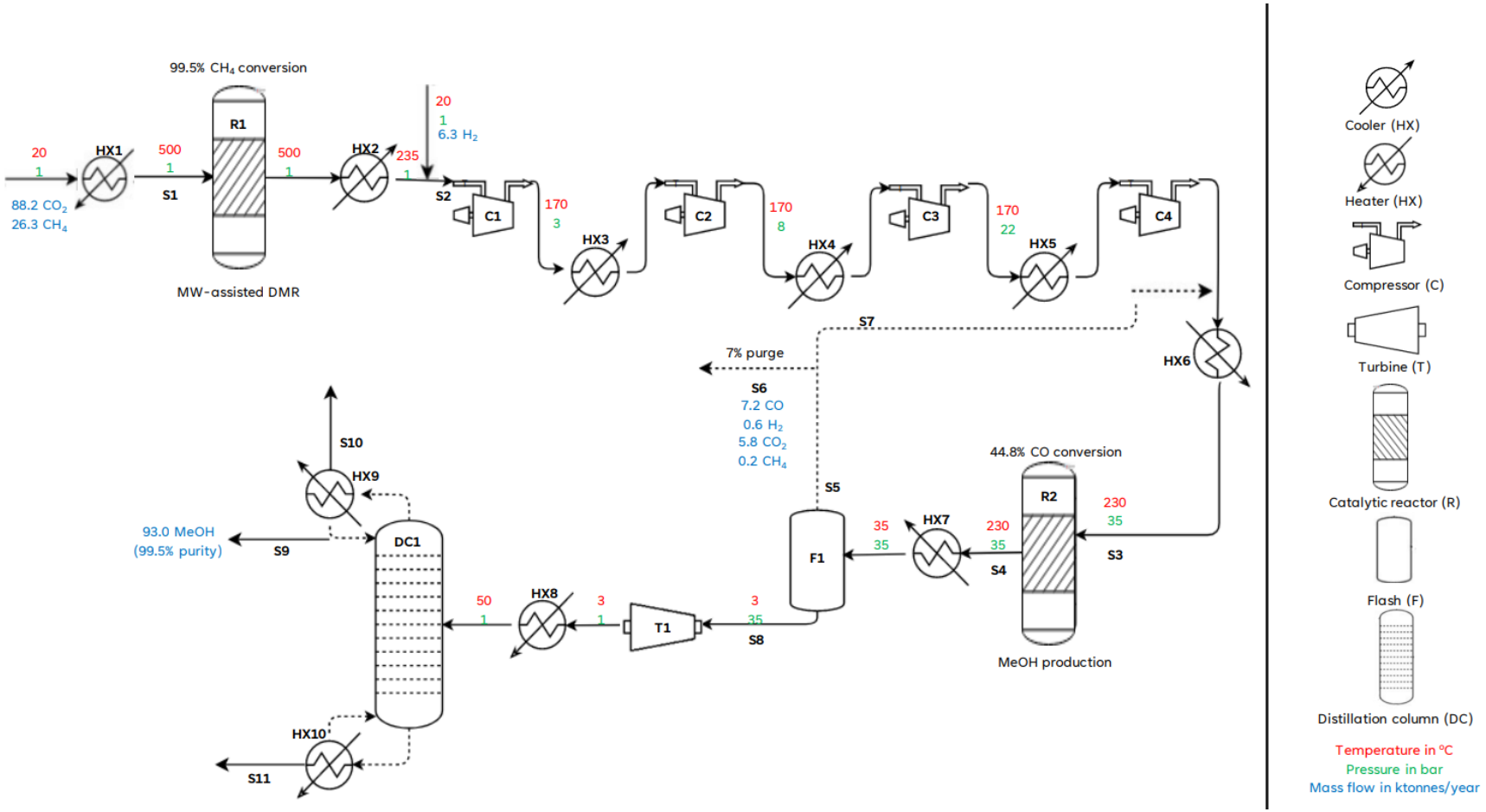

Figure 13: Process Flow Diagram for Case Study 2: Microwave assisted DMR with pure feed.

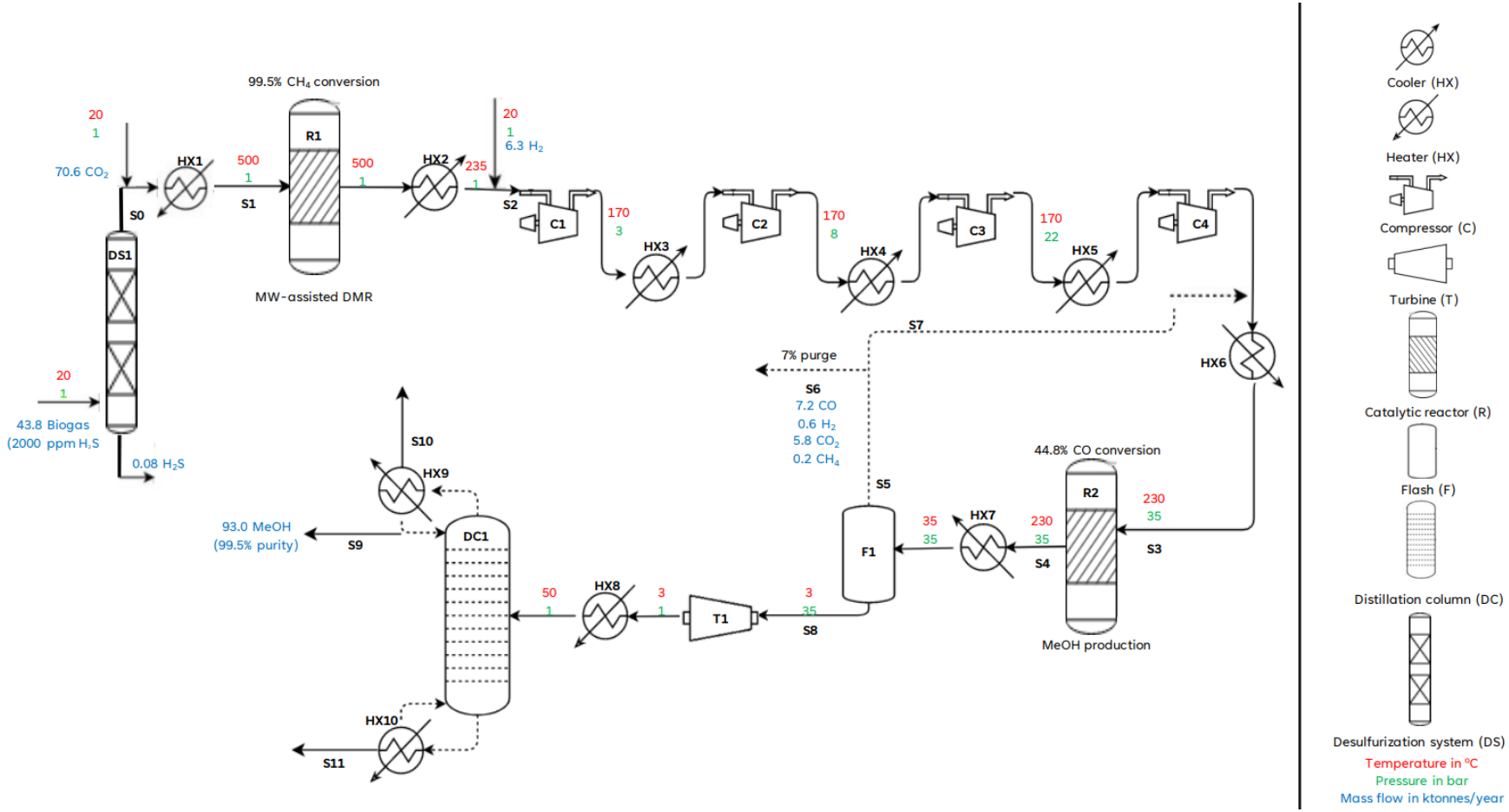

Figure 14: Process Flow Diagram for Case Study 3: Microwave assisted DMR with biogas feed.

2.2 Heat integration

In the process industries, several types of heat transfer equipment are employed. The shell-and-tube heat exchanger is by far the most common kind. This form of heat exchanger, as the name indicates, is made up of a shell (a huge pressure vessel) with a bundle of tubes inside it. To transfer heat between the two fluids, one fluid flows through the tubes and another fluid flows over the tubes (via the shell), as illustrated in Figure 15. Heat integration is the merging of process streams' heating and cooling demands, in heat exchangers, to eliminate the need for external heating and cooling in the form of hot and cold utilities. In systems comprising numerous heat or mass exchange components, known as exchanger networks, there's a specific point within the system where the driving force for energy or mass exchange reaches its lowest level. This point is referred to as a "pinch" or pinch point. The effective synthesis of these networks entails entails identifying the pinch point and utilizing the information at the pinch point to build the whole network. This design method is known as "pinch technology". [81] [82] In order to find the minimum utilities required the following algorithm is employed:

1. Select a minimum approach temperature (ΔT_{min}). This is the lowest temperature difference between two streams leaving or entering a heat exchanger. Typical temperatures range from 5 °C to 20 °C. For this study, the temperature is set at 10°C, with an awareness that alternative temperature methods will provide different outcomes.

2. Construction of a temperature interval diagram.

3. Construction of a cascade diagram and determination of the minimum utility requirements, as well as the pinch temperatures.

4. Determination of the minimum number of heat exchangers above and below the pinch.

5. Synthesis of the heat-exchanger network. [82]

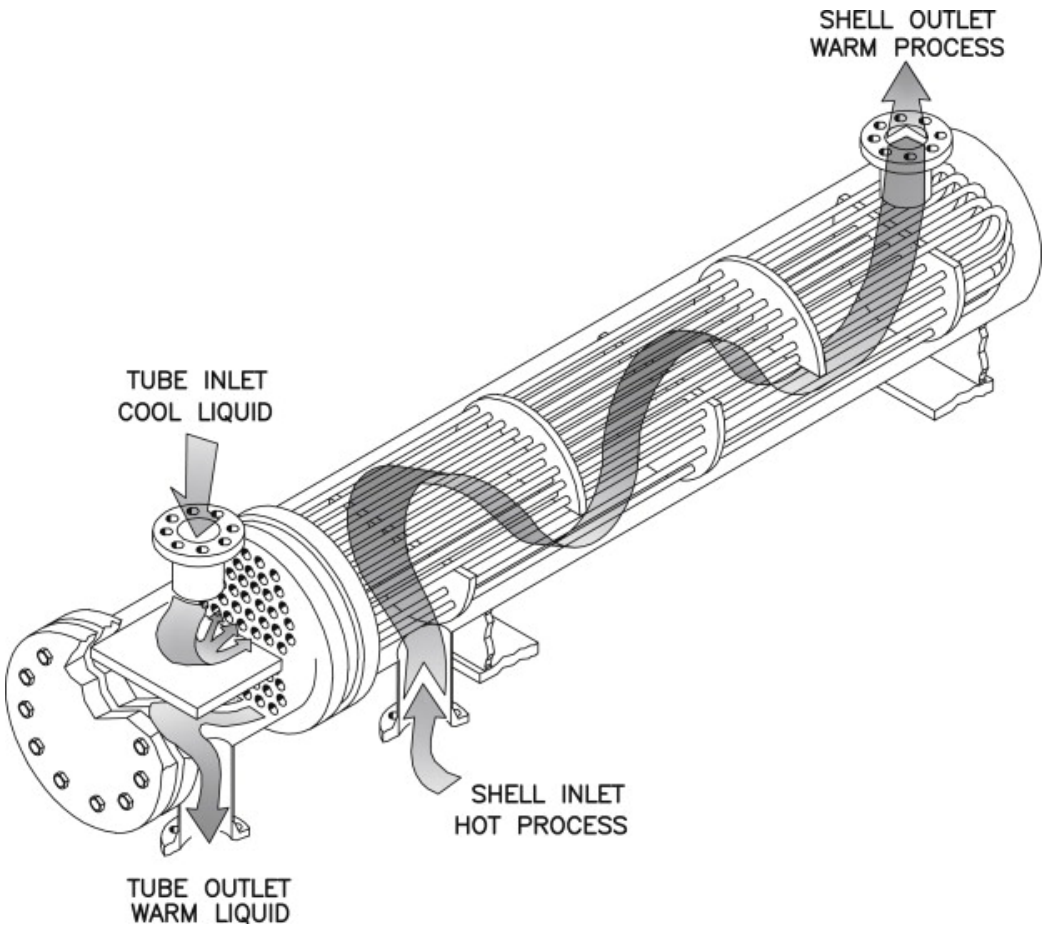

Figure 15: Internal view of a shell and tube exchanger.

In order to develop the heat-exchanger network (HEN) some necessary rules need to be employed:

1. Start at the pinch. The most restrictions regarding the number of feasible matches appear at the pinch point, where (ΔT_{min})exists between all hot and cold streams. By starting the design at the pinch, problems such as the use of temperature differences smaller than (ΔT_{min}) or excessive use of utilities, are avoided.

2. Heat capacity (CP) inequalities. Moving away from the pinch, temperature differences must increase. For that to be achieved two inequalities need to exist: Above the pinch, the CP of the cold stream must be bigger that the CP of the matched hot stream, while below the pinch the exact opposite must happen.

3. Threshold problems. In case that there is is no pinch point, the hot and cold streams' conditions are such that after cascading energy downward, there is either an excess of energy or the energy is perfectly balanced at every temperature interval. [82]

The utility requirements both in enthalpy and temperature terms can be obtained from the grand composite curve (GCC). The GCC shows the heat flow through the process against temperature (shifted and not actual - cold streams are represented $\Delta T_{min}/2$ times hotter and hot streams $\Delta T_{min}/2$ times colder than they are in practice).

Although the HEN lowers the total utility demand (reducing the operational cost), a supply of more heat exchangers is required (augmentation of capital cost). At the same time, the surface needed in the rest of the heat exchangers of the unit (that are relevant to the streams used in heat integration) drops, leading to reduction of capital cost. The heat transfer surface can be calculated approximately by using Equation 17, where A is the heat transfer area (m^2), Q is the heat duty (W), U is the heat transfer coefficient (W/m^2K) and ΔT_m is the logarithmic temperature difference. [82]

$$A = \frac{Q}{U * \Delta T_m} \tag{17}$$

Some typical values of the U are presented in Table 6. For this study, the reactors were not taken into account for the Heat Integration, given that for the DMR reactor, the heating takes place either by the use of furnace (CS1) or electricity (CS2). Regarding the MeOH synthesis reactor, the reaction is exothermic and the reactor isothermal, meaning that the cost of cold utility needed would be considerably low. Lastly, the reboiler of the distillation column was not considered for the HI. In Figure 32, Figure 33 and Figure 34 (Appendix) the Hot and Cold Composite Curve (CC), the Grand Composite

Curve (GCC), as well as the Grid Diagram (GD) for case study 1, 2 and 3 are presented, respectively. In Table 5 the pinch points, as well as the minimum hot and cold utilities needed, as resulted from the HI, for all case studies.

Table 5: The pinch points and the minimum hot and cold utilities needed, as resulted from the HI, for the three case studied.

	CS 1	CS 2	CS 3
pinch point (°C)	none	490	490
minimum hot utility (kW)	0	108	108
minimum cold utility (kW)	22,091	19,368	19,228

Table 6: Approximate values of heat transfer coefficient.

[83]

Conditions of heat transfer	U (W/m^2K)
gas/gas	5-50
gas/liquid	6-80
water/organic liquid	100-300
steam/organic liquid	200-1,200
water/water	1,000-4,000
steam/water	1,000-10,000

2.3 Economic analysis

The viable development of a chemical process unit is based on its ability to produce revenue. Consequently, the understanding of process economics is rather crucial. The three main goals are: to evaluate the design options and make the right decisions, to optimize the processes and to examine the overall project profitability. The total cost of a unit can be broken down into two main categories: the capital cost and the operational cost. [81] [82] In order to estimate these costs, a standardized cost estimation methodology for new technologies is applied. The methodology employs the factorial approach, in which costs are calculated using factors and percentages based on the cost of purchased equipment. The chosen approach relies on a comprehensive examination of existing literature concerning techniques and relevant data. The calculated estimations have a theoretical accuracy of ± 30%. [84] More specifically the results of the simulations were processed in MS Excel environment, by employing empirical equations, prices, assumptions and economic indicators found in process design handbooks, as well as in relevant publications and websites. Regarding the methanol production unit, a plant uptime of 8400 operating hours per year (350 days) was assumed, as well as a 20 years project lifespan. Lastly, the location of the unit was considered to be in central Europe (mean values of different countries, such as France and Germany were employed).

2.3.1 Capital cost

The overall investment required for a new design is divided into four key categories:

- Battery limits investment. Refers to the purchase of the buildings, as well as the individual plant equipment and its delivery and installation. Costs for equipment can be determined from equipment vendors or from published cost data, as its discussed below.
- Utility investment. It is the capital cost for the electricity and steam generation and distribution and the equipment needed for water processing.
- Off-site investment. It includes any auxiliary buildings, roads, systems and storage facilities.

- Working capital. It refers to the money that must be invested before there is a product to sell, in order to get the plant into productive operation. [81]

The overall capital cost of the process, services, and working capital may be calculated by multiplying the purchase price of individual parts of equipment with a relevant factor. Some typical factors for capital cost based on delivered equipment costs, for fluid processing units, are presented in Table 7. [81]

Table 7: Typical factors for capital cost based on delivered equipment costs (for fluid processing units).

[81] [82] [84]

Item	Factor
Direct costs	
Equipment delivered cost	1
Equipment erection	0.4
Piping (installed)	0.15
Instrumentation & controls (installed)	0.2
Electrical (installed)	0.1
Off-sites	0.2
Buildings (including services)	0.3
Site preparation	0.1
Total capital cost of installed equipment	3.4
Indirect costs	
Design, engineering and construction	1.0
Contingency (about 10% of fixed capital costs)	0.15
Total fixed capital cost	4.8
Working capital (15% of total capital cost)	0.7
Total capital cost	5.8

Some empirical equations have been developed to estimate the cost of various types of equipment by using characteristics of each type as inputs (such as height, heat transfer surface etc.), as presented in Equations 18, 19, 20, 21, 22, 23 and 24. Regarding the equation for the heat exchanger, it refers to a shell-and-tube heat exchanger, where A is considered the heat transfer

surface (in m^2). In case this surface is found to be greater than 1000 m_2, technical problems are created and more than one exchanger is taken into account, unless it concerns the condenser of the distillation column. For the compressors, the equation takes into account both the compressor cost, as well as its motor's cost and where P is the power of compressor in hp. For the turbine the P refers to Power in kW. As per the Flash, its weight (W - in kg), height (H - in m) and diameter (D - in m) must be considered. Following, the distillation column's cost is calculated by combining the cost of the column, the stages, the reflux pump, the reboiler and the condenser. For the last two the Equation 18 is considered. The column is calculated using its weight (W - in kg), height (H - in m), diameter (D - in m), number of stages (NT) and pump's power (P - in kW). Lastly, for the scenario of biogas as feedstock, a desulfurization unit is employed. It consists of 5 beds and an additional regeneration column. The equation used to specify the total equipment cost is the same as for the column (Equation 22). [80]

$$C_p(USD@1979) = exp(8.202 + 0.1506 * ln(A) + 0.06811 * ln(A)^2) \quad (HeatExchanger) \tag{18}$$

[85]

$$C_p(USD@2012) = 2.5 * exp(7.58 + 0.8 * ln(P)) + 2049 + 668.16 * P \quad (Compressor) \tag{19}$$

[86]

$$C_p(USD@2005) = 633000 * P^{0.398} \quad (Turbine) \tag{20}$$

[87]

$$C_p(USD@1979) = exp(8.6 - 0.21651 * ln(W) + 0.04576 * ln(W)^2) + 1017 * D^{0.7396} * H^{0.70684} \quad (Flash) \tag{21}$$

[85]

$$C_p(USD@1979) = exp(6.95 + 0.1808 * ln(W) + 0.02468 * ln(W)^2) + \\ + 834.86 * D^{0.63316} * H^{0.80161}) \ \ (Column) \tag{22}$$

[85]

$$C_p(USD@1979) = NT * 278.38 * EXP(0.05705 * D) * \\ * max(1, \frac{2.25}{1.0414^{NT}}) \ \ (Stages) \tag{23}$$

[85]

$$C_p(USD@2000) = 1970 * P^{0.35} \ \ (Pump) \tag{24}$$

[85]

For the reactors, the equipment cost estimation conducted by finding reactors of similar chemical units and by using Equations 25 and 26, as discussed below. Regarding the methanol synthesis from hydrogenation of carbon monoxide and dioxide reactor, the values presented in Table 8 were found in literature. The cost that was used was the mean of these values. As per the thermocatalytic DMR reactor, the cost is estimated based on the cost of a fired heater reformer furnace, due to its high operating temperature. Data from literature is obtained and converted to the capacity of this study. [88] Lastly, regarding the MW-assisted DMR reactor, the study of de la Fuente et al. for the cost of a microwave plasma reactor was considered. The main factor that determines the purchase cost is the generator of the microwaves in combination with the waveguide components needed for the operation. Due to the limitation of maximum output power of 100 kW at a frequency of 915 MHz that the magnetron has, a series of magnetrons need to be emplyed (the particular number of magnetrons is determined by dividing the kilowatts required by 100 and rounding up). As this study showed, with an increase in the maximum power (kW) per magnetron, the total equipment cost per produced kW decreases and reaches a plateau of around 1400 euro per kW. This equipment cost is likely to drop as technology evolves and magnetrons with higher microwave power output (more than 100 kW) are manufactured. [23]

Table 8: Literature data for the equipment cost of a methanol synthesis reactor and cost estimation for a unit with a capacity of approximately 100 ktonnes/year.

Base Capacity (ktonnes/year)	Base Cost (Meuro)	Year	Cost estimation (Meuro)	Reference
656	1.9	2022	0.6	[89]
16.3	1825	2020	3.7	[90]
23.8	1825	2014	4.1	[91]
1.2	3.9	2023	8.2	[92]

Each process in a unit has its own set of characteristics, one of which is the materials used to construct the equipment. These materials have a major effect on equipment capital costs. Furthermore, operating pressure and temperature affect the equipment capital cost due to thicker walls to handle increasing pressure and decreased allowable stress for construction materials as temperature rises. Table 9 provides some approximate average factors that relate the various materials and operating pressure and temperature with the equipment capital cost. Hence, Equation 25 may be used to calculate the actual cost of carbon steel equipment at moderate pressure and temperature, where C_E is the equipment cost for carbon steel at moderate pressure and temperature with capacity Q, C_B is the known base cost for equipment with capacity Q_B, N is a constant depending on equipment type and f_M, f_P and f_T are the correction factors for materials of construction, design pressure and design temperature respectively. The values of constant "N" vary between 0.30 and 0.84 and are related to the type of the equipment. A median value equal to 0.67 can be employed for approximate calculations for an average unit. [81] [82] [85]

$$C_E = C_B(\frac{Q}{Q_B})^N f_M f_P f_T \tag{25}$$

Table 9: Typical equipment material, pressure and temperature factors for equipment cost estimation.

[81]

Material	Correction factor (f_M)
Carbon steel	1.0
Aluminum	1.3
Stainless steel (low grades)	2.4
Stainless steel (high grades)	3.4
Hastelloy C	3.6
Monel	4.1
Nickel and inconel	4.4
Titanium	5.8
Design pressure (bar)	Correction factor (f_P)
0.01	2.0
0.1	1.3
0.5 to 7	1.0
50	1.5
100	1.9
Design temperature (°C)	Correction factor (f_T)
0–100	1.0
300	1.6
500	2.1

Cost data published in literature is frequently old, coming from a number of sources with varying dates. By using cost indexes, such data may be kept up to date and standardized. The equation used for this purpose is Equation 26, where C_1 is the equipment cost in year 1, C_2 is the equipment cost in year 2, $INDEX_1$ is the cost index in year 1 and $INDEX_2$ is the cost index in year 2. Commonly used indexes are the Chemical Engineering Plant Cost Index (CEPCI), the Marshall and Swift Index and the Nelson–Farrar Refinery Construction Index, the most useful of which is the CEPCI. [82] [81] In Table the evolution on the CEPCI over the years is presented.

$$\frac{C_1}{C_2} = \frac{INDEX_1}{INDEX_2} \tag{26}$$

Table 10: CEPCI evolution from 2001 to present.

[93]

Year	CEPCI	Year	CEPCI
1957-1959	100	2012	584.6
2001	394.3	2013	584.6
2002	395.6	2014	576.1
2003	402.0	2015	556.8
2004	444.2	2016	541.7
2005	468.2	2017	567.5
2006	499.6	2018	603.1
2007	525.4	2019	607.5
2008	575.4	2020	596.2
2009	521.9	2021	708.8
2010	550.8	2022	816.0
2011	585.7	2023 Apr	803.4

Lastly, the installation cost of each unit of equipment can be calculated by employing some factors, as presented in Table 11. It is important to be noted that these factors calculate the installed equipment cost, meaning that it includes the cost of the equipment. In order to determine only the cost of the installation the multiplying factor has to become (f_k-1). [94]

Table 11: Installation factors for the main industrial equipment.

[94]

Equipment	Installation Factor (f_k)
Reactor	4.05
Column	4.05
Reforming Heat Furnace	2.41
Compressor	2.50
Pump	2.97
Storage device	1.65
Shell-and-tube heat exchanger	3.22
Plate heat exchanger	1.70

2.3.2 Operational cost

Before assessing the economic feasibility of a particular process, the costs involved with daily operations of a chemical plant must be determined. Table 12 shows the primary factors influencing the Operating Cost of the production of a chemical product. The most expensive individual operational expense in most operations is raw materials. Their prices are obtained from the relevant suppliers, but in preliminary analysis they can be derived from publications and databases. Due to the price fluctuations over the time, the safer method is to obtain values from different sources and times and calculate the average material price. Some current price ranges for the raw materials used in this study are presented in Table 13.

Furthermore, a high operational cost is due to the utilities needed in various units of the plant, such as the heat exchangers (for heating and cooling), the reactors, the compressors etc. The main sources of these utilities are public or private producers and the company itself (from off-site facilities or self-production). The prices of the utilities (fuel, electricity, steam, cooling water, refrigeration, compressed air, inert gas) can be obtained in the same way as mentioned for the raw materials' prices. If the source is not updated, the CEPCI can be used in order to calculate more approximate prices for today, as shown in Table 13. [82] [81] The calculation of the total utility demand of this study is done through energy balances, taking into account the energy conversion efficiency (85% for compressors, 40% for the furnace and 90% for the microwaves). Water at 20 °C is used as the cooling utility for the condenser of the distillation column, the coolers and the methanol reactor (exothermic reaction). Low pressure (LP) steam (6 bar - 160 °C) is required for the column preheater and reboiler. High pressure (HP) steam (24 bar - 254 °C) is used for the preheat of the two reactor's inlet. In the case study of the conventional DMR heating, the reactor is heated via a furnace that burns natural gas. In the case of the MW-assisted DMR, the reactor is heated from the microwave plasma, by using electricity. Electricity is also required for the operation of the compressors, in all the scenarios. Lastly, for the the case scenario that uses biogas as feedstock, the adsorbent's regeneration column needs heating, which happens with the use of HP steam. The total demand is calculated using as a base the data obtained from the study of Aguilera et al., which indicates that for a capacity of 10000 cum/day, 422 kg of HP steam per hour are required. [80]

Following, for the cost estimation of the catalysts and adsorbents, prices from literature were obtained. For the methanol synthesis reactor, a bimetallic $Cu/ZnO/Al_2O_3$ is used as mentioned in Section 1.2. A price of 8 eur/kg and a loading of 132 kg that need to be replaced every two years were assumed. [89] [95] [96]. For the DMR reactor, in the first case study, with conventional heating, a Ni/Al_2O_3 catalyst with a price of 24 eur/kg and a loading of 1480 kg (changed every 4 years) was assumed [97]. Regarding the case study with the microwave heating DMR, the ruthenium-doped $SrTiO_3$ perovskite catalyst synthesized by Gangurde et al., as discussed in Section 1.3, with an estimated price of 8360, was employed. [20] Lastly, for the low-cost adsorbent (dried sewage sludge), a loading of 126 kg/year was calculated and a price equal to 0.1 eur/kg was assumed. [80]

Regarding the number of operators needed in a shift the empirical Equation 27 was employed, where N is the number of operators per shift and P is the number of processing steps including compression, heating and cooling, mixing, and reaction. For a plant with the characteristics of the one in this study, a total of 4 operators per shift can be calculated. [82]

$$N = (6.29 + 0.23 * P)^{0.5} \tag{27}$$

Finally, it is important to consider the exchange rate between the different currencies in the calculations that its needed (both for the capital and the operational costs). To convert US dollars to euros a rate of 0.91 (value obtained on 30/09/2023) was used. [98]

Table 12: Typical factors for operational costs (direct and indirect).

[81] [82]

Item	Factor
Direct manufacturing costs	
Operating labor	4 operators/shift, 3 shifts/day, 60000 USD/labor/year
Supervision	0.02 of operating labor
Maintenance & Repairs	0.06 of TFCC
Maintenance supplies	0.15 of maintenance and repairs
Laboratory charges	0.15 of operating labor
Fixed manufacturing costs	
Depreciation	0.1 of TFCC
Local taxes & insurance	0.03 of TFCC
Plant overhead costs	0.6 of Operating labor, Supervision and Maintenance & Repairs

Table 13: Raw material and utility prices.

Material	Price range (eur/tonne)	Reference	Assumed price (eur/tonne)
green hydrogen	2730-7280	[99] [100] [101] [102] [103]	1000
carbon dioxide	34-314	[104] [105] [106] [107] [108]	90
methane	210-458	[109] [110]	300
biogas	21-636	[111] [112] [113]	350
utility	Utility cost	Reference	Assumed price
cooling water	0.02 eur/cum	[93] [82] [98]	0.02 eur/cum
low temperature refrigerant (R-134a)	10.29 eur/GJ	[93] [82] [98]	10.29 eur/GJ
low pressure (LP) steam	2.46 eur/GJ	[93] [82] [98]	2.46 eur/GJ
high pressure (HP) steam	6.86 eur/GJ	[93] [82] [98]	6.86 eur/GJ
natural gas	3.83 eur/GJ	[93] [82] [98]	3.83 eur/GJ
electricity	0.08-0.12 eur/kW	[114] [115] [116]	0.10 eur/kW

2.3.3 Profitability

In the previous chapters there were provided the PFDs and the capital and operational cost estimations' methods. These can be utilized to carry out an economic analysis for the evaluation of profitability. The best method is to calculate the cash flows during the project's life. Table 14 shows the variables used, as well as the main assumptions and calculations made. Before the start of unit operation, some years to make the necessary studies and construct the plant are required. In these years a capital equal to the TCC is needed. Loans from banks, the company's issuing stock, and net cash flow from its profits accumulated over time, can all be used to fund new installations. The cost of financing a project varies depending on its funding source. Often, during the initial phases of a project, the source of funding remains uncertain. Nevertheless, there is a necessity to choose between different process options and conduct optimization considering both the capital and operational expenses. Achieving this becomes challenging unless both costs can be presented on a common basis. Capital costs can be annualized when assuming that the capital has been borrowed for a fixed period, typically ranging from 5 to 10 years, at a fixed interest rate. In that case, the capital cost can be annualized (Annualized Capital Cost - ACC) as per Equation 28, where LI is the Loan Installment, i is the fractional interest rate per year and n is the number of years. [81] For this study it was assumed that half of TCC is covered by loans, with an i=5% and years of payback equal to 5 (starting at year 1). [82] [81] [84] The rest half of TCC is covered by Equity Capital (EC). It is assumed that this capital will be paid back after the payoff of loans, meaning in years 6 until the end of plant's life. At the last year the unit will have a residual value, the calculation of which is shown in Table 14. This residual value was considered to be part of the equity payback. Regarding the income that is taxed it is calculated by subtracting OPEX and annual depreciation from revenue. [84] "Tax depreciation is the depreciation expense claimed by a taxpayer on a tax return to compensate for the loss in the value of the tangible assets used in income-generating activities." [117] Tax depreciation, like accounting depreciation, assigns depreciation expenditures across various periods. As a result, the tax values of depreciable assets decline steadily during their useful lifetimes. [117] Furthermore, the Economic Potentialcan give a preliminary estimation of the gross margin of the project. It may be calculated by Equation 29, where EP is the economic potential (eur/year), REV is the revenue from the

methanol sale (eur/year) and RM is the annual cost of raw materials (carbon dioxide and hydrogen for all cases, methane for CS 1 and 2 and biogas for CS 3). The prices of the raw materials were presented in Table 13. As per the methanol price, a mean value of 400 eur/tonne was considered. [118] [119] [10] [120] [121] [122]

$$ACC = LI * \frac{i(1+i)^n}{(1+i)^n - 1} \tag{28}$$

$$EP = REV - RM \tag{29}$$

As money could be invested to earn interest, money in the present has a higher value than the same amount at a future date. A project's net present value is the sum of the present values of every single cash flow. (As present is considered the start of the project.) The annual discounted cash flow is calculated by discounting the annual cash flow with the rate of interest. The higher the NPV, the more financially attractive the project is. A project with a negative NPV is not profitable and is therefore rejected. In a diagram of cumulative cash flow over time, the evolution of the NPV can be seen as well as the year in which it becomes positive (break-even point). This year, called the PayBack Period (PBP), is the moment when the positive cash flows equal the initial expenditure (NVP=0). [81] [82]

Table 14: Variables, assumptions and equations for the evaluation of profitability.

Variable	Description	Assumptions/Calculations
N_0	years for studies and construction	2
N	years of plant's life	18
TFCC	Total Fixed Capital Cost	calculated according to Section 2.3.1
WC	Working Capital	calculated according to Section 2.3.1
TCC	Total Capital Cost	TFCC + WC
REV	Revenue (value of products)	$unit's capacity * methanol price$
r_d	depreciation rate	5%
D	Depreciation	$r_d * TFCC$
N_k	years since the start of operating	$1 \leq N_k \leq N$
RV_k	Residual Value in year N_k	$TFCC - N_k * D$
RV	Residual Value in year N	$TFCC - N * D$
OPEX	Operational Expenditure	calculated according to Section 2.3.2
LI	Loan Installment	$\frac{TCC}{2}$
i	interest rate	5%
n_L	payback years for loans	5
I	Interest	$LI * \frac{i(1+i)^n_L}{(1+i)^n_L - 1}$, starting at year 1
EC	Equity Capital	$\frac{TCC}{2}$
n_E	payback years for equity capitals	13
EPB	annual Equity Payback	$\frac{EC-RV}{n_E}$, starting at year 6
T_k	Taxes in year N_k	$21\% * (REV - OPEX - N_k * D)$
CF_a	Cash Flow in the first five years	$REV - (OPEX + I + T_k)$
CF_b	Cash Flow in the years 6 to 18	$REV - (OPEX + EP + T_k)$
i_d	discount rate	7%
NPV	Net Present Value	$\Sigma_{n=1}^{N} \frac{CF_n}{(1+i_d)^n}$
IRR	Internal Rate of Return	i_d for which NPV=0

2.4 Preliminary GHG emissions estimation

Apart from the economic analysis, it is really important to evaluate the proposed processes in terms of environmental performance. A key indicator is the global warming potential (GWP100), measured in kg_{CO_2}-eq per reference unit. The data for this calculation were obtained from the Ecoinvent 3.9.1 (12/2022) database, as well as from the mass and energy balances extracted from Aspen Plus. The boundaries of the system were considered to be cradle-to-gate, given that the production and transportation of the raw materials and the manufacturing step were taken into account for the determination of the emissions. 93 ktonnes/year of methanol was set as the functional unit (f.u.). The method used for the determination of this indicator is the CML v4.8 2016 no LT. In Table 15 the indicators for each category are presented. Regarding the direct emissions, they include the CO_2 that was produced from the natural gas burning in the furnace of CS1 for the heating of the DMR reactor, and the CO_2 from the purge streams (MeOH reactor recycle and distillation column's top) after their burning in a flare.

Table 15: The global warming potential - GWP100 indicator for each component of the categories: raw materials, utilities, waste and direct emissions, obtained from the Ecoinvent 3.9.1 database and the CML v4.8 2016 no LT method.

Item	Reference unit	Global warming potential - GWP100 (kg_{CO_2}-eq)
Raw materials		
biogas (from anaerobic digestion)	cum	3.1E-01
hydrogen (from water electrolysis)	kg	8.2E-01
carbon dioxide	kg	0.0E+00
methane (from natural gas)	kg	5.9E-01
Utilities		
electricity	kWh	2E-02
steam (high pressure)	MJ	1.1E-01
natural gas (furnace)	MJ	3.9E-02
cooling water	kg	2.5E-05
refrigerant (R-134a)	kg	1.8E+01
Waste		
hydrogen sulfide	kg	5.5E-01
wastewater	cum	2.5E-01
Direct emissions		
carbon dioxide	kg	1.00E+00

Chapter 3

Results and discussion

The mass flows, as well as the conditions, for the main streams (as they appear on each PFD) were retrieved form Aspen Plus and are presented in Table 21 (Appendix). Given that all the main streams (S1-S11) are the same for all the case studies there was no need to design different tables for each case. The only thing that changes is the existence of a biogas stream in the third case study, which appears in the Table 21 as S0. After the desulfurization and the mix of the biogas with carbon dioxide, the stream that results finally is the same as the feed streams in the two previous case studies (pure feed). The mass balances, as well as the energy demand, are utilized for the calculation of some performance indicators (technical, economical and environmental).

3.1 Technical results

A Heat Exchanger Network was synthesized for each scenario, based on the criteria discussed in Section 2.2. The proposed HENs are illustrated in Figures 16, 17 and 18. The total energy savings from the HEN are presented in Table 16 alongside with the main technical results. The Heat Integration resulted in a reduction of energy demand of about 5.6%, 6.6% and 6.9% for scenario 1, 2 and 3 respectively.

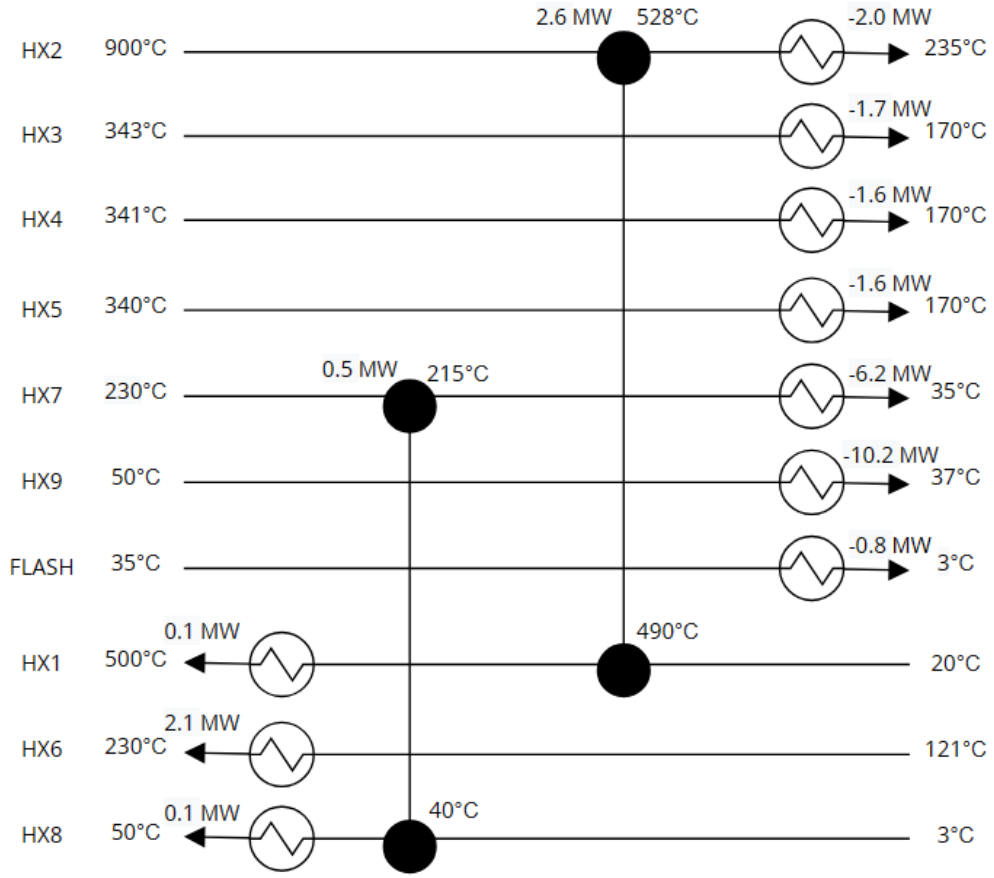

Figure 16: Synthesized Heat Exchanger Network for Case Study 1: Conventional DMR heating with pure feed.

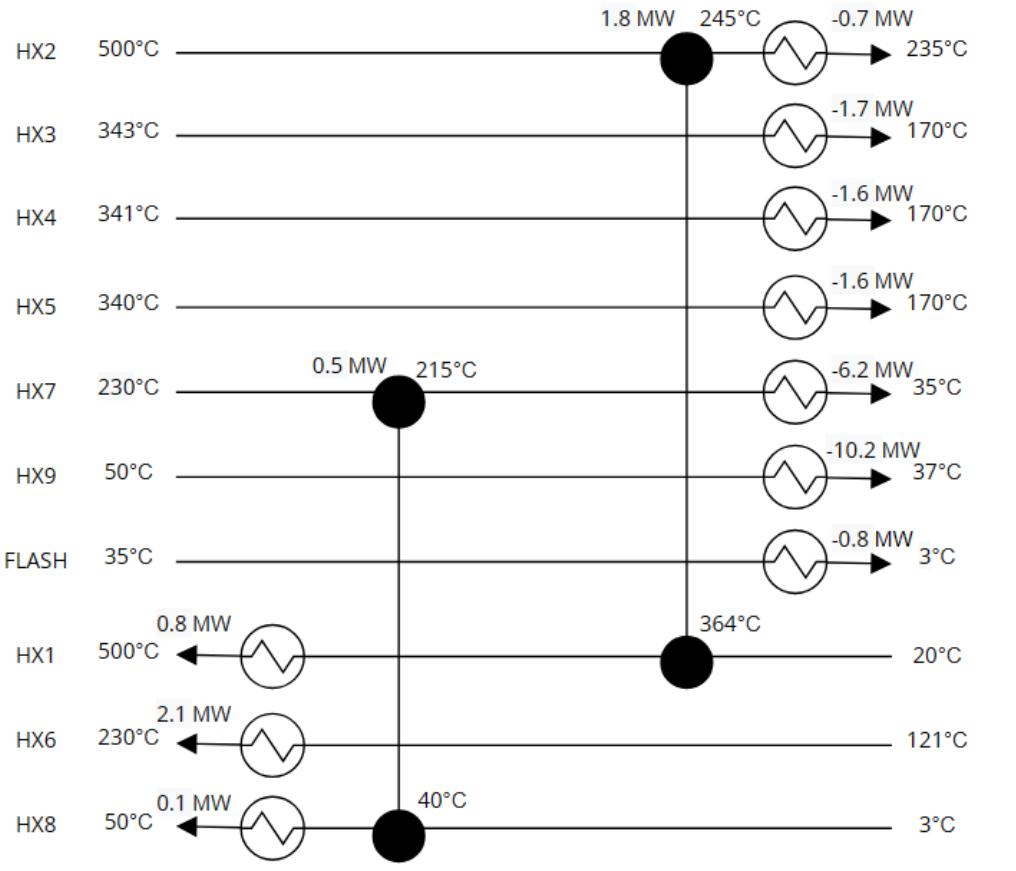

Figure 17: Synthesized Heat Exchanger Network for Case Study 2: MW-assisted DMR with pure feed.

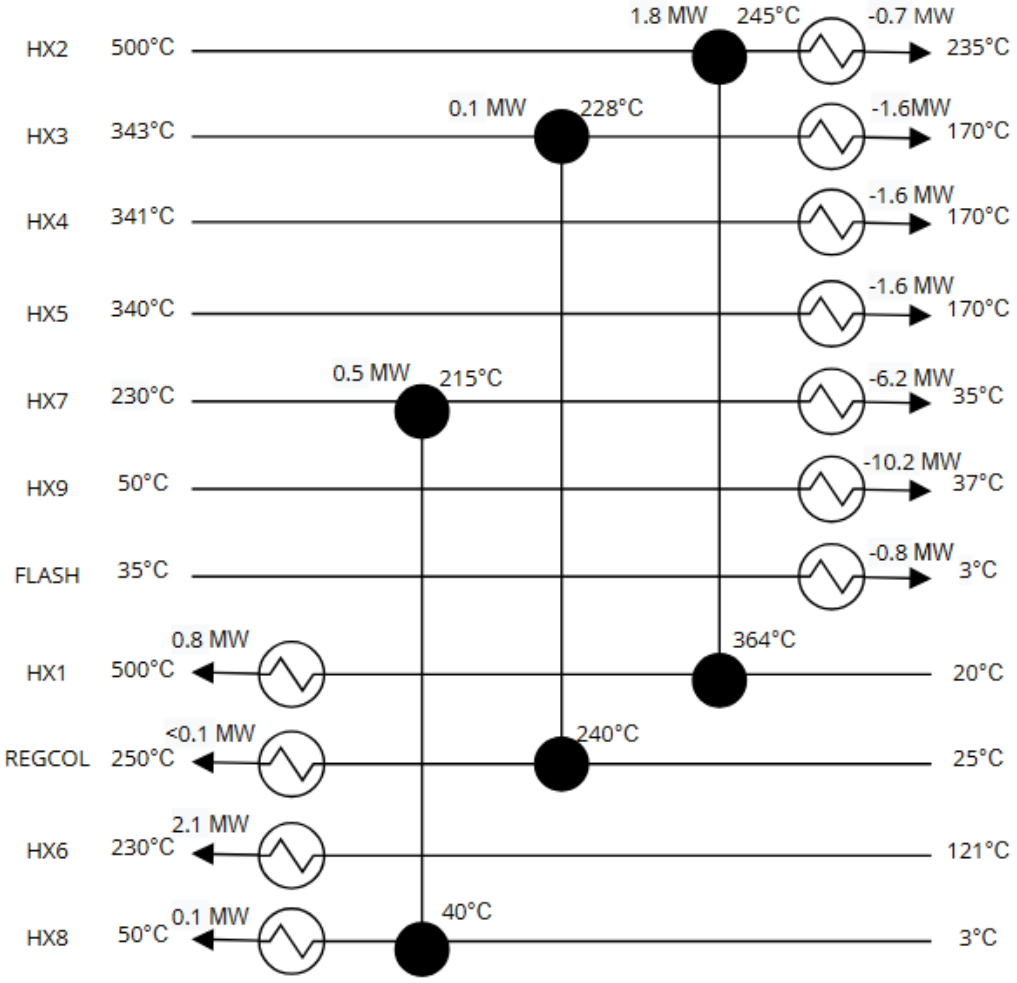

Figure 18: Synthesized Heat Exchanger Network for Case Study 3: MW-assisted DMR with biogas feed.

Table 16: Technical results for the three case studies.

Item	Case Study 1	Case Study 2	Case Study 3
methanol production (ktn/y)	100	100	100
methanol purity	99.5%	99.5%	99.5%
SEI (MJ/kg$_{MeOH}$)	12.1	11.2	11.3
total yield	73%	73%	73%
potential energy share of RES	9.5%	61.2%	60.9%
energy savings with HI (MW)	5.4	4.6	4.8
reduction of energy demand with HI	5.6%	6.6%	6.9%

As it appears in Table 16, the total yield (that was calculated by using the Equation 15) for the three scenarios is the same (0.73), given that the feed ratios, as well as the conversions for the two reactors, were the same for all scenarios. Regarding the specific energy demand (which was calculated by using the Equation 19), it occured to be equal to 12.1, 11.2 and 11.3 MJ/kg$_{MeOH}$ for CS 1, 2 and 3 respectively. For the case of conventional heating of the DMR reactor, it is elevated compared to the scenarios of heating via microwaves. This results from the fact that in the first case the reaction takes place at 900 °C, while for the other two cases at 500 °C. Furthermore, the efficiency of the conventional furnace, used in CS 1 to reach 900 °C, is 40%, leading to even higher energy needs. As seen in Figure 19, the energy demand driver is the heating of the DMR reactor, followed by the reboiler of the distillation column and the compressors. The energy demand of the regeneration column for the third case study is not significant compared to the energy needs of the rest plant. Thereafter, the energy share of renewable sources is, as expected, reduced in the first case study, because of the use of fossil fuels for the heating of the DMR reactor, compared to the "green" electricity (microwaves) used in case study 2 and 3. Then, in terms of energy savings from heat integration, the best results refer to the first scenario, as the outlet stream of the DMR reactor has a significantly higher energy content. Following, the third case study compared to the second had a bigger reduction of energy demand because more streams interfere with each other, as it appears in the HEN figures.

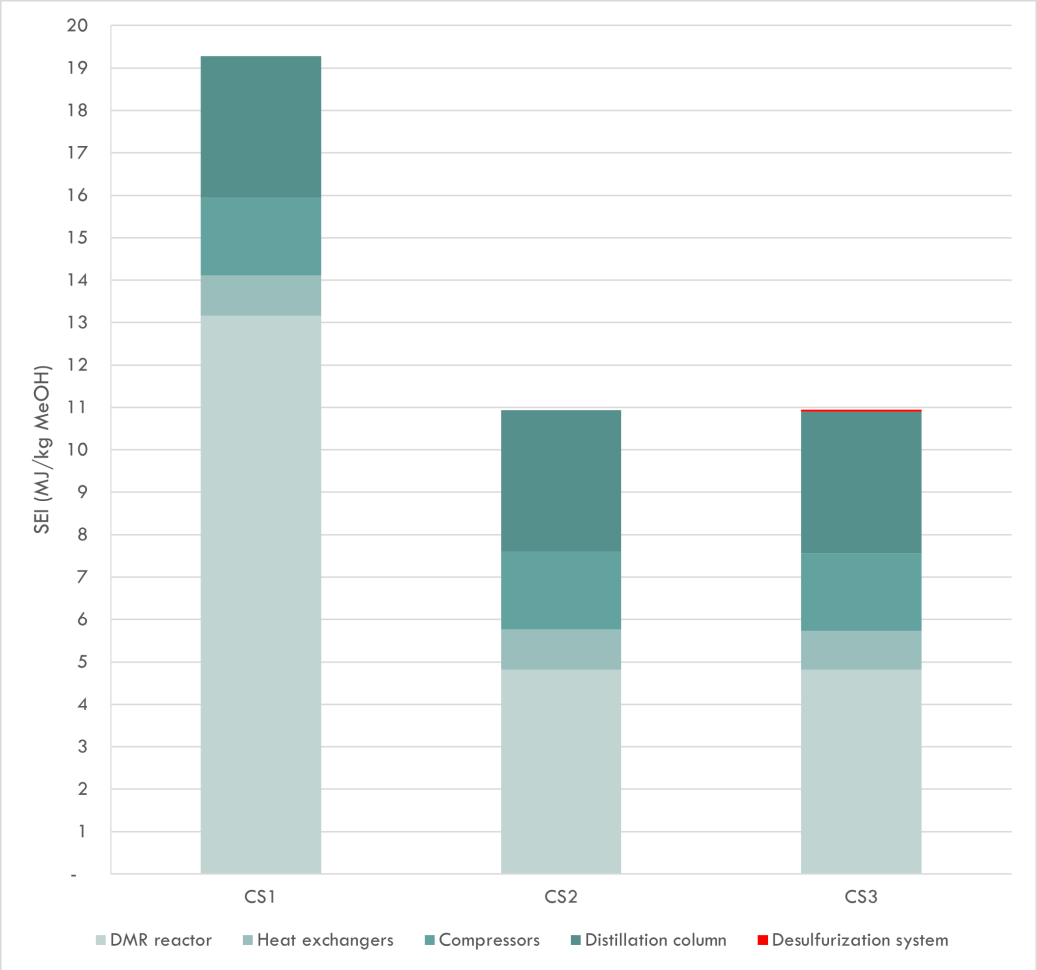

Figure 19: Breakdown bar for the Specific Energy Input.

3.2 Economic results

The economic analysis used as inputs all the equations and data discussed in the previous Chapter, as well as any information needed that resulted from the simulation in Aspen Plus. More specifically, the mass and energy balances and the characteristics of each unit (heat transfer surface, weight, height, diameter etc.) were utilized. It has to be noted that the utility savings resulted from the HEN where subtracted from the OPEX. Regarding the additional heat exchangers needed for the HEN, their cost was estimated (using the Equation 17) equal to 0.35, 0.29 and 0.34 million euros for CS 1, 2 and 3, respectively. At the same time, the heat exchangers, that already existed in the PFD and are related to the streams used for the HI, had a cost reduction due to the decrease of their heat transfer surface. Eventually, the difference between the cost of the extra heat exchangers and the money saved from the surface reduction was essentially small. With this reasoning, the equipment cost of heat exchangers remained the same after the Heat Integration.

Afterwards, the Figure 20 illustrates the distribution of cost for the installed equipment in each CS. The total cost of the equipment and its installation is significantly lower in the first case study (179 Meur compared to around 239 Meur for CS 2 and 3). This is due to the high cost of the microwave-assisted plasma reactor in the relevant cases (2 and 3), as seen in Figure 20. As discussed, this cost comes from the expensive magnetrons used for the MW reactor's operation. As for the installed equipment's cost, the compressors have the bigger influence, followed by the DMR reactors, especially in the case that they are microwave assisted.

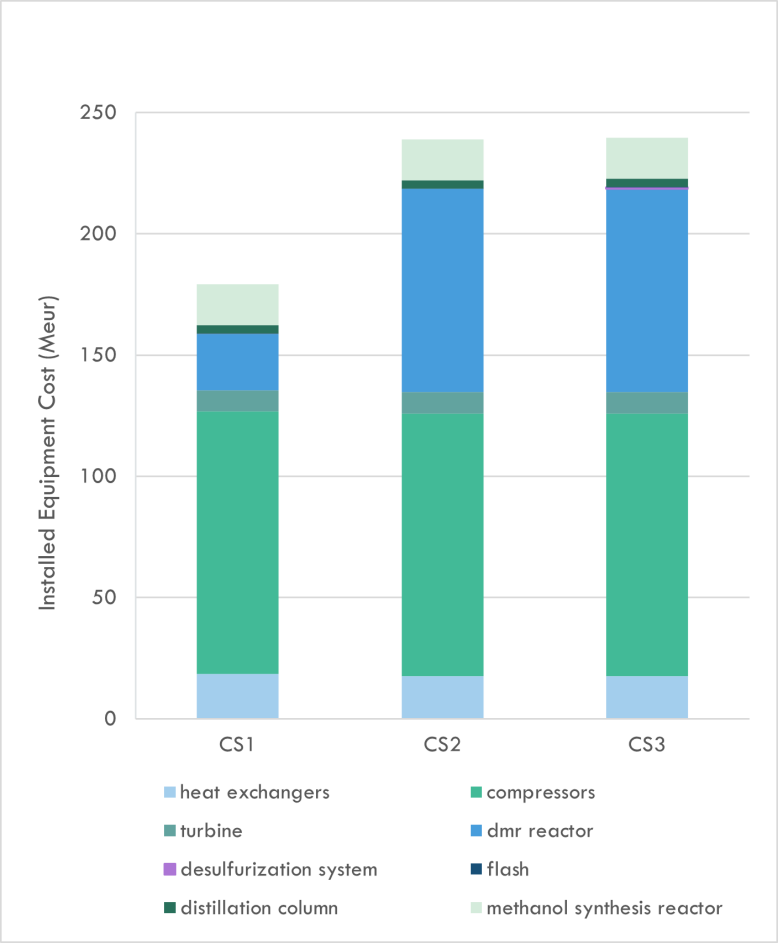

Figure 20: Allocation of total installed equipment cost to the different equipment categories for the three case studies.

Regarding the operational costs, they are higher for the two case studies including the MW-assisted DMR reactor (148 Meur/year for CS 1 compared to approximately 180 Meur/year for CS 2 and 3), even though the energy demand in these cases is lower (see Table 16). This is due to the high price of electricity compared to the natural gas burnt in furnace used for the DMR heating (see Table 13). In all the cases, the operating costs are approximately the 85% of the annual costs and as seen in Figure 21 the hydrogen, the HP steam and the electricity are the drivers of the operational, and consequently the total, cost.

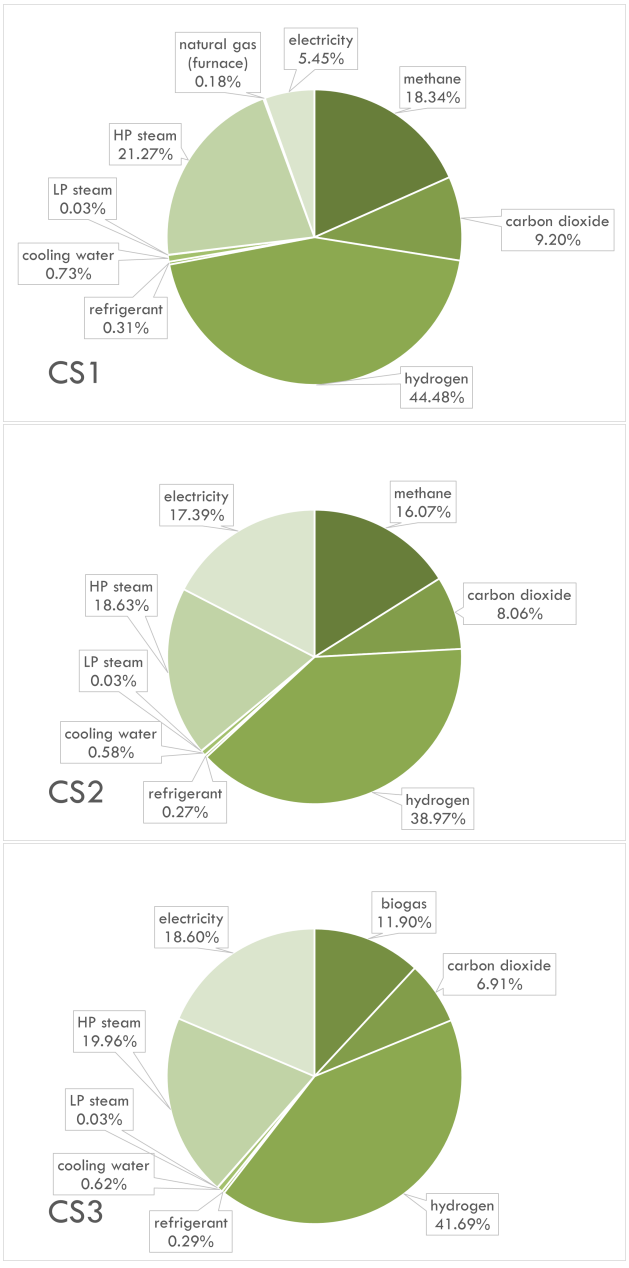

Figure 21: Cost distribution of the raw materials and the utilities for the three case studies.

In Table 17 the costs discussed in Section 2.3 are presented. As it was finally

calculated, the cost of methanol produced was around 1600 and 2300 eur per tonne, for the conventional heating case and the microwave-assisted cases, respectively. Even without consideration of any profit, this value is extremely elevated (4 to 6 times more) compared to the average price of methanol sold nowdays (400 eur/tonne), which was used for the calculation of the revenues (REV). That difference resulted in a negative economic potential for all cases (approximately -17 million dollars for all the cases), which led to a negative NPV. Finally, this project cannot be considered profitable, given that the plant would operate at a loss. More specifically, for 20 years of total existence, this project would result to a net loss of more than 1 billion euros (1.3 for CS 1 and 1.7 for CS 2 and 3).

Table 17: Calculation of the basic costs, as well as the economic potential and the net present value for the three case studies.

Item	CS 1	CS 2	CS 3
Total Purchsed Cost - TPC (Meur)	62.8	77.5	77.7
Total Capital Cost of Installed Equipment - TIC (Meur)	179.1	238.9	239.5
Total Fixed Capital Cost - TFCC (Meur)	289.1	374.6	375.5
Working capital - WC (Meur)	43.4	56.2	56.3
Total Capital Cost - TCC (Meur)	332.4	430.8	431.8
Annualized TCC - CAPEX (Meur/y)	26.7	34.6	34.6
Variable Cost of Production - VCP (Meur/y)	78.3	90.5	92.0
Fixed Cost of Production - FCP (Meur/y)	69.3	89.4	89.6
Operating Expenditure - OPEX (Meur/y)	147.6	179.9	181.7
Total Annual Cost - TAC (Meur/y)	174.3	214.5	216.3
Methanol cost (eur/tonne)	1874	2307	2326
OPEX percentage of TAC	85%	84%	84%
CAPEX percentage of TAC	15%	16%	16%
Revenues - REV (Meur/y)	37.2	37.2	37.2
Economic Potential - EP (Meur/y)	-17.0	-17.0	-18.5
Net Present Value - NPV (Meur)	-1331.2	-1721.4	-1739.4

3.3 Viability

The results of the economic analysis showed that the project is non profitable. Thus, a sensitivity analysis is performed to define the prices of raw materials, utilities and methanol that could result in profitable operation of the methanol production units (NPV higher than 0). By using the tool Solver in MS Excel, it was calculated that the break-even value of methanol is 1824, 2242 and 2261 eur/tonne for the CS 1, 2 and 3, a price non feasible in today's economy (2023 scenario). For the hydrogen and electricity no break-even value could be found. This is logical given that the cost of hydrogen is 12.8 Meur/year and of electricity 0.5-1.7 Meur/year, while the cash flow is, in the best case, -121 Meur/year. This means that even if the hydrogen and the electricity had no cost, the project would still be non feasible. For that reason, a feasibility study in a future economy, where RES will be dominant, was employed. The second case study (CS2), which utilizes more electricity than the first one, was considered for the analysis, because of the direction towards electrification in the industry (see Table 16 for energy share of RES). The third case (CS3) is the most costly, thus it was rejected. The cost drivers for the second case study are: hydrogen (12.5% of TAC), capex (16.0% of TAC), electricity (5.5% of TAC) and HP steam (5.7% of TAC). From these four drivers, the HP steam is fossil based and thus was not considered as a variable for the future analysis mentioned above, considering the expected decarbonization. Many studies have produced forecasts regarding the future prices of essential raw materials, including the ones used in this study, as well as of electricity. Some of these estimated values for the year 2050 are presented in Table 18.

Table 18: Prices of raw materials and electricity used in this study and predicted for the year 2050.

Variable	Used (2023)	Predicted (2050)	Reference
methanol (eur/tonne)	400	630	[11]
hydrogen (eur/tonne)	3000	1000	[123] [124]
carbon dioxide (eur/tonne)	90	34	[125]
electricity (eur/kWh)	0.1	0.02	[126]

Even with using the values of Table 18 for the 2050 scenario, the NPV is still bellow zero (-1.3 billion euros), but less negative compared to the 2023 NPV (-1.9 billion euros). The break-even value of methanol was calculated for the 2050 scenario, equal to 1986 eur/tonne (lower compared to 2242 eur/tonne for the 2023 scenario). However, the latter methanol price is well above the anticipated one for 2050 (i.e., 630 eur/tonne).

The economy of scale could also affect the methanol production cost. Thus a sensitivity analysis was performed to evaluate its impact on the economics (i.e., NPV) (Equation 25). The assumptions made for the economy of scale were the following: the N was considered equal to 0.6 (see Equation 25) and the total cost was calculated by adding the OPEX and the Annualized CAPEX (assuming that the total cost was covered by loans). As the capacity elevated, the OPEX elevated linearly, but the CAPEX elevated exponentially. That cost was subtracted from the revenues at each capacity, which were calculated by multiplying the estimated methanol price (630 eur/tonne) with the relevant capacity. The results showed that no positive value for the cash flow could be obtained, given that the economic potential was still negative, and as the evolution of both the revenues and the OPEX is linear, the EP would never become positive. For that reason, a "trial and error" method was employed in order to find the lowest price of methanol for which a higher capacity than the 100 ktonnes/year would make the project profitable. The capacity had to be in an industrial acceptable range (i.e. 350-3500 ktonnes/year [90] [12] [127]). The results showed that with a MeOH price of 1720 eur/tonne, the NPV became zero at a capacity equal to 3500 tonnes_{MeOH}/year, as seen in Figure 22.

Figure 22: The evolution of NPV as a function of capacity, with the method of economy of scale, for the second case study, in year 2050, and for a methanol price of 1720 eur/tonne.

This price (1700 eur/tonne) is still high -i.e., 3 times more than the forecasted one-. Another concept that could be taken into account is the capital cost reduction due to the maturity of technology. The Technology Readiness Level (TRL) is a method that determines the maturity of technologies during the acquisition phase of a project. The more mature a technology is the lower the CAPEX can become, especially the cost of purchasing and installing the equipment. More specifically a reduction of 10-40% can be considered, according to the TRL. [128] For example, in the future, there are high chances in reduction of the MW-assisted DMR reactor's cost as a result of the construction of more efficient and less expensive magnetrons [23]. In Figure 23 the NPV reduction as a function of CAPEX reduction due to evolution of maturity of technology is presented. The values used are the ones of Table 18. As it appears, the examined CAPEX reduction (i.e., 10-40%) cannot result in a positive NPV, although the NPV values get closer to zero as the reduction percentage rises. This means that the maturity of technology by itself cannot create a positive NPV.

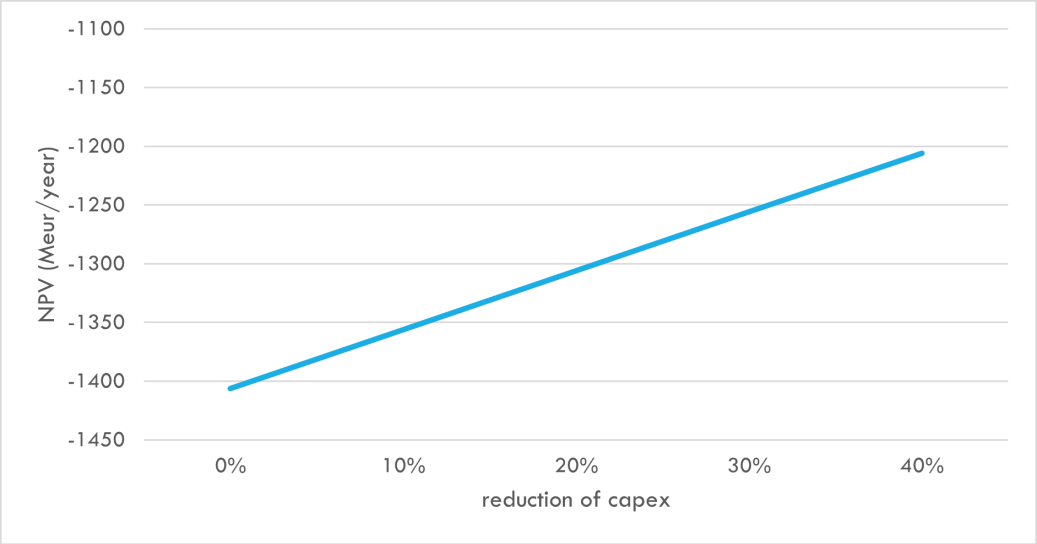

Figure 23: The evolution of NPV as a function of CAPEX reduction, due to increase of maturity of technology, for the second case study, in year 2050, and for a methanol price of 630 eur/tonne.

Consequently, from the all the above analysis, the result is that neither the reduction of OPEX (2050 prices), nor the economy of scale, nor the CAPEX reduction according to TRL, are able, by themselves, to create a positive NPV. A synergy of all the above is required. For that scenario the following were considered:

- The estimated prices for the raw materials and the utilities (2050 - Table 18).
- A capacity of 3500 ktonnes/year, according to the economy of scale. (see Figure 22)
- A CAPEX reduction equal to 40%, in accordance with the concept of TRL.

Considering the above, a break-even value of methanol price was calculated, by zeroing the NPV with the tool Solver of MS Excel. The result was a methanol price equal to 1674 eur/tonne, which is still a lot higher than the predicted one (2 to 3 times). All the methanol prices that were mentioned in this study are presented together in Table 19. Overall, the project is

not considered profitable unless the methanol price rises to more than 1674 eur/tonne in 2050, while utility and material prices fall to 1000 eur/tonne for hydrogen, 34 eur/tonne for CO_2, and 0.02 eur/kWh for electricity, capacity rises to 3500 ktonne/year, and CAPEX falls by 40% due to the evolution of technology maturity.

Table 19: The prices of methanol for 2023 and 2050, mentioned in this study, for CS2. For the literature values the references of Tables 13 and 18 were used. The break-even values refer to the MeOH price for which NPV=0. For the economy of scale case the value is the break-even one for a capacity of 3500 ktonnes/year. Synergy refers to the break-even value for a combination of 2050 utility and material prices, 3500 ktonne/year capacity and 40% reduction of CAPEX due to technology maturity.

Case	Methanol price (eur/tonne)
2023 - literature	400
2023 - break-even	2462
2050 - prediction in literature	630
2050 - break-even	1986
2050 - economy of scale	1720
2050 - synergy	1674

Lastly, it has to be noted that the European union has made a plan of investments for the next decades, based on the Green Deal, regarding the financing of green technologies that will lead to net zero emissions and decarbonization. According to the European Commission, at least one trillion euros is needed to found over the next decade. The EU budget should provide the most money, 503 billion euros, with national governments contributing another 114 billion euros. The remaining money will come from the private sector and various programs that support climate and environmental projects, such as agricultural grants, Horizon Europe, the Life program, and regional and cohesion funds. [129] [130] [131] In this logic, EU's green subsidies could be used for the implementation of a project that utilizes CO_2 emissions, biomethane, green hydrogen and that it's main energy demands are covered by electricity that is generated by RES.

3.4 Preliminary GHG emissions estimation results

Table 22 (Appendix) depicts the CO_2 equivalent emissions of the processes studied. The total specific emissions for CS 1, 2 and 3 were 1.82, 1.30 and 1.68 $kg_{CO_2-equivalent}/kg_{MeOH}$, respectively. The allocation of these emissions is illustrated in Figure 24. The most emissions were produced for CS 1, due to the burning of natural gas in the furnace for heating the DMR reactor (29% of total emissions). The emissions drivers for all the cases are the refrigerant (29% of total emissions for CS1 and 39% for CS 2 and 3), the HP steam (24% for CS1 and 32% for CS 2 and 3) and the methane/biogas (9% for CS1, 12% for CS2 and 11% for CS3). The utilization of a refrigerant that is more "environmental friendly" could reduce significantly the emissions due to this factor. Electricity has a small contribution (0.02 kg_{CO_2-eq}/kg_{MeOH} in the CS 2 and 3 where electricity is used for the heating of the DMR reactor), due to the RES (wind) used for its generation. Lastly, it should be noted that direct CO_2 emissions, accounted for approximately 7% of the total emissions in all cases. Thus, these CO_2 emissions could be decreased by employing a new MeOH synthesis technique that improves CO_2 conversion and by utilizing the purge streams and the off-gases from the natural gas burning in the CS1's furnace, instead of emitting them to the atmosphere.

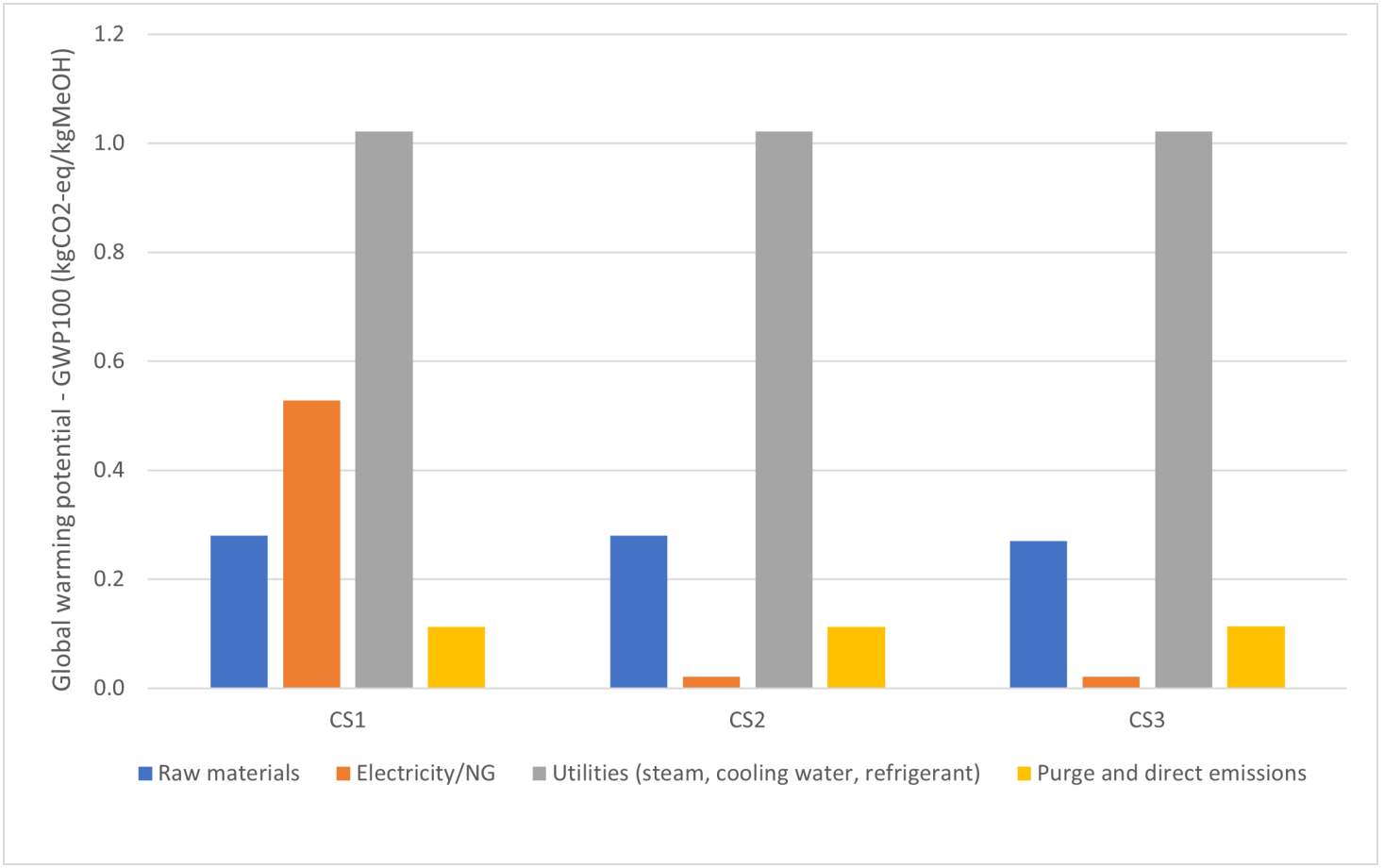

Figure 24: Allocation of global warming potential expressed in kg_{CO_2-eq}/kg_{MeOH}, to every component of each category (raw materials, utilities, waste, direct emissions) of each case study, using the Ecoinvent 3.9.1 (12/2022) database and the CML v4.8 2016 no LT method.

3.5 Overall comparison

Comparing the CSs investigated in this study with literature, some conclusions can be made. The three case studies seem to have a better performance regarding the total yield (0.73), meaning that more of the feed is utilized for the synthesis of the total product compared to the other methods. Especially in the case of biomass gasification almost half of the feed is wasted (not converted into methanol). This happens because there is a WGS reactor in order to increase the H_2 content of syngas (to attain the S required for methanol reactor). This implies that CO_2 is also produced in WGS reactor. The latter CO2 is separated upstream the methanol reactor, resulting in a CO_2 bleeding stream (thus part of carbon content is emitted as CO_2). The value of SEI of the case studies is in between the SEI values of the other cases. The studies with lower SEI than the proposed are the vacuum residue gasification (0.3), the hydrogenation of captured carbon (8.7) and the biogas steam reforming (2.0), whose values are not significantly apart from the CSs' ones. The carbon emissions of the three CS appear to be low compared to the rest studies. The only lower values are for the combined tri and dry methane reforming (0.01), the hydrogenation of captured carbon (0.02) and the vacuum residue gasification (1.25). The only category that the CSs do not have the desired performance compared to the other studies is the cost of methanol. For that reason, although the project investigated in this study is environmental viable, it is not profitable in today's economy, given that there are studies that propose ways for methanol production which are ten times less costly (shale gas partial SMR and vacuum residue gasification).

Table 20: Comparison of total yield, SEI, final product cost and CO_2 equivalent emissions of the three case studies investigated in this study, as well as of other methods for methanol production.

Method for MeOH production	Capacity (ktonne/year)	Yield (kg_{MeOH}/kg_{feed})	Specific Energy Input (MJ/kg)	Methanol cost (eur/tonne)	Carbon emissions (kg_{CO_2}/kg_{MeOH})	Reference
DMR with conventional heating	100	0.73	12.1	1874	1.94	this study
MW-assisted DMR	100	0.73	11.2	2307	1.44	this study
MW-assisted DMR with biogas feed	100	0.73	11.3	2326	1.43	this study
coke-oven gases SMR	134	-	19.2	338	1.37	[132]
vacuum residue gasification	-	-	0.3	288	1.25	[133]
biomass gasification	525	0.51*	-	1183	-	[91]
hydrogenation of captured carbon	1750	0.60*	8.7	396	0.02	[90]
green hydrogen and captured CO_2	4	0.60*	41.1	960	-	[92]
biogas steam reforming	20	0.78*	2.0	379	1.37	[134]
electrochemical reduction of CO_2	17.5	-	100.8	423	5.55	[135]
combined tri and dry CH_4 reforming	629	-	60.3	434	0.01	[89]
shale gas partial oxidation/SMR	3500	-	4.0-13.7	240-369	12.5-19.8	[127]

*Calculated using Equation 15, where the F_{feed} is the process feed and not the MeOH reactor feed.

Chapter 4

Conclusions

In this thesis, the process design of indirect methanol production via dry reforming of methane was investigated. Three scenarios for the DMR were studied regarding the way of reactor heating, as well as the feed used. In the first two scenarios captured carbon dioxide and methane where used as a feed to the DMR reactor, while in the third one desulfurized biogas was combined with captured CO_2 and inserted as a feed. In the first case study a thermocatalytic, fossil-based heated DMR reactor, was considered, while in the other two cases the employed DMR reactor was heated by microwaves. Following, the syngas, produced in either of the three ways, was combined with hydrogen, produced from water electrolysis, and inserted into the methanol synthesis reactor. The produced methanol was downstream purified. These processes were modeled in Aspen Plus V11 software and later on the optimization, heat integration, techno-economic evaluation and carbon emissions' calculation were carried out. Overall, all the scenarios resulted in a high yield, feasible energy demand and viable carbon emissions, compared to other methods found in literature. On the other hand, the total product cost of methanol was around 5 times more than today's market prices (1874-2326 eur/tonne compared to approximately 400 eur/tonne), leading to non-profitability and net loss (negative economic potential and consequently net present value in all the cases). In order to lower the total cost, two main categories of changes could be investigated: adjustments in the processes and alterations in the economy.

Regarding the first category, future studies could research the following:

- Reduction of purge stream and utilization of the off gases and waste

water produced rather than entering the environment.

- Development of carbon capture, water electrolysis, electricity generation and biomethanol production technologies in order to self produce the raw materials and utilities needed and interfere the processes to lower the overall cost
- Energy demand reduction by applying a better heat integration than the one proposed and by taking advantage of others streams' energy load coming from this unit or other units of the plant.
- Increase the unit's capacity, according to the economies of scale, which, as indicated in the Viability Chapter, can result to profitability.
- Employment of new techniques for methanol synthesis (e.g., reactor and catalyst) in order to improve the CO conversion resulting in less purged gases, smaller size of the reactor and lower CO2 emissions.

Although this project did not appear to be profitable in today's economy, there is some potential for it to become feasible in the next decades. European Union has made a commitment to invest into renewable energy sources, waste management, industrial electrification and decarbonization and generally "green" technologies that will eventually lead to zero net emissions in the next 30 years. Electricity can be generated by RES resulting in lower cost, viability and significantly lower carbon emissions compared to the conventional fossil based generation. Hydrogen can be produced from electrolysis, with extremely low carbon footprint and a price that can reach the 1 euro per kg, considering the utilization of renewable electricity and also the EU's funding. Carbon Capture and Utilization has the potential to become even more lucrative, given that the studies for the CCU technology are constantly increasing and also that the taxation of carbon emissions is expected to rise enormously. Furthermore, methane could be obtained from bio-sources such as biogas and landfill gas resulting to a twofold advantage: management of waste and utilization of low or zero cost raw materials. In addition, methanol demand, and consequently its price, is expected to rise significantly in the next years, due to the many uses that it has in various fields and also due to the capability of e- and bio- production. Today, methanol is produced by thermocatalytic pathways based on fossil resources, while the production cost varies between 100 and 450 eur/ton, depending on the feed, the processes and the capacity of the installation. Bearing in mind the reduction

of hydrogen and electricity cost and the increased carbon emission tax that may be imposed in the future, the proposed method of methanol production may compete with conventional state-of-the-art thermocatalytic processes, which are very carbon intensive. Considering the objectives to limit carbon emissions during the production of methanol, the comparison of the proposed processes with existing industrial methods should be done not only on an economic basis, but also on an environmental one, with the conduction of Life Cycle Analysis and the determination of various indicators regarding the effects on the human health and the society. Apart from the prices of the raw materials, the utilities and the final product, a significant cost driver for the proposed method is the integration of microwaves into the industrial processes. In order to scale-up the laboratory findings and create MW-assisted reactors that are competitive to the conventional thermocatalytic reactors, it is essential to develop power sources of high output (>100 kW for microwave plasma), to design reactors that are efficiently powered by multiple generators, to develop materials for the reactor's construction and catalysts that are suitable for the microwave processes and also low-cost and generally to improve the stability and the overall reliability of the MW plasma processes.

All in all more studies need to be conducted in order to optimize the processes proposed even more, in terms of efficiency, energy consumption, total cost and environmental impacts. The future must become "greener" which means that the industries, the research centers and the governments worldwide need to collaborate and act fast and efficiently.

Chapter 5

Bibliography

[1] *Putting CO2 to Use – Analysis*. en-GB. 2019. URL: https://www.iea.org/reports/putting-co2-to-use (visited on 08/23/2023).

[2] Mohd Hanifa et al. "A review on CO2 capture and sequestration in the construction industry: Emerging approaches and commercialised technologies". In: *Journal of CO2 Utilization* 67 (Jan. 2023), p. 102292. ISSN: 2212-9820. DOI: 10.1016/j.jcou.2022.102292.

[3] *World Emissions Clock*. URL: https://worldemissions.io/ (visited on 08/23/2023).

[4] *A European Green Deal*. en. July 2021. URL: https://commission.europa.eu/strategy-and-policy/priorities-2019-2024/european-green-deal_en (visited on 08/25/2023).

[5] *Industry and the Green Deal*. en. URL: https://commission.europa.eu/strategy-and-policy/priorities-2019-2024/european-green-deal/industry-and-green-deal_en (visited on 08/25/2023).

[6] *Outlook for biogas and biomethane: Prospects for organic growth – Analysis*. en-GB. URL: https://www.iea.org/reports/outlook-for-biogas-and-biomethane-prospects-for-organic-growth (visited on 08/28/2023).

[7] Francesco Dalena et al. "Chapter 1 - Methanol Production and Applications: An Overview". In: *Methanol*. Ed. by Angelo Basile and Francesco Dalena. Elsevier, Jan. 2018, pp. 3–28. ISBN: 978-0-444-63903-5. DOI: 10.1016/B978-0-444-63903-5.00001-7.

[8] Jörg Ott et al. “Methanol”. en. In: *Ullmann’s Encyclopedia of Industrial Chemistry*. Ed. by Wiley-VCH. 1st ed. Wiley, Oct. 2012. ISBN: 978-3-527-30385-4 978-3-527-30673-2. DOI: 10.1002/14356007.a16_465.pub3.

[9] Sebastian Verhelst et al. “Methanol as a fuel for internal combustion engines”. In: *Progress in Energy and Combustion Science* 70 (Jan. 2019), pp. 43–88. ISSN: 0360-1285. DOI: 10.1016/j.pecs.2018.10.001.

[10] *The Methanol Industry*. en-US. URL: https://www.methanol.org/the-methanol-industry/ (visited on 08/26/2023).

[11] IRENA. “Innovation Outlook: Renewable Methanol”. en. In: ().

[12] Xudong Zhen and Yang Wang. “An overview of methanol as an internal combustion engine fuel”. In: *Renewable and Sustainable Energy Reviews* 52 (Dec. 2015), pp. 477–493. ISSN: 1364-0321. DOI: 10.1016/j.rser.2015.07.083.

[13] Francesco Dalena et al. “Advances in Methanol Production and Utilization, with Particular Emphasis toward Hydrogen Generation via Membrane Reactor Technology”. In: *Membranes* 8.4 (Oct. 2018), p. 98. ISSN: 2077-0375. DOI: 10.3390/membranes8040098.

[14] *Hydrogen Production: Natural Gas Reforming*. en. URL: https://www.energy.gov/eere/fuelcells/hydrogen-production-natural-gas-reforming (visited on 08/26/2023).

[15] T. T.Phuong Pham et al. “Microwave-assisted dry reforming of methane for syngas production: a review”. In: *Environmental Chemistry Letters* 18.6 (Nov. 2020), pp. 1987–2019. ISSN: 1610-3653. DOI: 10.1007/s10311-020-01055-0.

[16] John Crelling and Hans Hagemann. “Coal”. en. In: *Ullmann’s Encyclopedia of Industrial Chemistry*. Ed. by Wiley-VCH. 1st ed. Wiley, Oct. 2012. ISBN: 978-3-527-30385-4 978-3-527-30673-2. DOI: 10.1002/14356007.a07153.pub2.

[17] Evangelos Delikonstantis et al. “An assessment of electrified methanol production from an environmental perspective”. en. In: *Green Chemistry* 23.18 (2021). Publisher: Royal Society of Chemistry, pp. 7243–7258. DOI: 10.1039/D1GC01730F.

[18] Ignacio de Dios García, Andrzej Stankiewicz, and Hakan Nigar. "Syngas production via microwave-assisted dry reforming of methane". In: *Catalysis Today*. 1st International Conference on Unconventional Catalysis, Reactors and Applications: Catalysis Beyond the Reactor 362 (Feb. 2021), pp. 72–80. ISSN: 0920-5861. DOI: 10.1016/j.cattod.2020.04.045.

[19] Evangelos Delikonstantis, Marco Scapinello, and Georgios D. Stefanidis. "Investigating the Plasma-Assisted and Thermal Catalytic Dry Methane Reforming for Syngas Production: Process Design, Simulation and Evaluation". en. In: *Energies* 10.9 (Sept. 2017). Number: 9 Publisher: Multidisciplinary Digital Publishing Institute, p. 1429. ISSN: 1996-1073. DOI: 10.3390/en10091429.

[20] Lalit S. Gangurde et al. "Synthesis, characterization, and application of ruthenium-doped SrTiO3 perovskite catalysts for microwave-assisted methane dry reforming". In: *Chemical Engineering and Processing - Process Intensification* 127 (May 2018), pp. 178–190. ISSN: 0255-2701. DOI: 10.1016/j.cep.2018.03.024.

[21] Peter Sorknæs et al. "Electrification of the industrial sector in 100% renewable energy scenarios". In: *Energy* 254 (Sept. 2022), p. 124339. ISSN: 0360-5442. DOI: 10.1016/j.energy.2022.124339.

[22] *Electrification - Energy System*. en-GB. URL: https://www.iea.org/energy-system/electricity/electrification (visited on 08/27/2023).

[23] Javier F de la Fuente et al. "Microwave plasma emerging technologies for chemical processes". en. In: *Journal of Chemical Technology & Biotechnology* 92.10 (2017), pp. 2495–2505. ISSN: 1097-4660. DOI: 10.1002/jctb.5205.

[24] Lalit S. Gangurde et al. "Complexity and Challenges in Noncontact High Temperature Measurements in Microwave-Assisted Catalytic Reactors". In: *Industrial & Engineering Chemistry Research* 56.45 (Nov. 2017). Publisher: American Chemical Society, pp. 13379–13391. ISSN: 0888-5885. DOI: 10.1021/acs.iecr.7b02091.

[25] Peter Priecel and Jose Antonio Lopez-Sanchez. "Advantages and Limitations of Microwave Reactors: From Chemical Synthesis to the Catalytic Valorization of Biobased Chemicals". In: *ACS Sustainable Chem-*

istry & Engineering 7.1 (Jan. 2019). Publisher: American Chemical Society, pp. 3–21. DOI: 10.1021/acssuschemeng.8b03286.

[26] A. Domínguez et al. "Biogas to Syngas by Microwave-Assisted Dry Reforming in the Presence of Char". In: *Energy & Fuels* 21.4 (July 2007). Publisher: American Chemical Society, pp. 2066–2071. ISSN: 0887-0624. DOI: 10.1021/ef070101j.

[27] A. Domínguez et al. "Microwave-assisted catalytic decomposition of methane over activated carbon for CO2-free hydrogen production". In: *International Journal of Hydrogen Energy* 32.18 (Dec. 2007), pp. 4792–4799. ISSN: 0360-3199. DOI: 10.1016/j.ijhydene.2007.07.041.

[28] B. Fidalgo et al. "Microwave-assisted dry reforming of methane". In: *International Journal of Hydrogen Energy* 33.16 (Aug. 2008), pp. 4337–4344. ISSN: 0360-3199. DOI: 10.1016/j.ijhydene.2008.05.056.

[29] B. Fidalgo and J. A. Menéndez. "Study of energy consumption in a laboratory pilot plant for the microwave-assisted CO2 reforming of CH4". In: *Fuel Processing Technology* 95 (Mar. 2012), pp. 55–61. ISSN: 0378-3820. DOI: 10.1016/j.fuproc.2011.11.012.

[30] B. Fidalgo, A. Arenillas, and J. A. Menéndez. "Influence of porosity and surface groups on the catalytic activity of carbon materials for the microwave-assisted CO2 reforming of CH4". In: *Fuel* 89.12 (Dec. 2010), pp. 4002–4007. ISSN: 0016-2361. DOI: 10.1016/j.fuel.2010.06.015.

[31] Taiwo Odedairo et al. "Influences of doping Cr/Fe/Ta on the performance of Ni/CeO2 catalyst under microwave irradiation in dry reforming of CH4". In: *Journal of Solid State Chemistry* 233 (Jan. 2016), pp. 166–177. ISSN: 0022-4596. DOI: 10.1016/j.jssc.2015.10.025.

[32] Fusen Zhang et al. "Factors influencing CH4CO2 reforming reaction over Fe catalyst supported on foam ceramics under microwave irradiation". In: *International Journal of Hydrogen Energy* 43.20 (May 2018), pp. 9495–9502. ISSN: 0360-3199. DOI: 10.1016/j.ijhydene.2018.03.171.

[33] Oscar H. Ojeda-Niño, Francisco Gracia, and Carlos Daza. "Role of Pr on Ni–Mg–Al Mixed Oxides Synthesized by Microwave-Assisted Self-Combustion for Dry Reforming of Methane". In: *Industrial &*

Engineering Chemistry Research 58.19 (May 2019). Publisher: American Chemical Society, pp. 7909–7921. ISSN: 0888-5885. DOI: 10.1021/acs.iecr.9b00557.

[34] B. Fidalgo, A. Arenillas, and J. A. Menéndez. "Mixtures of carbon and Ni/Al2O3 as catalysts for the microwave-assisted CO2 reforming of CH4". In: *Fuel Processing Technology* 92.8 (Aug. 2011), pp. 1531–1536. ISSN: 0378-3820. DOI: 10.1016/j.fuproc.2011.03.015.

[35] Jose M. Bermudez et al. "Mixtures of Steel-Making Slag and Carbons as Catalyst for Microwave-Assisted Dry Reforming of CH4". In: *Chinese Journal of Catalysis* 33.7 (July 2012), pp. 1115–1118. ISSN: 1872-2067. DOI: 10.1016/S1872-2067(11)60386-0.

[36] Longzhi Li et al. "Methane dry and mixed reforming on the mixture of bio-char and nickel-based catalyst with microwave assistance". In: *Journal of Analytical and Applied Pyrolysis* 125 (May 2017), pp. 318–327. ISSN: 0165-2370. DOI: 10.1016/j.jaap.2017.03.009.

[37] Longzhi Li et al. "Methane dry reforming with microwave heating over carbon-based catalyst obtained by agriculture residues pyrolysis". In: *Journal of CO2 Utilization* 28 (Dec. 2018), pp. 41–49. ISSN: 2212-9820. DOI: 10.1016/j.jcou.2018.09.010.

[38] Longzhi Li et al. "Performance of bio-char and energy analysis on CH4 combined reforming by CO2 and H2O into syngas production with assistance of microwave". In: *Fuel* 215 (Mar. 2018), pp. 655–664. ISSN: 0016-2361. DOI: 10.1016/j.fuel.2017.11.107.

[39] Longzhi Li et al. "Fe-rich biomass derived char for microwave-assisted methane reforming with carbon dioxide". In: *Science of The Total Environment* 657 (Mar. 2019), pp. 1357–1367. ISSN: 0048-9697. DOI: 10.1016/j.scitotenv.2018.12.097.

[40] Rahul Kadam and N. L. Panwar. "Recent advancement in biogas enrichment and its applications". In: *Renewable and Sustainable Energy Reviews* 73 (June 2017), pp. 892–903. ISSN: 1364-0321. DOI: 10.1016/j.rser.2017.01.167.

[41] Matthew J. Palys and Prodromos Daoutidis. "Power-to-X: A review and perspective". In: *Computers & Chemical Engineering* 165 (Sept. 2022), p. 107948. ISSN: 0098-1354. DOI: 10.1016/j.compchemeng.

2022.107948. URL: https://www.sciencedirect.com/science/article/pii/S009813542200285X (visited on 08/28/2023).

[42] Irini Angelidaki et al. "Biogas upgrading and utilization: Current status and perspectives". In: *Biotechnology Advances* 36.2 (Mar. 2018), pp. 452–466. ISSN: 0734-9750. DOI: 10.1016/j.biotechadv.2018.01.011.

[43] Olumide Wesley Awe et al. "Laboratory-scale investigation of the removal of hydrogen sulfide from biogas and air using industrial waste-based sorbents". In: *Journal of Environmental Chemical Engineering* 5.2 (Apr. 2017), pp. 1809–1820. ISSN: 2213-3437. DOI: 10.1016/j.jece.2017.03.023.

[44] James G. Speight. "3 - Unconventional gas". In: *Natural Gas (Second Edition)*. Ed. by James G. Speight. Boston: Gulf Professional Publishing, Jan. 2019, pp. 59–98. ISBN: 978-0-12-809570-6. DOI: 10.1016/B978-0-12-809570-6.00003-5.

[45] Gerhard Rettenberger. "Chapter 9.4 - Utilization of Landfill Gas and Safety Measures". In: *Solid Waste Landfilling*. Ed. by Raffaello Cossu and Rainer Stegmann. Elsevier, Jan. 2018, pp. 463–476. ISBN: 978-0-12-818336-6. DOI: 10.1016/B978-0-12-407721-8.00023-1.

[46] Francois Pouliquen et al. "Hydrogen Sulfide". en. In: *Ullmann's Encyclopedia of Industrial Chemistry*. John Wiley & Sons, Ltd, 2000. ISBN: 978-3-527-30673-2.

[47] Fabiano Bisinella Scheufele et al. "Mathematical modeling of low-pressure H2S adsorption by babassu biochar in fixed bed column". In: *Journal of Environmental Chemical Engineering* 9.1 (Feb. 2021), p. 105042. ISSN: 2213-3437. DOI: 10.1016/j.jece.2021.105042.

[48] Abhimanyu Pudi et al. "Hydrogen sulfide capture and removal technologies: A comprehensive review of recent developments and emerging trends". In: *Separation and Purification Technology* 298 (Oct. 2022), p. 121448. ISSN: 1383-5866. DOI: 10.1016/j.seppur.2022.121448.

[49] H. Pourzolfaghar and M. H. S. Ismail. "Study of H2S Removal Efficiency of Virgin Zeolite in POME Biogas Desulfurization at Ambient Temperature and Pressure". en. In: *Developments in Sustainable Chemical and Bioprocess Technology*. Ed. by Ravindra Pogaku, Awang

Bono, and Christopher Chu. Boston, MA: Springer US, 2013, pp. 295–301. ISBN: 978-1-4614-6208-8. DOI: 10.1007/978-1-4614-6208-8_35.

[50] Waseem Ahmad et al. "Hydrogen sulfide removal using diatomite". In: *AIP Conference Proceedings* 2124.1 (July 2019), p. 020005. ISSN: 0094-243X. DOI: 10.1063/1.5117065.

[51] Amvrosios G. Georgiadis et al. "Adsorption of Hydrogen Sulfide at Low Temperatures Using an Industrial Molecular Sieve: An Experimental and Theoretical Study". In: *ACS Omega* 6.23 (June 2021). Publisher: American Chemical Society, pp. 14774–14787. DOI: 10.1021/acsomega.0c06157. (Visited on 08/28/2023).

[52] Linda Barelli et al. "13X Ex-Cu zeolite performance characterization towards H2S removal for biogas use in molten carbonate fuel cells". In: *Energy* 160 (Oct. 2018), pp. 44–53. ISSN: 0360-5442. DOI: 10.1016/j.energy.2018.05.057.

[53] Piero Bareschino et al. "Biogas purification on Na-X Zeolite: Experimental and numerical results". In: *Chemical Engineering Science* 223 (Sept. 2020), p. 115744. ISSN: 0009-2509. DOI: 10.1016/j.ces.2020.115744.

[54] Soheil Bahraminia, Mansoor Anbia, and Esmat Koohsaryan. "Hydrogen sulfide removal from biogas using ion-exchanged nanostructured NaA zeolite for fueling solid oxide fuel cells". In: *International Journal of Hydrogen Energy* 45.55 (Nov. 2020), pp. 31027–31040. ISSN: 0360-3199. DOI: 10.1016/j.ijhydene.2020.08.091.

[55] Zehua Pan et al. "Regenerable Co-ZnO-based nanocomposites for high-temperature syngas desulfurization". In: *Fuel Processing Technology* 201 (May 2020), p. 106344. ISSN: 0378-3820. DOI: 10.1016/j.fuproc.2020.106344.

[56] Mengmeng Wu et al. "Mesoporous Zn-Fe-based binary metal oxide sorbent with sheet-shaped morphology: Synthesis and application for highly efficient desulfurization of hot coal gas". In: *Chemical Engineering Journal* 389 (June 2020), p. 123750. ISSN: 1385-8947. DOI: 10.1016/j.cej.2019.123750.

[57] Yongtae Ahn et al. "Removing hydrogen sulfide from a feed stream using suitable adsorbent materials". In: *Journal of Cleaner Production* 272 (Nov. 2020), p. 122849. ISSN: 0959-6526. DOI: 10.1016/j.jclepro.2020.122849.

[58] Chao Yang et al. "ZnFe2O4/activated carbon as a regenerable adsorbent for catalytic removal of H2S from air at room temperature". In: *Chemical Engineering Journal* 394 (Aug. 2020), p. 124906. ISSN: 1385-8947. DOI: 10.1016/j.cej.2020.124906.

[59] H.W. Ou et al. "Long-term evaluation of activated carbon as an adsorbent for biogas desulfurization". In: *Journal of the Air & Waste Management Association* 70.6 (June 2020). Publisher: Taylor & Francis _eprint: https://doi.org/10.1080/10962247.2020.1754305, pp. 641–648. ISSN: 1096-2247. DOI: 10.1080/10962247.2020.1754305.

[60] Nurul Noramelya Zulkefli et al. "Application of Response Surface Methodology for Preparation of ZnAC2/CAC Adsorbents for Hydrogen Sulfide (H2S) Capture". en. In: *Catalysts* 11.5 (May 2021). Number: 5 Publisher: Multidisciplinary Digital Publishing Institute, p. 545. ISSN: 2073-4344. DOI: 10.3390/catal11050545.

[61] Chao Yang et al. "Bifunctional ZnO-MgO/activated carbon adsorbents boost H2S room temperature adsorption and catalytic oxidation". In: *Applied Catalysis B: Environmental* 266 (June 2020), p. 118674. DOI: 10.1016/j.apcatb.2020.118674.

[62] Yankai Pan et al. "Two-dimensional CaO/carbon heterostructures with unprecedented catalytic performance in room-temperature H2S oxidization". In: *Applied Catalysis B: Environmental* 280 (Jan. 2021), p. 119444. ISSN: 0926-3373. DOI: 10.1016/j.apcatb.2020.119444.

[63] Lin Chen et al. "A regenerable N-rich hierarchical porous carbon synthesized from waste biomass for H2S removal at room temperature". In: *Science of The Total Environment* 768 (May 2021), p. 144452. ISSN: 0048-9697. DOI: 10.1016/j.scitotenv.2020.144452.

[64] Zhengfa Yu et al. "Nitrogen-doped mesoporous carbon nanosheets derived from metal-organic frameworks in a molten salt medium for efficient desulfurization". In: *Carbon* 117 (June 2017), pp. 376–382. ISSN: 0008-6223. DOI: 10.1016/j.carbon.2017.02.100.

[65] Minghui Sun et al. “Nitrogen-rich hierarchical porous carbon nanofibers for selective oxidation of hydrogen sulfide”. In: *Fuel Processing Technology* 191 (Aug. 2019), pp. 121–128. ISSN: 0378-3820. DOI: 10.1016/j.fuproc.2019.03.020.

[66] Yankai Pan et al. “Probing the room-temperature oxidative desulfurization activity of three-dimensional alkaline graphene aerogel”. In: *Applied Catalysis B: Environmental* 262 (Mar. 2020), p. 118266. ISSN: 0926-3373. DOI: 10.1016/j.apcatb.2019.118266.

[67] Nidhika Bhoria et al. “Functionalization effects on HKUST-1 and HKUST-1/graphene oxide hybrid adsorbents for hydrogen sulfide removal”. In: *Journal of Hazardous Materials* 394 (July 2020), p. 122565. ISSN: 0304-3894. DOI: 10.1016/j.jhazmat.2020.122565.

[68] Nishesh Kumar Gupta et al. “Fabrication of Cu(BDC)0.5(BDC-NH2)0.5 metal-organic framework for superior H2S removal at room temperature”. In: *Chemical Engineering Journal* 411 (May 2021), p. 128536. ISSN: 1385-8947. DOI: 10.1016/j.cej.2021.128536.

[69] Abolfazl Atash Jameh et al. “Synthesis and modification of Zeolitic Imidazolate Framework (ZIF-8) nanoparticles as highly efficient adsorbent for H2S and CO2 removal from natural gas”. In: *Journal of Environmental Chemical Engineering* 7.3 (June 2019), p. 103058. ISSN: 2213-3437. DOI: 10.1016/j.jece.2019.103058.

[70] Snezana Reljic et al. “Structural Deterioration of Well-Faceted MOFs upon H2S Exposure and Its Effect in the Adsorption Performance”. en. In: *Chemistry – A European Journal* 26.71 (2020), pp. 17110–17119. DOI: 10.1002/chem.202002473.

[71] Jitong Wang et al. “Polyethyleneimine-functionalized mesoporous carbon nanosheets as metal-free catalysts for the selective oxidation of H2S at room temperature”. In: *Applied Catalysis B: Environmental* 283 (Apr. 2021), p. 119650. ISSN: 0926-3373. DOI: 10.1016/j.apcatb.2020.119650.

[72] Georgia Basina et al. “Mesoporous silica “plated” copper hydroxides/oxides heterostructures as superior regenerable sorbents for low temperature H2S removal”. In: *Chemical Engineering Journal* 398 (Oct. 2020), p. 125585. ISSN: 1385-8947. DOI: 10.1016/j.cej.2020.125585.

[73] Chao Yang et al. “Facile and Versatile Sol–Gel Strategy for the Preparation of a High-Loaded ZnO/SiO2 Adsorbent for Room-Temperature H2S Removal”. In: *Langmuir* 35.24 (June 2019). Publisher: American Chemical Society, pp. 7759–7768. ISSN: 0743-7463. DOI: 10.1021/acs.langmuir.9b00853.

[74] Qiang Geng et al. “Room-temperature hydrogen sulfide removal with zinc oxide nanoparticle/molecular sieve prepared by melt infiltration”. In: *Fuel Processing Technology* 185 (Mar. 2019), pp. 26–37. ISSN: 0378-3820. DOI: 10.1016/j.fuproc.2018.11.013.

[75] Mirzokhid Abdirakhimov, Mohsen H. Al-Rashed, and Janusz Wójcik. “Recent Attempts on the Removal of H2S from Various Gas Mixtures Using Zeolites and Waste-Based Adsorbents”. en. In: *Energies* 15.15 (Jan. 2022). Number: 15 Publisher: Multidisciplinary Digital Publishing Institute, p. 5391. ISSN: 1996-1073. DOI: 10.3390/en15155391.

[76] Huanan Wu et al. “H2S adsorption by municipal solid waste incineration (MSWI) fly ash with heavy metals immobilization”. In: *Chemosphere* 195 (Mar. 2018), pp. 40–47. ISSN: 0045-6535. DOI: 10.1016/j.chemosphere.2017.12.068.

[77] Guofeng Shang et al. “Kinetics and mechanisms of hydrogen sulfide adsorption by biochars”. In: *Bioresource Technology* 133 (Apr. 2013), pp. 495–499. ISSN: 0960-8524. DOI: 10.1016/j.biortech.2013.01.114.

[78] Omid Jalalvandi et al. “Removal of H2S and Mercaptan from Outlet Gases of Kermanshah Refinery Using Modified Adsorbents (Bentonite and Sludge)”. en. In: *Iranian Journal of Oil and Gas Science and Technology* 8.2 (Apr. 2019). Publisher: Petroleum University of Technology, pp. 1–14. ISSN: 2345-2412. DOI: 10.22050/ijogst.2018.110934.1429.

[79] Muhammad Usman, W. M. A. Wan Daud, and Hazzim F. Abbas. “Dry reforming of methane: Influence of process parameters—A review”. In: *Renewable and Sustainable Energy Reviews* 45 (May 2015), pp. 710–744. ISSN: 1364-0321. DOI: 10.1016/j.rser.2015.02.026.

[80] P. G. Aguilera and F. J. Gutiérrez Ortiz. “Techno-economic assessment of biogas plant upgrading by adsorption of hydrogen sulfide on treated sewage–sludge”. In: *Energy Conversion and Management*

126 (Oct. 2016), pp. 411–420. ISSN: 0196-8904. DOI: 10.1016/j.enconman.2016.08.005.

[81] Robin Smith. *Chemical Process Design and Integration*. en. Wiley, 2005.

[82] Richard Turton. *Analysis Synthesis and Design of Chemical Processes*. Pearson Education, 2018.

[83] George D. Saravacos Maroulis Zacharias B. *Transport Properties of Foods*. Boca Raton: CRC Press, Apr. 2014. ISBN: 978-0-429-07973-3. DOI: 10.1201/9781482271010.

[84] Stanil Y. Ereev. "Standardized cost estimation for new technologies (SCENT) methodology and tool". English. In: *Journal of Business Chemistry* (2012).

[85] Ioannis Koukos. *INTRODUCTION TO CHEMICAL PLANT DESIGN*. TZIOLA, 2019. ISBN: 978-960-418-696-9.

[86] William L. Luyben. "Capital cost of compressors for conceptual design". In: *Chemical Engineering and Processing - Process Intensification* 126 (Apr. 2018), pp. 206–209. ISSN: 0255-2701. DOI: 10.1016/j.cep.2018.01.020.

[87] Antonio C. Caputo et al. "Economics of biomass energy utilization in combustion and gasification plants: effects of logistic variables". en. In: *Biomass and Bioenergy* 28.1 (Jan. 2005), pp. 35–51. ISSN: 09619534. DOI: 10.1016/j.biombioe.2004.04.009.

[88] Ebrahim Rezaei and Stephen Dzuryk. "Techno-economic comparison of reverse water gas shift reaction to steam and dry methane reforming reactions for syngas production". In: *Chemical Engineering Research and Design* 144 (Apr. 2019), pp. 354–369. ISSN: 0263-8762. DOI: 10.1016/j.cherd.2019.02.005.

[89] Mohammad Osat and Faryar Shojaati. "Techno-economic-environmental evaluation of a combined tri and dry reforming of methane for methanol synthesis with a high efficiency CO2 utilization". In: *International Journal of Hydrogen Energy* 47.14 (Feb. 2022), pp. 9058–9070. ISSN: 0360-3199. DOI: 10.1016/j.ijhydene.2021.12.207.

[90] Judit Nyári et al. "Techno-economic barriers of an industrial-scale methanol CCU-plant". In: *Journal of CO2 Utilization* 39 (July 2020), p. 101166. ISSN: 2212-9820. DOI: 10.1016/j.jcou.2020.101166.

[91] Zhihai Zhang et al. "Simulation and techno-economic assessment of bio-methanol production from pine biomass, biochar and pyrolysis oil". In: *Sustainable Energy Technologies and Assessments* 44 (Apr. 2021), p. 101002. ISSN: 2213-1388. DOI: 10.1016/j.seta.2021.101002.

[92] Stefano Sollai et al. "Renewable methanol production from green hydrogen and captured CO2: A techno-economic assessment". In: *Journal of CO2 Utilization* 68 (Feb. 2023), p. 102345. ISSN: 2212-9820. DOI: 10.1016/j.jcou.2022.102345.

[93] *Cost Indices – Towering Skills*. URL: https://toweringskills.com/financial-analysis/cost-indices/ (visited on 09/05/2023).

[94] Alain Chauvel, Gilles Fournier, and Claude Raimbault. *Manual of Process Economic Evaluation*. en. Editions TECHNIP, 2003. ISBN: 978-2-7108-0836-7.

[95] Igor L. Wiesberg et al. "Carbon dioxide management by chemical conversion to methanol: HYDROGENATION and BI-REFORMING". In: *Energy Conversion and Management*. Sustainable development of energy, water and environment systems for future energy technologies and concepts 125 (Oct. 2016), pp. 320–335. ISSN: 0196-8904. DOI: 10.1016/j.enconman.2016.04.041.

[96] *Cuo Zno Al2o3 Catalyst Price - Search - IndexBox*. en. URL: https://www.indexbox.io/search/cuo-zno-al2o3-catalyst-price/ (visited on 09/06/2023).

[97] Frederick G. Baddour et al. "Estimating Precommercial Heterogeneous Catalyst Price: A Simple Step-Based Method". en. In: *Organic Process Research & Development* 22.12 (Dec. 2018), pp. 1599–1605. ISSN: 1083-6160, 1520-586X. DOI: 10.1021/acs.oprd.8b00245.

[98] *USD to EUR Exchange Rate*. URL: https://www.bloomberg.com/quote/USDEUR:CUR (visited on 09/05/2023).

[99] *Executive summary – Global Hydrogen Review 2021 – Analysis*. en-GB. URL: https://www.iea.org/reports/global-hydrogen-review-2021/executive-summary (visited on 09/06/2023).

[100] This text provides general information Statista assumes no liability for the information given being complete or correct Due to varying update cycles and Statistics Can Display More up-to-Date Data Than Referenced in the Text. *Topic: Green hydrogen*. en. URL: https://www.statista.com/topics/7783/green-hydrogen/ (visited on 09/06/2023).

[101] *Europe: green hydrogen costs 2030*. en. URL: https://www.statista.com/statistics/1312286/europe-green-hydrogen-production-and-import-costs-2030/ (visited on 09/06/2023).

[102] *Imported hydrogen can beat EU production costs by 2030 - study — Reuters*. URL: https://www.reuters.com/business/energy/imported-hydrogen-can-beat-eu-production-costs-by-2030-study-2023-01-24/ (visited on 09/06/2023).

[103] *Hydrogen cost and sales prices — H2Valleys*. URL: https://h2v.eu/analysis/statistics/financing/hydrogen-cost-and-sales-prices (visited on 09/06/2023).

[104] William J. Schmelz, Gal Hochman, and Kenneth G. Miller. "Total cost of carbon capture and storage implemented at a regional scale: northeastern and midwestern United States". In: *Interface Focus* 10.5 (Aug. 2020). Publisher: Royal Society, p. 20190065. DOI: 10.1098/rsfs.2019.0065.

[105] *How much is captured CO2 worth? — MIT Climate Portal*. URL: https://climate.mit.edu/ask-mit/how-much-captured-co2-worth (visited on 09/06/2023).

[106] *EU-ETS carbon pricing 2023*. en. URL: https://www.statista.com/statistics/1322214/carbon-prices-european-union-emission-trading-scheme/ (visited on 09/06/2023).

[107] *EU carbon hits 100 euros taking cost of polluting to record high — Reuters*. URL: https://www.reuters.com/markets/carbon/europes-carbon-price-hits-record-high-100-euros-2023-02-21/ (visited on 09/06/2023).

[108] *Cost of carbon capture by approach or technology*. en. URL: https://www.statista.com/statistics/1304575/global-carbon-capture-cost-by-technology/ (visited on 09/06/2023).

[109] *United States Natural Gas Industrial Price (Dollars per Thousand Cubic Feet)*. URL: https://www.eia.gov/dnav/ng/hist/n3035us3m.htm (visited on 09/06/2023).

[110] *U.S. natural gas price for industry 2022*. en. URL: https://www.statista.com/statistics/1383403/us-industry-sector-average-natural-gas-price/ (visited on 09/06/2023).

[111] Jessies Birman. *Biogas Cost Reductions to Boost Sustainable Transport*. en. Mar. 2017. URL: https://www.irena.org/news/articles/2017/Mar/Biogas-Cost-Reductions-to-Boost-Sustainable-Transport (visited on 09/06/2023).

[112] Purwanta et al. "Techno-economic analysis of reactor types and biogas utilization schemes in thermophilic anaerobic digestion of sugarcane vinasse". In: *Renewable Energy* 201 (Dec. 2022), pp. 864–875. ISSN: 0960-1481. DOI: 10.1016/j.renene.2022.10.087.

[113] Alberto T. Penteado et al. "Techno-economic evaluation of a biogas-based oxidative coupling of methane process for ethylene production". en. In: *Frontiers of Chemical Science and Engineering* 12.4 (Dec. 2018), pp. 598–618. ISSN: 2095-0187. DOI: 10.1007/s11705-018-1752-5.

[114] *Executive summary – Electricity Market Report – Update 2023 – Analysis*. en-GB. URL: https://www.iea.org/reports/electricity-market-report-update-2023/executive-summary (visited on 09/06/2023).

[115] *European electricity prices fell significantly in May — GMK Center*. en-US. URL: https://gmk.center/en/posts/european-electricity-prices-fell-significantly-in-may/ (visited on 09/06/2023).

[116] *Electricity price Europe 2023 monthly*. en. URL: https://www.statista.com/statistics/1267500/eu-monthly-wholesale-electricity-price-country/ (visited on 09/06/2023).

[117] *Tax Depreciation*. en-US. URL: https://corporatefinanceinstitute.com/resources/accounting/tax-depreciation/ (visited on 09/07/2023).

[118] *Monthly methanol spot prices by region*. en. URL: https://www.statista.com/statistics/1323381/monthly-methanol-spot-prices-worldwide-by-region/ (visited on 09/09/2023).

[119] *Pricing*. en-CA. URL: https://www.methanex.com/about-methanol/pricing/ (visited on 09/09/2023).

[120] *Methanol - 2023 Data - 2014-2022 Historical - 2024 Forecast - Price - Quote - Chart*. URL: https://tradingeconomics.com/commodity/methanol (visited on 09/09/2023).

[121] *Methanol Price and Supply/Demand*. en-US. URL: https://www.methanol.org/methanol-price-supply-demand/ (visited on 09/09/2023).

[122] *Methanol price index - businessanalytiq*. URL: https://businessanalytiq.com/procurementanalytics/index/methanol-price-index/ (visited on 09/09/2023).

[123] Jake Stones. *EU Hydrogen Bank could bring renewable hydrogen costs below €1/kg*. en-US. URL: https://www.icis.com/explore/resources/news/2023/04/05/10873154/eu-hydrogen-bank-could-bring-renewable-hydrogen-costs-below-1-kg (visited on 09/06/2023).

[124] Harry Morgan (6318a5139c91e). *OPINION — Why market dynamics will reduce the average price of green hydrogen to $1.50/kg by 2030*. en. Section: energy_transition. Sept. 2022. URL: https://www.rechargenews.com/energy-transition/opinion-why-market-dynamics-will-reduce-the-average-price-of-green-hydrogen-to-1-50-kg-by-2030/2-1-1292801 (visited on 09/06/2023).

[125] Franziska Holz et al. "A 2050 perspective on the role for carbon capture and storage in the European power system and industry sector". In: *Energy Economics* 104 (Dec. 2021), p. 105631. ISSN: 0140-9883. DOI: 10.1016/j.eneco.2021.105631.

[126] Eero Vartiainen and Gaetan Masson. *PV LCOE in Europe 2014-30*. July 2015. DOI: 10.13140/RG.2.1.4669.5520.

[127] Laura M. Julián-Durán et al. "Techno-Economic Assessment and Environmental Impact of Shale Gas Alternatives to Methanol". In: *ACS Sustainable Chemistry & Engineering* 2.10 (Oct. 2014). Publisher: American Chemical Society, pp. 2338–2344. DOI: 10.1021/sc500330g.

[128] Jaroslaw Gracel and Piotr Łebkowski. "The Concept of Industry 4.0 Related Manufacturing Technology Maturity Model (Manutech Maturity Model, MTMM)". en. In: *Decision Making in Manufacturing and Services* 12 (2018), pp. 17–31. ISSN: 2300-7087. DOI: 10.7494/

dmms.2018.12.1-2.17. URL: https://journals.agh.edu.pl/dmms/article/view/2779 (visited on 09/14/2023).

[129] Fiona Harvey and Jennifer Rankin. "What is the European Green Deal and will it really cost €1tn?" en-GB. In: *The Guardian* (Mar. 2020). ISSN: 0261-3077. (Visited on 09/10/2023).

[130] *EU invests €3.6 billion of emissions trading revenues*. en. Text. URL: https://ec.europa.eu/commission/presscorner/detail/en/ip_23_3787 (visited on 09/10/2023).

[131] *Europe's one trillion climate finance plan — News — European Parliament*. en. Jan. 2020. URL: https://www.europarl.europa.eu/news/en/headlines/society/20200109STO69927/europe-s-one-trillion-climate-finance-plan (visited on 09/10/2023).

[132] Sunghoon Kim and Jiyong Kim. "The optimal carbon and hydrogen balance for methanol production from coke oven gas and Linz-Donawitz gas: Process development and techno-economic analysis". In: *Fuel* 266 (Apr. 2020), p. 117093. ISSN: 0016-2361. DOI: 10.1016/j.fuel.2020.117093. URL: https://www.sciencedirect.com/science/article/pii/S0016236120300880 (visited on 09/10/2023).

[133] Fayez Nasir Al-Rowaili et al. "Techno-economic evaluation of methanol production via gasification of vacuum residue and conventional reforming routes". In: *Chemical Engineering Research and Design* 177 (Jan. 2022), pp. 365–375. ISSN: 0263-8762. DOI: 10.1016/j.cherd.2021.11.004. URL: https://www.sciencedirect.com/science/article/pii/S0263876221004652 (visited on 09/10/2023).

[134] Riccardo Rinaldi et al. "Techno-economic analysis of a biogas-to-methanol process: Study of different process configurations and conditions". In: *Journal of Cleaner Production* 393 (Mar. 2023), p. 136259. ISSN: 0959-6526. DOI: 10.1016/j.jclepro.2023.136259. URL: https://www.sciencedirect.com/science/article/pii/S0959652623004171 (visited on 09/10/2023).

[135] Fangfang Li et al. "Energy, Cost, and Environmental Assessments of Methanol Production via Electrochemical Reduction of CO2 from Biosyngas". In: *ACS Sustainable Chemistry & Engineering* 11.7 (Feb. 2023). Publisher: American Chemical Society, pp. 2810–2818. DOI: 10.1021/acssuschemeng.2c05968. URL: https://doi.org/10.1021/acssuschemeng.2c05968 (visited on 09/11/2023).

Chapter 6

Appendix

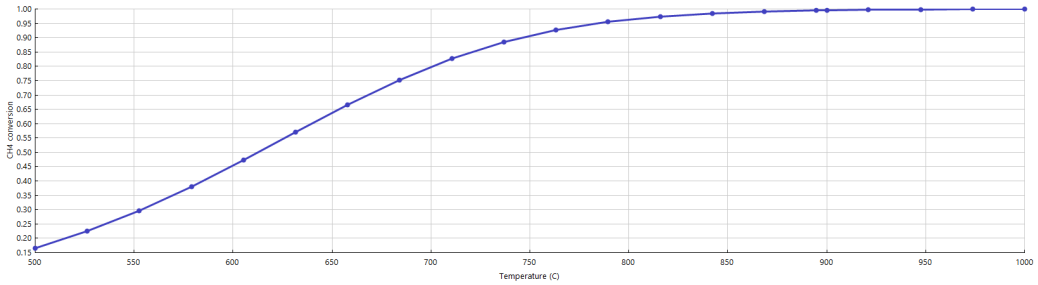

Figure 25: Sensitivity analysis using Aspen Plus (RGibbs unit) for the effect of temperature on CH_4 conversion in the Dry Methane Reforming reaction.

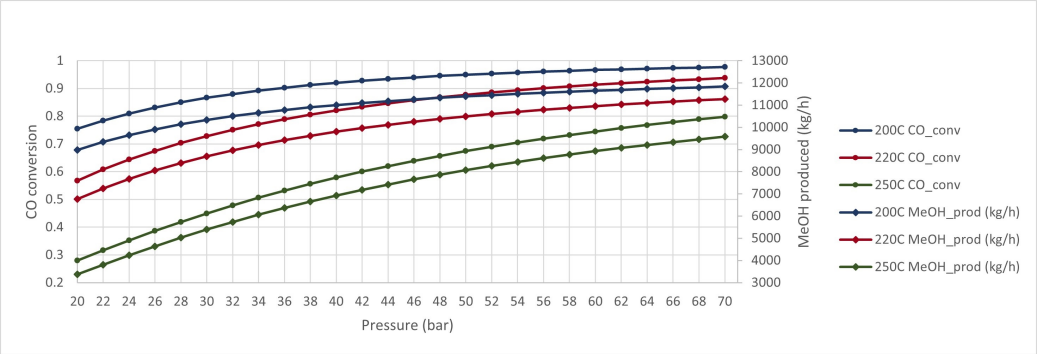

Figure 26: Sensitivity analysis using Aspen Plus for the effect of pressure on CO conversion in the methanol synthesis reactor.

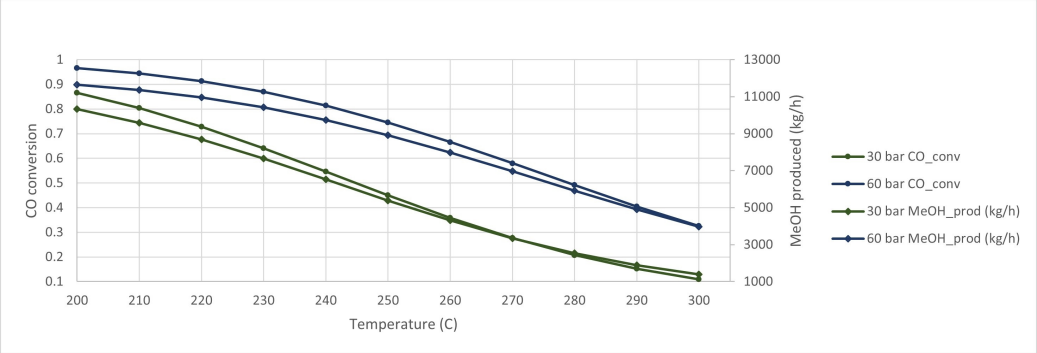

Figure 27: Sensitivity analysis using Aspen Plus for the effect of temperature on CO conversion in the methanol synthesis reactor.

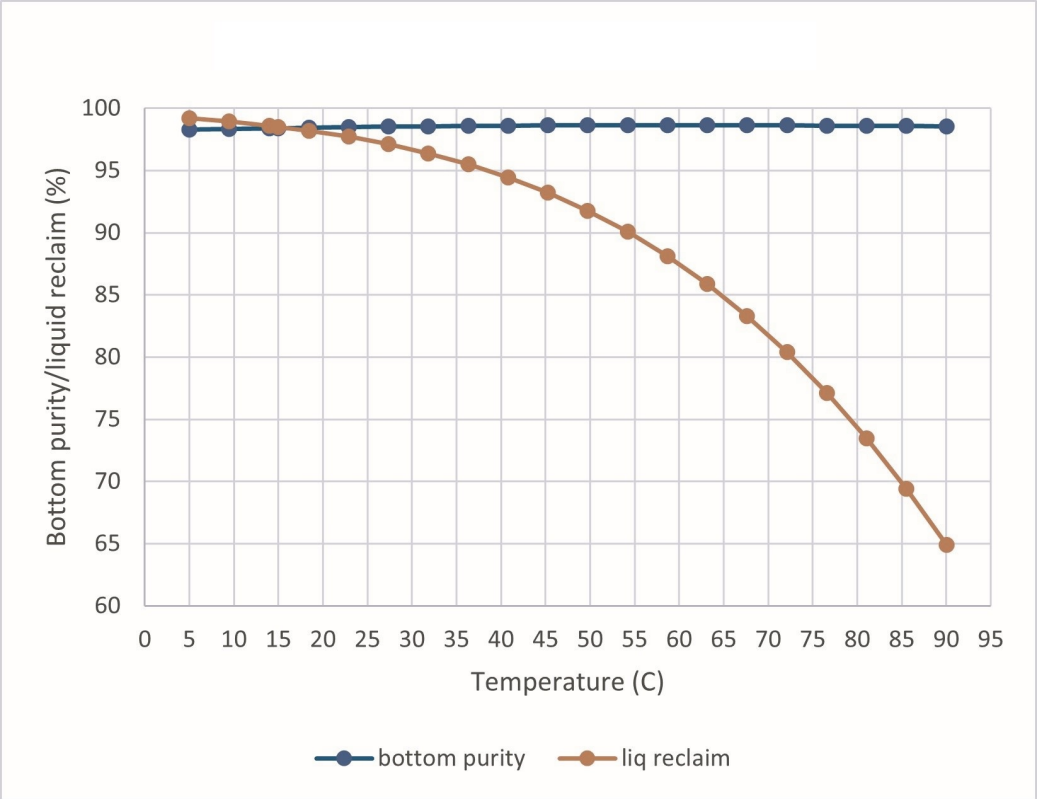

Figure 28: Sensitivity analysis using Aspen Plus at 35 bar, for the effect of temperature on methanol and water reclaim at the bottom of the Flash, as well as the bottom's purity in terms of the gaseous impurities.

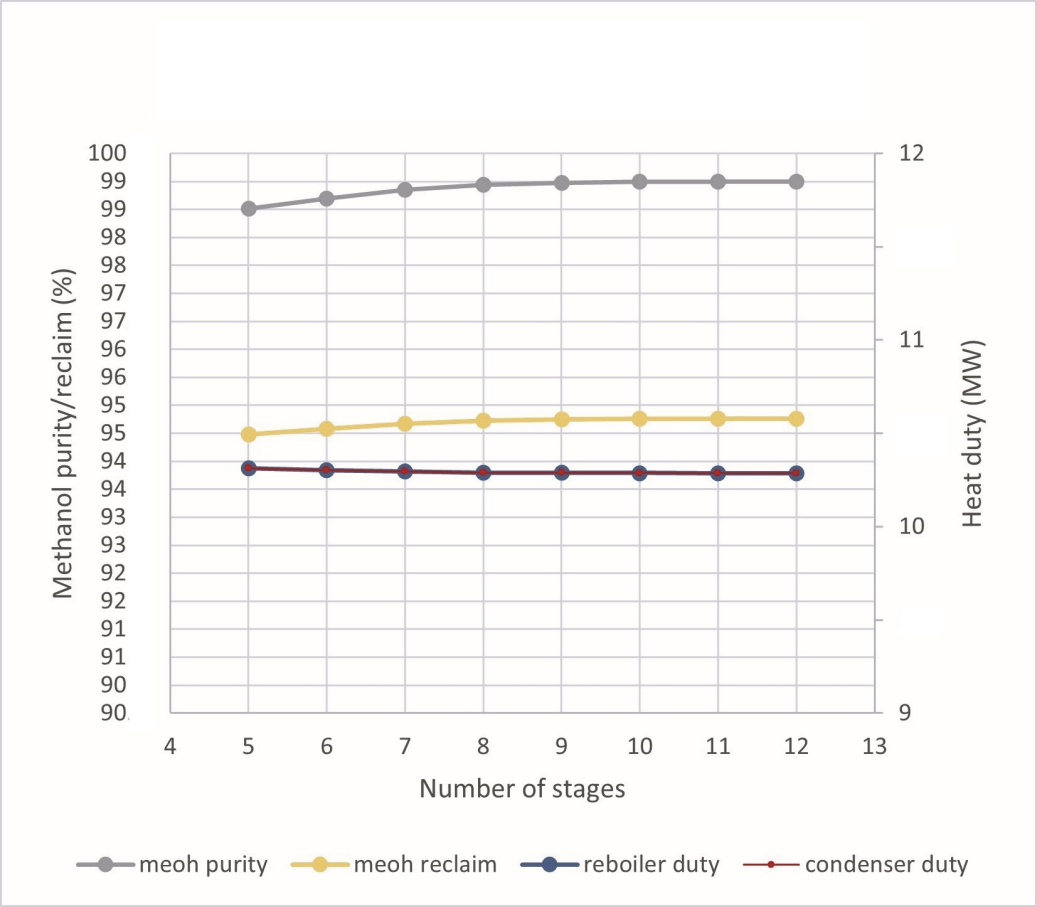

Figure 29: Sensitivity analysis using Aspen Plus for the effect of number of stages on methanol reclaim and purity, as well as the reboiler and condenser duty, keeping the reflux ratio at 1.6 and the distillate vapor fraction at 0.1.

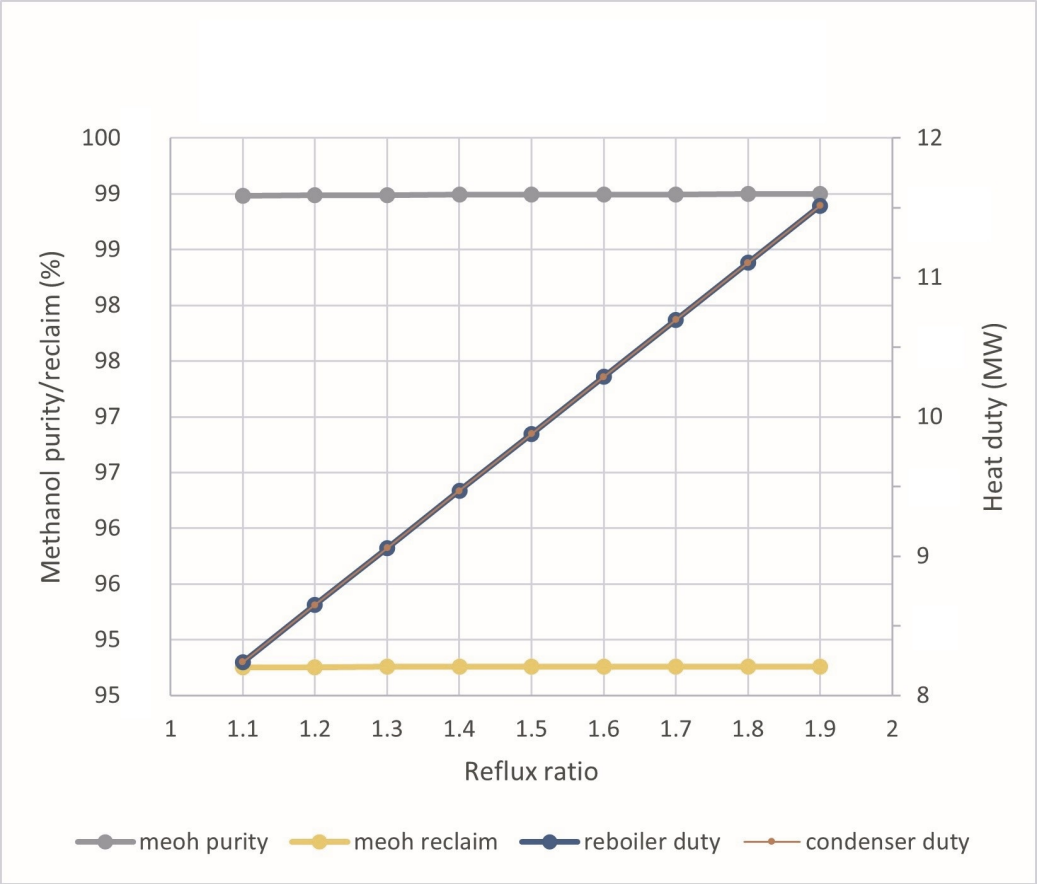

Figure 30: Sensitivity analysis using Aspen Plus for the effect of reflux ratio on methanol reclaim and purity, as well as the reboiler and condenser duty, keeping the number of stages at 11 and the distillate vapor fraction at 0.1.

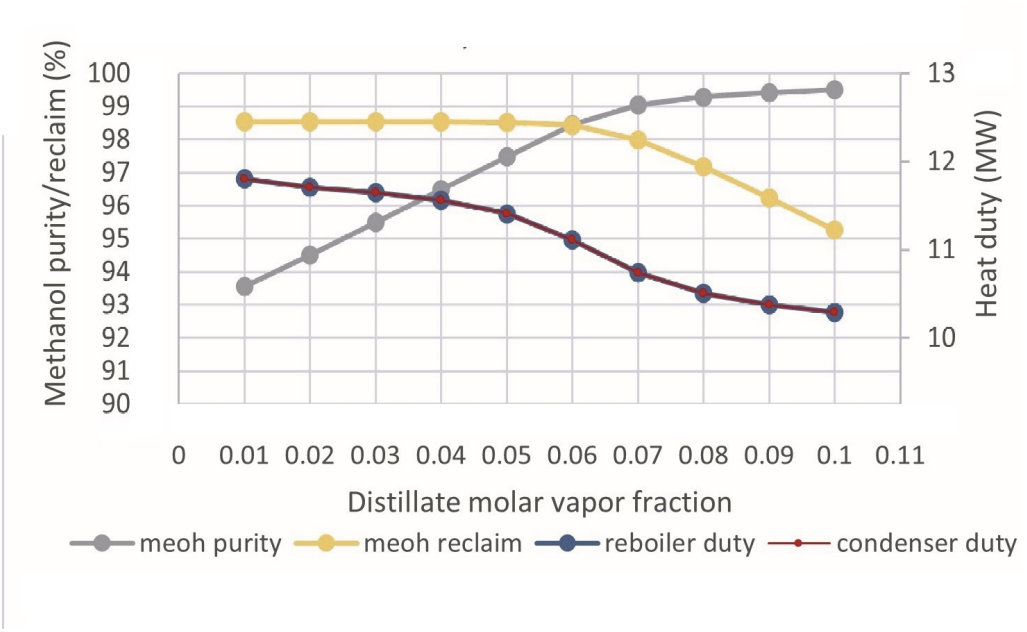

Figure 31: Sensitivity analysis using Aspen Plus for the effect of the distillate vapor fraction on methanol reclaim and purity, as well as the reboiler and condenser duty, keeping the number of stages at 11 and the reflux ratio at 1.6.

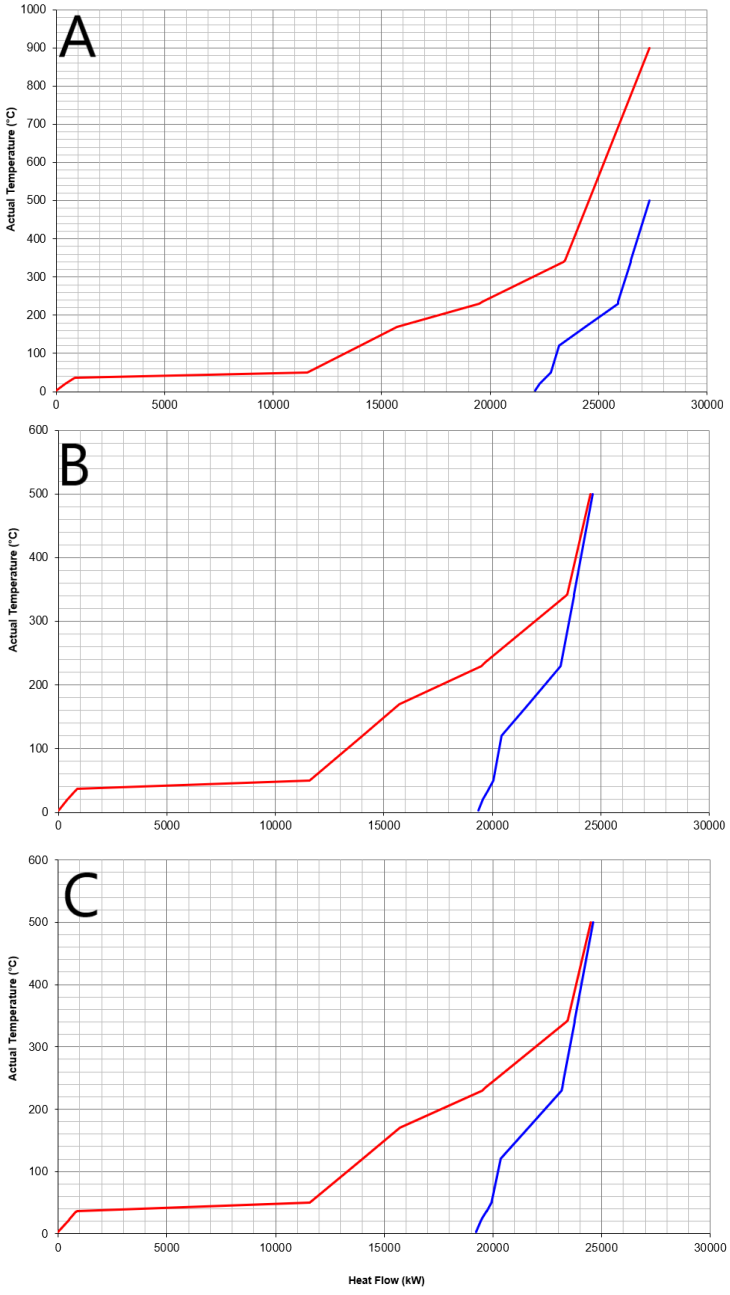

Figure 32: Hot and Cold Composite Curves for the three case studies. (A): conventional DMR heating, (B): MW-assisted DMR and (C): MW-assisted DMR with biogas feed. With red appears the hot composite stream, while with blue the cold.

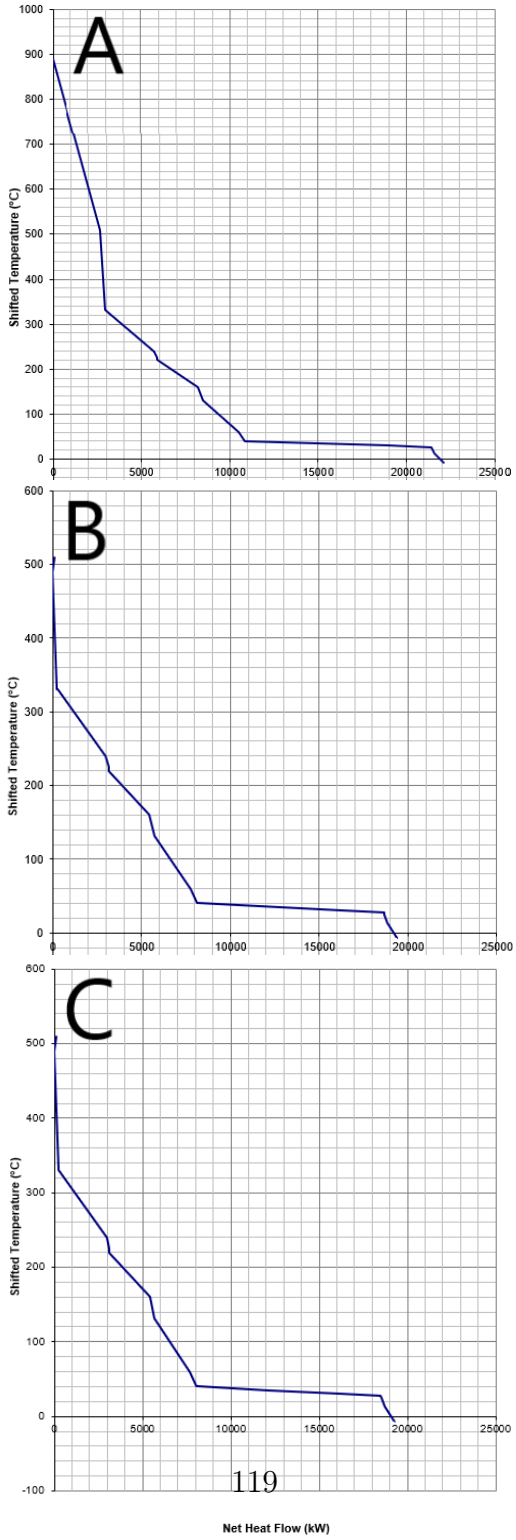

Figure 33: Grand Composite Curves for the three case studies.

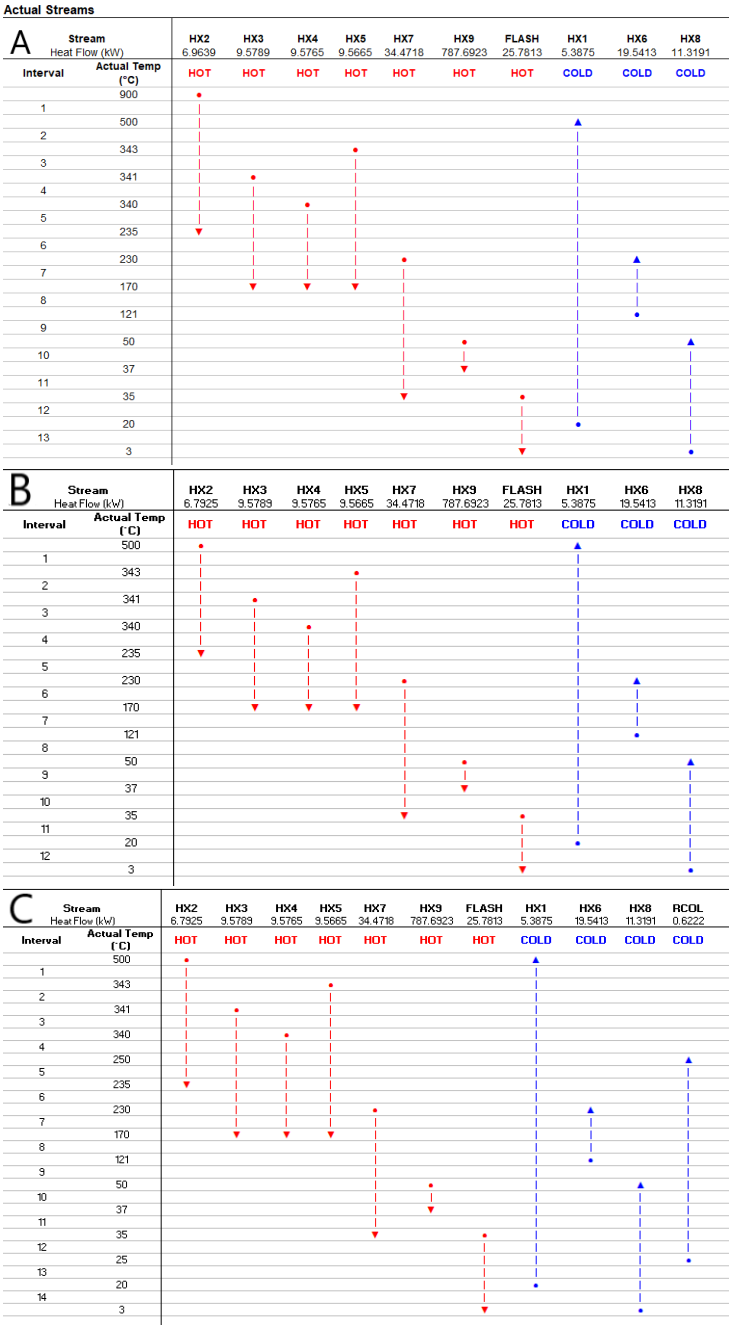

Figure 34: Grid Diagrams for the three case studies. (A): conventional DMR heating, (B): MW-assisted DMR and (C): MW-assisted DMR with biogas feed.

Table 21: Mass balances and conditions of the main streams of the three case studies, extracted from Aspen Plus.

Streams	S0	S1	S2	S3	S4	S5	S6	S7	S8	S9	S10	S11
Phase		Vapor	Vapor	Vapor	Vapor	Vapor	Vapor	Vapor	Liquid	Liquid	Vapor	Liquid
Temperature (°C)	20.0	500.0	170.00	230	230	3	3	3	3	37.25	37.25	69.33
Pressure (bar)	1.0	1.0	1	35	35	35	35	35	35	1	1	1
Mole Fractions												
CH_4	0.00	0.45	0.00	0.01	0.02	0.02	0.02	0.02	0.00	0.00	0.01	0.00
CO_2	0.00	0.55	0.04	0.11	0.16	0.18	0.18	0.18	0.07	0.00	0.67	0.00
CO	0.00	0.00	0.32	0.34	0.27	0.36	0.36	0.36	0.00	0.00	0.02	0.00
H_2	0.00	0.00	0.64	0.54	0.33	0.44	0.44	0.44	0.00	0.00	0.01	0.00
H_2O	0.00	0.00	0.00	0.00	0.00	0.00	0.00	0.00	0.01	0.00	0.00	0.32
biogas (20 ppm H_2S)	1.00	0.00	0.00	0.00	0.00	0.00	0.00	0.00	0.00	0.00	0.00	0.00
MeOH	0.00	0.00	0.00	0.00	0.22	0.00	0.00	0.00	0.92	0.99	0.31	0.68
Mass Flows (ktn/y)	43.80	114.5	120.7	305.8	305.8	199.0	13.9	185.0	106.8	93.0	11.8	1.8
CH_4	0.0	26.3	0.3	3.4	3.4	3.4	0.2	3.1	0.0	0.0	0.0	0.0
CO_2	0.0	88.2	16.8	94.2	93.2	83.2	5.8	77.4	10.0	0.4	9.4	0.0
CO	0.0	0.0	90.9	186.5	102.9	102.8	7.2	95.6	0.1	0.0	0.1	0.0
H_2	0.0	0.0	12.8	21.2	9.0	9.0	0.6	8.4	0.0	0.0	0.0	0.0
H_2O	0.0	0.0	0.0	0.0	0.4	0.0	0.0	0.0	0.4	0.0	0.0	0.4
biogas (20 ppm H_2S)	43.8	0.0	0.0	0.0	0.0	0.0	0.0	0.0	0.0	0.0	0.0	0.0
MeOH	0.0	0.0	0.0	0.5	96.8	0.6	0.0	0.5	96.3	92.6	2.3	1.4
Mass Fractions												
CH_4	0.00	0.23	0.00	0.01	0.01	0.02	0.02	0.02	0.00	0.00	0.00	0.00
CO_2	0.00	0.77	0.14	0.31	0.30	0.42	0.42	0.42	0.09	0.01	0.74	0.00
CO	0.00	0.00	0.75	0.61	0.34	0.52	0.52	0.52	0.00	0.00	0.01	0.00
H_2	0.00	0.00	0.11	0.07	0.03	0.05	0.05	0.05	0.00	0.00	0.00	0.00
H_2O	0.00	0.00	0.00	0.00	0.00	0.00	0.00	0.00	0.00	0.00	0.00	0.21
biogas (20 ppm H_2S)	1.00	0.00	0.00	0.00	0.00	0.00	0.00	0.00	0.00	0.00	0.00	0.00
MeOH	0.00	0.00	0.00	0.00	0.32	0.00	0.00	0.00	0.90	0.99	0.25	0.79
Volume Flow (m^3/h)	5640.0	26717.1	59853.1	2695.1	1832.5	755.5	52.9	702.6	14.6	13.5	932.6	0.3

Table 22: Global warming potential expressed in kg_{CO_2-eq}/kg_{MeOH}, for every component of each category (raw materials, utilities, waste, direct emissions) of each case study, using the Ecoinvent 3.9.1 (12/2022) database and the CML v4.8 2016 no LT method.

	global warming potential - GWP100 (kg_{CO_2-eq}/kg_{MeOH})		
	CS1	CS2	CS3
Raw materials			
biogas (from anaerobic digestion)	-	-	0.16
hydrogen (from water electrolysis)	0.11	0.11	0.11
carbon dioxide	0.00	0.00	0.00
methane (from natural gas)	0.17	0.17	-
total	0.28	0.28	0.27
Utilities			
electricity	0.01	0.02	0.02
steam (high pressure)	0.46	0.46	0.46
natural gas (furnace)	0.52	-	-
cooling water	0.00	0.00	0.00
refrigerant (R-134a)	0.56	0.56	0.56
total	1.55	1.04	1.04
Waste			
hydrogen sulfide	-	-	0.00
wastewater	0.00	0.00	0.00
total	0.00	0.00	0.01
Direct emissions			
carbon dioxide	0.10	0.10	0.10
Total	1.94	1.44	1.43